EXPERIMENTAL STUDIES ON REDUCTVE EXTRACTION OF ACTINIDES FROM MOLTEN SALT UNDER HIGHLY STRATIFYING CONDITIONS

By
S. VANNIA PERUMAL

ENGG02201104005

Indira Gandhi Centre for Atomic Research,
Kalpakkam-603102, Tamil Nadu, India

A thesis submitted to the

Board of Studies in Engineering Sciences

In partial fulfillment of requirements

for the Degree of

DOCTOR OF PHILOSOPHY

of

HOMI BHABHA NATIONAL INSTITUTE

August, 2015

Homi Bhabha National Institute

Recommendations of the Viva Voce Board

As members of the Viva Voce Board, we certify that we have read the dissertation prepared by **S.Vannia Perumal** entitled **"Experimental studies on reductive extraction of actinides from molten salt under highly stratifying conditions**" and recommend that it may be accepted as fulfilling the dissertation requirement for the Degree of Doctor of Philosophy.

_____ **Date:**

Chairman - Dr. P. M. Sathya Sai

_____ **Date:**

Guide/Convener - Prof. Sreenivas Jayanti

_____ **Date:**

Co-guide - Dr.B. Prabhakara Reddy

_____ **Date:**

Member 1 - Dr. T. Gnanasekaran

_____ **Date:**

Examiner

Final approval and acceptance of this dissertation is contingent upon the candidate's submission of the final copies of the dissertation to HBNI.

I hereby certify that I have read this dissertation prepared under my direction and recommend that it may be accepted as fulfilling the dissertation requirement.

Date: **Prof. Sreenivas Jayanti**

Place: **(Supervisor/ Convener)**

CERTIFICATE

I hereby certify that I have read this dissertation prepared under my direction and recommend that it may be accepted as fulfilling the dissertation requirement

Prof. Sreenivas Jayanti
(Guide)

Date:

Place: Indian Institute of Technology

Chennai

STATEMENT BY AUTHOR

This dissertation has been submitted in partial fulfillment of requirements for an advanced degree at Homi Bhabha National Institute (HBNI) and is deposited in the Library to be made available to borrowers under rules of the HBNI.

Brief quotations from this dissertation are allowable without special permission, provided that accurate acknowledgement of source is made. Requests for permission for extended quotation from or reproduction of this manuscript in whole or in part may be granted by the Competent Authority of HBNI when in his or her judgment the proposed use of the material is in the interests of scholarship. In all other instances, however, permission must be obtained from the author.

(S. Vannia Perumal)

DECLARATION

I, hereby declare that the investigation presented in the thesis has been carried out by me. The work is original and has not been submitted earlier as a whole or in part for a degree / diploma at this or any other Institution / University.

S. Vannia Perumal

List of Publications arising from the thesis

Journal

1. "Actinides drawdown process for pyrochemical reprocessing of spent metal fuel", S. Vannia Perumal, B. Prabhakara Reddy, G. Ravisankar, K. Nagarajan, *Radiochemica Acta*, 2015, *103(4)*, 287-292.

2. "Effect of impeller type and density difference on draw down of low density microsphere", S. Vannia Perumal, S. Jayanti, K. Nagarajan, *Chem. Eng. Res. Design*, Dec'2015,104 , 571-578.

Conferences

1. "Actinides drawdown process for pyrochemical reprocessing of spent metal fuel", S. Vannia Perumal, B. Prabhakara Reddy, G. Ravisankar, K. Nagarajan, SESTEC-2014, BARC, Mumbai, February 25-28, 2014

S. Vannia Perumal

DEDICATIONS

Dedicated to my parents and all well wishers

ACKNOWLEDGEMENTS

My sincere thanks

to all those people

I came across

CONTENTS

Page No.

SYNOPSIS v
LIST OF FIGURES ix
LIST OF TABLES xi
Nomenclature xiii
Chapter 1 1
INTRODUCTION 1
1.1 Energy Requirements in India 1
1.2 Fast Reactor Fuels 1
1.3 Fast Reactor Fuel Cycle 2
1.4 Reprocessing of Spent Fuel 4
1.5 Metallic Fuels for FBRs 5
1.6 Indian Fast Reactor Program 6
1.6.1 Molten salt electrorefining process for metallic fuel reprocessing 7
1.6.2 Electrolyte salt waste treatment 11
1.6.3 Actinide drawdown process (ADDP) 11
1.7 Solvent Extraction 13
1.8 Organization of the Thesis 16
Chapter 2 19
LITERATURE REVIEW AND OBJECTIVE OF THE WORK 19
2.1 Introduction 19
2.2 Literature Review 19
2.3 Need for Hydrodynamic Studies 23
2.4 Literature on Solid–liquid Dispersion 24
2.4.1 Dense solid particle suspension studies 24
2.4.2 Floating particle drawdown studies 29
2.5 Objectives and Scope of the Present Work 34
2.5.1 Objectives 35
2.5.2 Scope of the work 35

Chapter 3 37
EXPERIMENTAL INVESTIGATION OF STRATIFICATION USING FLOATING SOLIDS 37
3.1 Introduction 37
3.2 Experimental 38
3.2.1 Materials 38
3.2.2 Experimental setup 40
3.2.3 Drawdown criteria 43
3.3 Results and Discussion 43
3.3.1 Effect of parameters 44
3.3.1.1 Effect of liquid medium 44
3.3.1.2 Effect of impeller type: 46
3.3.1.4 Effect of submergence (s/Da): 49
3.4 Correlation of Data and Prediction of N_{crit} 50
3.4.1 Correlations from cold flow dispersion studies 50
3.4.2 Prediction of N_{crit} for eutectic salt/cadmium alloy dispersion 54
3.5 Effect of Multiple Impellers on N_{crit} 55
3.5 Summary 57
Chapter 4 59
EXPERIMENTAL STUDY OF DRAWDOWN PROCESS FOR RECOVERY OF ACTINIDE FROM MOLTEN SALT 59
4.1 Introduction 59
4.2 Experimental 59
4.2.1 Facility 59
4.2.2 Heater power calculation 67
4.2.3 Flow control system 70
4.2.4 Safety measures - high level detector in extractor 72
4.3 Argon Atmosphere Glove Box System 73
4.3.1 Argon gas analyzer 74
4.3.2 Regeneration of argon gas purification tower 75
4.4 Chemicals 75
4.4.1 Drying of eutectic salt 75
4.4.2 Cleaning of cadmium balls 77
4.4.3 Preparation of UCl_3 loaded LiCl-KCl salt mixture 77

4.4.4 Analytical methods 78
4.4.4.1 Inductively Coupled Plasma – Optical Emission Spectroscopy (ICP-OES) ... 78
4.4.4.2 Inductively Coupled Plasma – Mass Spectroscopy (ICP-MS) 78
4.4.4.3 Atomic Absorption Spectroscopy (AAS): 79
4.4.4.4 High Performance Liquid Chromatography (HPLC) 79
4.4.4.5 Davies –Gray Potentiometric method 79
4.5 Experimental Procedure 80
4.6 Results and Discussion 81
4.6.1 Continuous runs 81
4.6.2 Material balance of U in salt and alloy phases 84
4.6.3 Mass transfer coefficient 85
4.6.4 Reductive extraction at higher U concentration in batch mode 88
4.7 Challenges Encountered During the Experiments 90
4.8 Summary 92
Chapter 5 93
SCALE UP STUDIES 93
5.1 Scale Up Principles 93
5.1.1 Similarities 93
5.2 Experimental 94
5.3 Results and Discussion 96
5.3.1. Effect of vessel size 96
5.3.2 Effect of impeller diameter 99
5.3.3 Correlation of data 101
5.3.4 Multistage impeller results 102
5.4 Summary 104
Chapter 6 105
CONCLUSIONS AND FUTURE STUDIES 105
6.1 Conclusions 105
6.2 Scope for Future Studies 106
REFERENCES 107

SYNOPSIS

The recovery of the fissile material from the spent fuel discharged from the nuclear reactors is the main focus of nuclear reprocessing industry. By adopting suitable reprocessing methods, the fissile material is recovered for reuse in reactors. The conventional aqueous reprocessing, mainly PUREX (Plutonium Uranium Extraction) process, is well established and is in use for treating oxide and carbide fuels from the fast reactors. For treating metallic fuel from the fast breeder reactors the non-aqueous pyroreprocessing by molten salt electrorefining has certain advantages over the conventional process. Department of Atomic Energy, India is pursuing the development of metal fuel fast breeder reactors which offer higher breeding ratio and power density along with closed fuel cycle. For reprocessing the spent metallic fuel, a high temperature electrorefining process employing an eutectic LiCl-KCl salt which offers high radiation stability towards high burn up (atom %) and short cooled fuel is proposed. The minor actinides partitioning (such as Np, Am and Cm) along with U and Pu gives an additional advantage of nuclear proliferation resistance.

In pyrochemical reprocessing, LiCl-KCl eutectic salt with wide electrochemical window is employed as the electrolyte for selective separation of the actinides. The spent fuel coming out of the reactor contains many elements in the periodic table. The separation of the actinides here is based on the difference in thermodynamic stability (reduction potential) of their chlorides. The elements in the spent fuel are grouped based on the thermodynamic stability of their chlorides. Chlorides of alkali, alkali earth and rare earth fission products are very stable. Chlorides of actinides are intermediately stable and chlorides of noble metals are less stable. In the electrorefiner, very stable fission products are dissolved and accumulated in the molten salt whereas the actinide elements having intermediate stability are selectively electro transported and deposited on the cathode. The noble metal fission products and cladding materials remain in the anode basket. The accumulation of fission products in the electrolyte

salt enforces periodic cleaning in order to maintain the decontamination factor of the actinide which is accomplished by treating with an ion exchange resin (zeolite). Prior to the reconditioning of the electrolyte, the actinides present in the electrolyte are removed by Actinide drawdown process (ADDP). The objective of this thesis work is to investigate actinide drawdown process using natural U as the representive. The proposed work involves designing an experimental facility to operate at high temperature ensuring the mixing of molten salt and Li-Cd alloy phase. The experiment needs to be carried out in an inert gas glove box because of the hygroscopic nature of the molten salt and the high reactivity of Li-Cd alloy towards oxygen. It is a continuous reductive liquid- liquid extraction operation wherein the molten salt is contacted with Li-Cd alloy phase containing lithium as the reducing agent. As the melting temperatures of the salt and alloy phases are high, the setup is designed to operate at 773K. The molten salt eutectic containing 0.5 wt % U is contacted with molten Li- Cd alloy phase (Li~ 300 ppm) at 723 K. The extraction was carried out by maintaining the flow rates of salt and cadmium phases at 25 ml/min each and the mixing was performed by a specially designed continuous contactor provided with 3- impellers. Extraction efficiency of up to 99 percent is obtained for uranium in typical runs.

In addition to these complexities, the effect of large difference in density between the cadmium phase (8000 kg/m^3) and salt phase (1600 kg/m^3) that can lead to stratification of the phases is also investigated to understand the dispersion of the phases. The relative difference in density between the molten salt and molten cadmium is 0.80. Considering the difficulties in observing the dispersion at high temperature operation with molten materials, it is proposed to carry out the fluid dynamic studies under cold flow condition.

The two phase solid -liquid system with relative difference in density varying from 0.13 to 0.63 is considered as the representative for the liquid-liquid dispersion. The low density (680 kg/m^3) microspheres having average sizes 100, 230 and 325 μm were used as the floating solid

particles and liquids with varying density from 778 to 1830 kg/m^3 with dynamic viscosity from 0.3 to 19 cP were used in the experiments. Three impeller system generally used for the low viscous fluids was considered and the effect of impeller type, impeller submergence, and solid/liquid properties on drawdown of floating particles was experimentally studied. The critical impeller speed required for uniform dispersion of the particles was experimentally determined for different conditions. It is observed that the density difference between the phases and impeller submergence are having strong effect on the dispersion. Based on the studies, a correlation in the form of non-dimensional numbers (Froude number, Archimedes number, density ratio, impeller submergence and particle diameter) to predict the critical impeller speed required for the dispersion of floating particles is proposed. This correlation was used to predict the impeller speed required for the dispersion of molten eutectic salt in alloy phase at high temperature. The effect of scale up on two phase dispersion was studied with 1:10 volume ratio. The experimental results were analyzed using general scale up criteria. The findings of this work are discussed here.

LIST OF FIGURES

No.	Title of the figures	Page no.
1.1	Schematic of the fast reactor fuel cycle	3
1.2	Radio-toxicity vs. cooling time	4
1.3	Pyrochemical reprocessing flow sheet based on molten salt electrorefining process	8
1.4	Schematic diagram of the electrorefining process	9
1.5	Resistances in the two phase mass transfer	15
3.1	Schematic of the stirred vessel, a) radial impeller, b) axial impeller	42
3.2	Stages of solid-liquid dispersion	45
3.3	N_{crit} vs. $\Delta\rho/\rho$ for (a) radial (b) axial downward and (c) axial upward impeller	48
3.4	Fluid flow pattern in radial and axial type impellers	49
3.5	Effect of impeller submergence on N_{crit}	51
3.6	Parity chart N_{crit} vs actual impeller speed using correlation 3.2 for radial, PD and PU impellers with ±20 % deviation lines.	54
4.1	Process flow diagram of actinide drawdown process	60
4.2	Photograph of the extraction system, without heaters.	60
4.3	Schematic of the continuous extractor	64
4.4	Process flow diagram with thermocouple locations.	65
4.5	Photograph of (a) Line heater and (b) Vessel heaters used in the setup	65
4.6	Photograph of the high temperature molten salt extraction setup with heaters	69

4.7	Photograph of glove box signal transfer devices a) signal feed through-inside, b) feed through-outside c) wireless signal transmitter, d) signal receiver	69
4.8	Schematic of the 1 mm dia. capillary in the salt and cadmium phase feed line.	70
4.9	Simplified schematic of molten salt flow control system.	71
4.10	Inert atmosphere glove box with argon purification system	76
4.11	Photograph showing a) feed eutectic salt and cadmium balls, b) UCl_3 loaded eutectic salt	78
4.12	Photograph of salt samples at various stages	82
4.13	Schematic illustrating mass transfer across the interface in the extractor	86
5.1	Schematic of a) the experimental set up and b) impellers	95
5.2	Effect of vessel volume on (a) Tip speed (b) N_{Re}, (c) N_{Fr}, (d) P/V and (e) Q_V/H.	98
5.3	Effect of impeller diameter on (a) Tip speed (b) N_{Re} (c) N_{Fr} (d) P/V and (e) Q_V/H.	100
5.4	Parity chart comparing experimental impeller speed with predicted values	102
5.5	Photograph of a) experimental set up and b) 3-stage impeller	103

LIST OF TABLES

No.	Title of the tables	Page no.
1.1	Fuels for Liquid cooled fast breeder reactors	6
1.2	Gibbs energy of formation of chlorides at 773 K	10
2.1	Separation factor for actinides and rare earths in LiCl-KCl/Cd systems at 773±5K	20
2.2	The properties of the liquids used for suspension studies in literature	25
2.3	Details of the particles used for suspension studies in literature	29
2.4	The details of the floating particles used in literature	29
2.5	The details of the floating particle used in literature	31
3.1	Properties of solids and fluids employed in this study	40
3.2	Experimental setup dimensions	42
3.3	Measured Critical impeller speed, N_{crit} (rpm) at which solid particles dispersed uniformly throughout the medium for radial and axial impellers at impeller location S/D_a =0.5, 1.0, 1.5.	47
3.4	Non-dimensional group used in correlation-1	52
3.5	Exponents' values in correlation given in equation (3.1)	53
3.6	N_{crit} predicted for molten salt system	55
3.7	Effect of multiple impellers	56
4.1	Pressure vessel design calculation for salt and cadmium feed tank.	62
4.2	Physical properties of the reagents	63
4.3	Thermocouple tag number and location details	66
4.4	Details of various heaters used in the setup	68

4.5	Percentage recovery of U in different experimental runs	82
4.6	Uranium material balance	85
4.7	Uranium concentration in batch extraction experiments	89
4.8	Uranium material balance in batch experiments	90
5.1	Scale up criteria generally used in stirred vessels	94
5.2	Variables in the scale up experiments	96
5.3	Vessel dimensions in scale up studies	96
5.4	Effect of scale up (1:10) on critical impeller speed. N_{crit} (rpm) in small and large vessel with three impeller submergence	97
5.5	Effect of impeller dia. on critical impeller speed in large vessel. N_{crit} (rpm) in 5 liter stirred vessel with 60 and 90 mm diameter impeller	99
5.6	Exponent of correlation equation, from the large scale vessel data.	101
5.7	Effect of 3-stage impellers compared with single stage impeller	103

NOMENCLATURE

a	Interfacial area, m^2
A_o	Cross sectional area of the orifice, m^2
A	Cross sectional area of the feed line, m^2
Ar	Archimedes number, Ar = $\frac{g\, {D_p}^3 \rho\, \Delta\rho}{\mu^2}$
C', C''	Constants in the correlation equations
C	Solute concentration, wt %
C_o	Orifice discharge coefficient
C_p	Specific heat capacity , kJ/kg-K
D_a	impeller diameter, mm
D_T	vessel diameter, mm
E	Weld efficiency
f	Darcy's friction factor
F	Flow rate, m^3/s
g	Acceleration due to gravity, m/s^2
h_L	Frictional loss in the Bernoulli's equation (4.3)
Fr	Froude number, Fr =$\frac{\rho N^2 D_a^2}{g\Delta\rho D_p}$
H	height of the liquid in the tank, m
J	Baffle width, m
k	Mass transfer coefficient, cm/s
m	Mass of the material (kg)
N_{crit}	critical impeller speed, rpm
P	Impeller power, W
P_1, P_2	Pressure in the Bernoulli's equation (4.3)
Re	Reynolds number, Re =$\frac{{D_a}^2 N\rho}{\mu}$

R	Vessel inner radius, m
R_c	Radius of curvature, m
R_k	Knuckle radius, m
s	Impeller submergence from the top interface, m
S	Maximum allowable stress , N/m^2
t	Wall thickness, m
V	Volume of the liquid, m^3
V_1, V_2	Velocity in the Bernoulli's equation (4.3)
W	Impeller blade height, mm
Z_1, Z_2	Elevation in the Bernoulli's equation (4.3)

Greek letters

μ	Dynamic viscosity, kg/m-s
ϑ	kinematic viscosity, m^2/s
α , β, γ, δ	Exponents in the correlations
ρ	Density of the liquid, kg/m^3
$\Delta\rho$	density difference between particle and liquid medium, kg/m^3
k	Turbulent kinetic energy, m^2/s^2
ϵ_{avg}	Average energy dissipation rate, m^2/s^3

List of Abbreviations

AAS	Atomic Absorption Spectroscopy
ADDP	Actinide Drawdown Process
CCT	Cadmium Collection Tank
CFL	Cadmium Feed Line
CFT	Cadmium Feed Tank
EXT	Extractor
FBR	Fast Breeder Reactor
HPLC	High Performance Liquid Chromatography
ICP-OES	Inductively Coupled Plasma- Optical Emission Spectroscopy
MA	Minor Actinides
PID	Proportional- Integral -Derivative controller
PD	Pitched Downward impeller
PU	Pitched Upward impeller
PUREX	Plutonium Uranium Extraction
SCL	Salt Collection Line
SFT	Salt Feed Tank
UHP	Ultra High Purity argon gas
TRU	TRansUranium elements

CHAPTER 1
INTRODUCTION

1.1 Energy Requirements in India

The world energy consumption has increased tremendously in the last three decades and majority of the world's primary energy consumption is from fossil fuels [1]. Energy consumption plays a significant role in policy decisions in developed as well as developing countries [1, 2]. Electricity production using nuclear energy is one of the important non-conventional energy sources[3]. As of 2010, nuclear fuel based energy generation supplies roughly 5 % of the total energy consumed [1]. With concerns about global warming and its harmful effects on the environment, the non-conventional energy sources have attracted more attention [4-8]. The share of nuclear energy in the total energy production is expected to rise over a period of time [9].

The energy requirement in India in 2050 is projected to be around 1000 GWe [10]. Per capita energy consumption is an indicator of the quality of life and increasing energy production in India is an important goal to be reached [11]. India has a large reserve of thorium ores [12-14], which can be converted into fissile material (U^{233}) in breeder reactors. Metal fuel breeder reactors can convert fertile materials (thorium) to fissile materials (uranium).

1.2 Fast Reactor Fuels

The currently operating nuclear power plant are based on the energy produced during nuclear fission. There are two types of power reactors, thermal and fast, depending on the energy of the neutron causing fission[15]. The reactors based on lower energy neutrons are known as thermal while those based on higher energy neutrons are called fast reactors. The present work is of relevance to the fast reactor fuels and hence the discussion will be pertaining to fast reactors. The fast nuclear fuel generally comprises the oxides, carbides, nitrides or alloys

of uranium alone or with plutonium. Uranium and plutonium are known as fuel materials. For the fabrication of a fast reactor fuel, the required fuel materials are obtained from the treatment of thermal reactor fuels. In nuclear reactor, during irradiation, the fissile materials (such as U-235, U-233 and Pu-239) undergo fission and releases fission energy along with the release of two to three neutrons and a wide range of fission products. The fertile materials, U-238 and Th-232 capture neutrons and undergo transmutation to form the fissile materials, U-233 and Pu-239. All the actinides absorb neutrons and form heavy elements like neptunium, Americium, Curium known as Minor Actinides (MA). Some of the fission products having high neutron absorption cross section act as neutron poison which leads to the reduction in the number of neutrons available for sustaining the chain reaction. The fuel pin cladding material (AISI-316 and D9 alloy in fast reactor) [16] under the influence of prolonged neutron flux (irradiation) loses the structural integrity and this increases the risk of clad failure and subsequent release of radioactivity. Hence it is necessary to discharge the fuel undergoing irradiation, even though all the fissile materials have not been consumed completely. The irradiated fuel or the spent fuel discharged from reactors will consist of the fuel materials, U and Pu (in significant amount), the fission products and the Minor Actinides (MA).

1.3 Fast Reactor Fuel Cycle

The valuable fuel materials, U and Pu, from the spent fuel may be recovered by subjecting the spent fuel to chemical processing and using the fuel materials for fabrication of the fast reactor fuel for irradiation[10]. The processing of the spent fuel is known as reprocessing. In a reprocessing operation, the fuel materials, U, Pu and minor actinides are separated and the fission products are disposed off as waste to the repository. The string of operations starting from the fast reactor fuel fabrication, irradiation in a fast reactor, reprocessing, and waste management and going back to refabrication of the fuel is known as a fast reactor fuel cycle. The operations up to the irradiation in the reactor are known as front end

of the fuel cycle and the back-end starts from the spent fuel handling from the reactor and various processes related to fuel reprocessing. A fast reactor fuel recycle is shown in Fig.1.1.

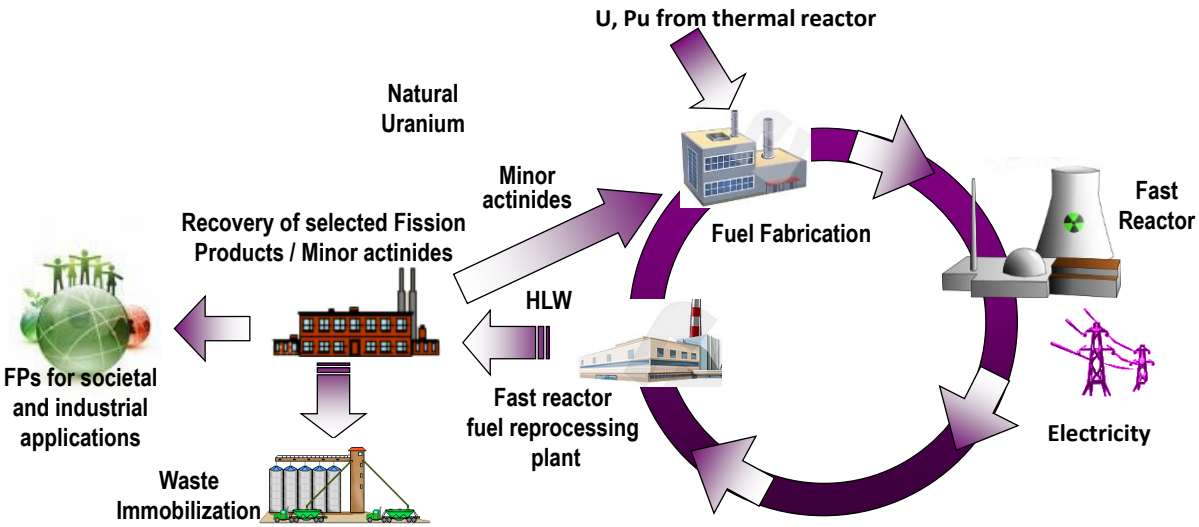

Fig. 1.1 Schematic of the fast reactor fuel cycle (adopted from www.iaea.org)

This kind of fuel cycle is known as the closed fuel cycle and certain countries opt to dispose of the spent fuel as waste without processing and the fuel cycle is known as open fuel cycle [17-19]. The advantages of the closed fuel cycle are the effective utilization of the fuel materials by recycling them and the reduction in the volume and radiotoxicity of the waste making waste management easier [20]. The closed fuel cycle enhances the uranium utilization factor to above 60 % [21]. Fig.1.2 shows the contributions of the various constituents to the radiotoxicity of the spent fuel and the time required for the activity levels to come down so that they can be left unmonitored. As can be seen, if the spent fuel is discharged as waste as in open fuel cycle, it will take 10^6 years to decay to natural background level whereas if all the actinides, U, Pu and MA are recovered and fission products are disposed as waste it will take a few hundred years only to decay. India is one of the countries that have opted for closed fuel cycle in which reprocessing plays an important role.

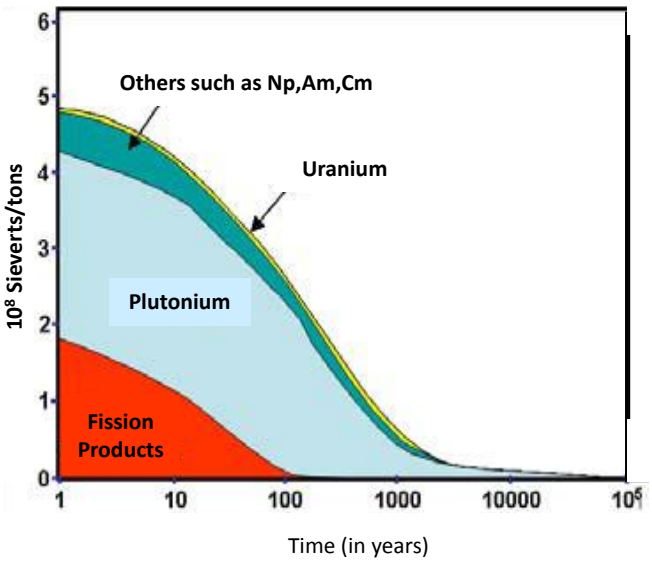

Fig. 1.2 Radio-toxicity *vs.* cooling time (adopted from [22])

1.4 Reprocessing of Spent Fuel

The present day large scale reprocessing plants utilize an aqueous processes based on solvent extraction by using n-tributyl phosphate. The process known as the PUREX (Plutonium Uranium EXtraction) is a well-developed and commonly used in reprocessing [23-26]. In this process, the irradiated fuel is chopped into small pieces and the fuel is selectively dissolved in nitric acid. The un-dissolved cladding material is disposed off as solid waste known as hulls. The solution containing uranium, plutonium and fission products as nitrates is then contacted with 30% Tri-butyl phosphate (TBP) in kerosene/dodecane which selectively extracts uranium and plutonium. Most of the fission products remain in the aqueous phase. Uranium and plutonium are then separated using a reducing agent and further purifications is carried out using either solvent extraction or ion exchange methods.

A number of non-aqueous processes have also been evaluated for this purpose but have not yet been used in large scale plants [27]. Among the non-aqueous processes, some are based primarily on gas-solid reactions and others on the use of non-aqueous media such as molten salts and alloys for the chemical separation. The family of non-aqueous reprocessing methods

that utilize oxidation -reduction reaction to effect chemical separation at elevated temperatures are called pyrochemical processes [28-31]. These include oxide electro-winning and molten salt electrorefining which are based on molten salt electrochemical technology and fluoride volatility process using the volatilization for separation of fuel materials. Pyrochemical reprocessing methods using high temperature molten salt media have significant advantages over the PUREX process. The molten salt media used for pyroprocessing have high radiation stability compared to the organic solvents of PUREX process providing the advantage of handling higher amounts of radioactivity in the fuel processed [32]. The equipment are potentially more compact than those of the aqueous process and so it enables co-deployment of separation facility with reactor which will lessen the shipment of spent nuclear fuel and special nuclear materials. The other advantages of this process are treating short cooled and high burn up irradiated fuels which reduces the out of pile inventory and overall doubling time, minor actinide recycling, proliferation resistance and less number of process steps. The inherent characteristics of incomplete separation of fission products (i.e less decontamination factor) also pose challenges such as requirement of remote fabrication of fuel from materials recovered from non-aqueous technology.

1.5 Metallic Fuels for FBRs

As mentioned above, all FBR fuels are based on U alone or with plutonium. But the chemical forms could be different. The various choices of fuel for fast breeder reactor are oxide, carbide, metal and nitride [33]. Each one has advantages and limitations and the selection of the fuel is based on the experience and available technology on fuel cycle. The comparison of fuel types are shown in the Table-1.1.

Table 1.1 Fuels for liquid cooled fast breeder reactors [34]

Properties	$(U_{0.8}Pu_{0.2})O_2$	$(U_{0.8}Pu_{0.2})C$	$(U_{0.8}Pu_{0.2})N$	U-19Pu-10Zr
Theoretical density, g/cc	11.04	13.58	14.32	15.73
Melting point, ºK	3080	2750	3070	1400
Thermal conductivity,(W/m-ºK) 1000 ºK 2000 ºK	2.6 2.4	18.8 21.2	15.8 20.1	40
Breeding ratio	1.1 - 1.15	1.2 - 1.25	1.2 – 1.25	1.35 – 1.4
Swelling	Moderate	High	-	high
Handling	Easy	Pyrophoric	Inert atmosphere	Inert atmosphere
Compatibility -Clad Coolant	Average Average	Carburization Good	Good good	Eutectics good
Reprocessing	Good	Demonstrated	Risk of C^{14}	Pyroreprocessing
Fabrication/Irradiation Experience	Large/good	Limited	Very little	limited

As can be seen, metallic fuels offer the highest thermal conductivity besides highest breeding ratios. High thermal conductivity is advantageous because the linear power rating, the power that can be produced per unit length of the fuel pin is decided by the thermal conductivity and the breeding ratio is decided by the fissile atom density. Though metallic fuels offer these advantages, the experience with metallic fuels in commercial reactors is very less compared to the oxide fuels which have been by far the choice of FBRs worldwide.

1.6 Indian Fast Reactor Program

India is keen on developing the fast reactor technology due to the paucity of uranium resources and availability of abundant thorium resources [12]. The only way to utilize the abundant thorium is to use the available uranium in thermal reactors (I stage) to produce plutonium and use the plutonium in FBRs (II stage) to produce U-233 using thorium as blanket in FBRs. Then Th-U233 combination can be used in thermal reactors in the III stage. This is

known as the three stage nuclear program. To develop the FBR technology, a test reactor known as Fast Breeder Test Reactor (FBTR) was set up and has been operating since 1985 at Kalpakkam. Based on the experience, a 500 MWe Prototype Fast Breeder Reactor is being constructed following which two more such reactors are planned. PFBR and these reactors will use oxide fuels. For the FBRs of future, India proposes to introduce metallic fuels to take advantage of the highest breeding ratios. Hence development of FBR fuel cycle is important.

1.6.1 Molten salt electrorefining process for metallic fuel reprocessing

As mentioned above, among the pyrochemical methods, namely, molten salt electrorefining, oxide electro-winning and fluoride volatility, the molten salt electrorefining process is ideally suited for reprocessing metallic fuels because the fuel is maintained in the metallic state throughout the process [28, 35] and hence the number of process steps are less. The other two methods are suitable for reprocessing of oxide fuels. Molten salt electrorefining process was developed by Argonne National laboratory [36] for processing the U-Pu-Zr alloy fuel of the Integral Fast Reactor (IFR). Besides the reduction in the number of steps, the molten salt electrorefining process offers other advantages over the PUREX process as well.

Besides the advantages of compatibility with short cooled and high burn up fuels which are highly radioactive and the compactness of the plants (discussed earlier) the volume of waste is lower, since most of the waste is in solid form. There are fewer criticality problems owing to the absence of aqueous reagents (neutron moderator). Another advantage of the molten salt electrorefining process is the ‘minor actinide recycling’. The minor actinides, Np, Am and Cm are not separated from plutonium and hence are recycled back into the reactor and are burnt producing energy and at the same time reducing the High level Liquid Waste (HLW) management problems. The pyrochemical flow sheet for the pyrochemical based on molten salt electrorefining process is shown in Fig.1.3. The key step is the molten salt electrorefining process.

A schematic diagram of the electrorefining process proposed by Argonne National Laboratory for reprocessing U-Pu-Zr alloy fuel is shown in Fig.1.4. This process exploits the differences in the thermodynamic stabilities of the chlorides of fuel materials and fission products, to separate them. The actinides (U, Pu, Am, Cm, etc.) and the fission products (alkali, alkaline earth and rare earth elements) in the spent fuel are, thus, separated based on the difference in their reduction potential. The eutectic salt (58.5 mol % LiCl and 41.5 mol % KCl) is used as the electrolyte. This eutectic salt has the low eutectic temperature 634 K [37]. The inorganic salt has wide electrochemical window and high stability to irradiation. The elctrorefining process is carried out at 773 K.

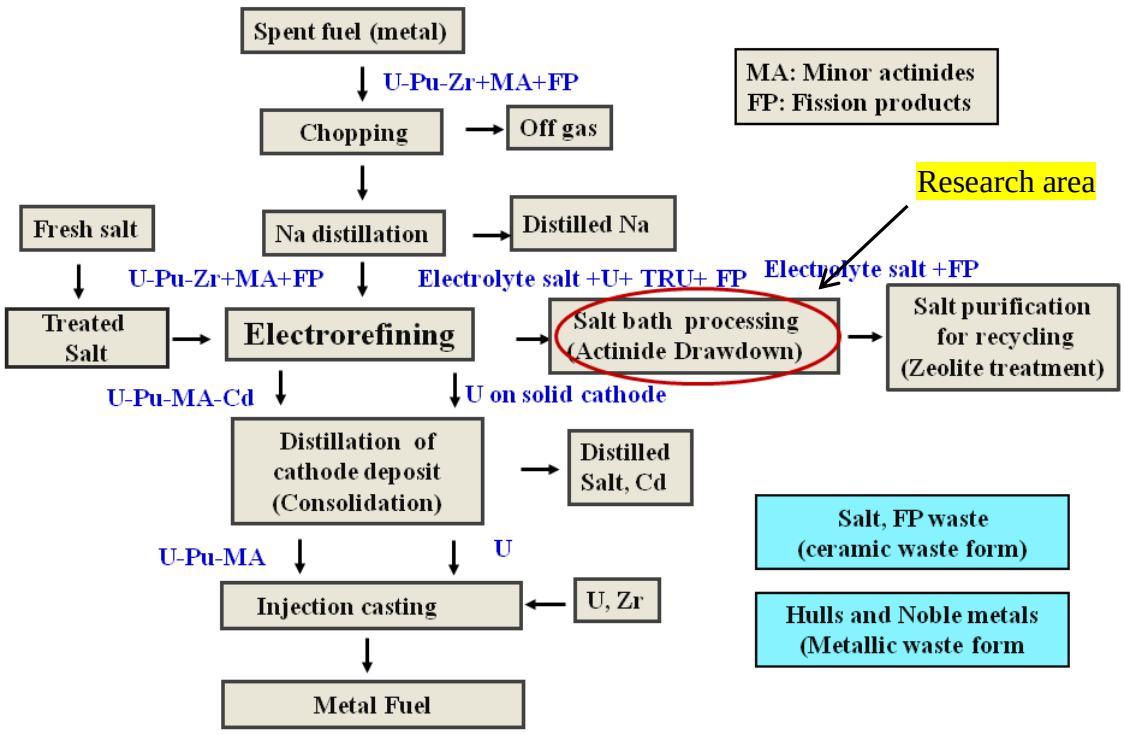

Fig. 1.3 Pyrochemical reprocessing flow sheet based on molten salt electrorefining process

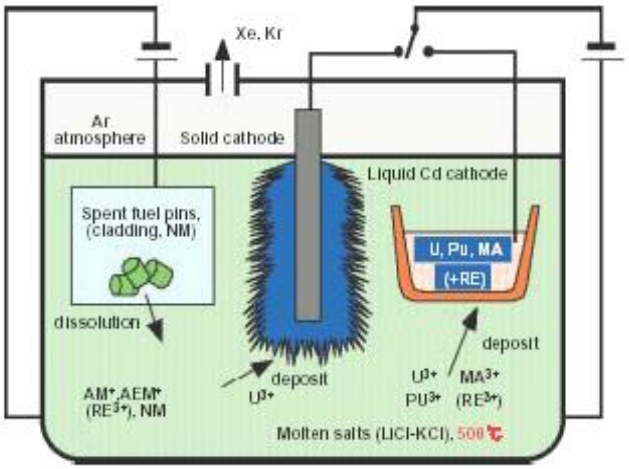

Fig.1.4 Schematic diagram of the electrorefining process. (Here AM- Alkali metals, AEM- Alkaline Earth Metals, MA- Minor Actinides, and REE- Rare Earth Elements)

The chopped spent fuel is loaded in basket and immersed in the molten salt electrolyte. The fuel materials, U and Pu are selectively electro-transported and deposited on suitable cathodes of the electrorefining cell. On a solid cathode, U alone gets deposited. Due to the high stability of its chloride, plutonium does not get reduced at the applied potentials. However, on a liquid cadmium cathode, uranium, plutonium and MA get co-deposited. This is due to lowering of the reduction potentials due to the reduced thermodynamic activities of actinides and MA in cadmium. The co-deposition of MA along with U and Pu is unavoidable and it offers the advantage of recycling the MA into the fuel, known as Actinide Recycle Potential. The chlorides of the elements constituting spent fuel can be classified according to their stability as indicated in Table 1.2. As shown in the Table, the elements in the spent fuel could be grouped as follows based on the electrochemical or thermodynamic stability of their chlorides: very stable chlorides (alkali, alkaline earth and rare earth elements Na, Ba, Sr, Cs, Ce, Nd, etc.), chlorides of intermediate stability (actinides and minor actinides U, Pu, Np, Am, Pu, Cm) and less stable chlorides (Cd, Fe, Nb, Mo, Tc, Rh, Pd, etc.).

Table 1.2 Gibbs energy of formation of chlorides at 773 K ($-\Delta G_f^0$, kJ/mole of chlorine) [28]

High stability		Electro-transportable		Low stability	
compound	$-\Delta G_f^0$	compound	$-\Delta G_f^0$	compound	$-\Delta G_f^0$
$BaCl_2$	367.8	$CeCl_3$	287.0	$CdCl_2$	135.1
CsCl	367.4	$NdCl_3$	284.1	$FeCl_2$	122.5
KCl	362.8	YCl_3	272.4	$NbCl_5$	111.7
$SrCl_2$	354.4	$AmCl_3$	267.8	$MoCl_2$	70.3
LiCl	345.2	$CmCl_3$	267.8	$TcCl_4$	46.0
NaCl	339.3	$PuCl_3$	261.1	$RhCl_3$	41.8
$CaCl_2$	337.6	$NpCl_3$	243.1	$PdCl_2$	37.7
$LaCl_3$	293.7	UCl_3	231.0	$RuCl_4$	25.1
$PrCl_3$	288.7	$ZrCl_4$	195.0		

During the electrorefining process, the less stable elements remain in the anode basket. chlorides (Cd, Fe, Nb, Mo, Tc, Rh, Pd, etc.). During the electrorefining process, the less stable elements remain in the anode basket. The intermediate group of actinides and MA are converted into chlorides. The chlorides dissolve into the electrolyte salt and are selectively reduced and deposited on the cathode as metals. On the other hand, fission product elements whose chlorides are very stable are converted into chlorides and remain dissolved in the electrolyte, as they are not easily reduced.

Although these fission product elements are expected to mainly remain in the electrolyte, if they are present in high concentrations, they also tend to get deposited on the cathode affecting the purity of the actinide metals deposited at the cathode. Presence of significant amounts of fission products in the cathode deposit is unacceptable due to their high neutron absorption cross section [23]. Further, loading of the fission product chlorides would also increase the melting temperature of the electrolyte salt leading to possible solidification at the operating temperature of 773 K. Hence the concentration of chlorides of fission products in the electrolyte should not exceed the permissible limit which is about 4 to 5 weight percent. In order to maintain the purity of the cathode deposit, the electrolyte needs to be either treated

to remove the fission products and recycled, or should be discarded and fresh salt must be used as the electrolyte. In the latter case, the volume of solid waste will be high and in addition to that, there will be loss of valuable actinides which are present in the electrolyte. Therefore, the best choice is treatment of electrolyte and recycling. This is achieved by treating the eutectic salt containing chlorides of fission products with zeolite ion exchange resins. Prior to this zeolite treatment, the actinides, which are also in the electrolyte salt along with these fission products and are very valuable, must be recovered from the salt by actinide drawdown process (ADDP). Otherwise, the actinides would result in the waste.

1.6.2 Electrolyte salt waste treatment

Various choices, such as fractional crystallization, solvent extraction using metal alloy phase, exhaustive electrolysis and ultra-filtration on an inorganic membrane, are available for the separation of actinides from the fission products present in the waste salt. Among these, solvent extraction and electrolysis (both combined or separately) are more adoptable than other choices for industrial application and hence are considered for the development in the Indian nuclear program. The current work is on the development of solvent extraction for the removal of actinide from molten salt using cadmium alloy phase as the solvent.

1.6.3 Actinide drawdown process (ADDP)

In this process, the LiCl-KCl molten salt electrolyte containing the actinides, fission products and the MA as their chlorides at 773 K is brought in contact with the cadmium alloy containing a reducing agent so as to reduce the actinide chlorides selectively and the reduced actinides would be brought to the cadmium alloy phase leaving the fission product chlorides in the salt. The major consideration in the selection of the solvent phase (alloy phase) in actinide drawdown process are mainly from the melting temperature of the alloy so that it remains molten at the process temperature of 773 K and the other is the thermodynamic stability of its

chloride should not be high otherwise it will act as the reducing agent and get transferred to the salt as chloride. The choices are cadmium and bismuth. Of the two, cadmium was chosen because liquid cadmium is used as the cathode in the electrorefining process and is also kept at the bottom of the electro-refiner to collect any loose deposits from the solid cathode that may fall from the cathode. Since the chloride of lithium is of the highest stability, lithium is chosen as the reducing agent. The actinides, which are present as the chlorides in the salt phase are reduced to their metallic states and extracted into the cadmium alloy (metal) phase whereas the alkali, alkaline earth and lanthanide fission product elements remain as chlorides in the salt phase. The reductive extraction of actinides is based on the difference of the thermodynamic stabilities of the lithium chloride and the chlorides of the actinides.

$$MCl_{n\ (\text{salt phase})} + n\ Li_{(\text{Cd phase})} \rightarrow M_{(\text{Cd phase})} + n\ LiCl_{(\text{salt phase})} \qquad \Delta G_{rxn} = -ve \qquad (1.1)$$

where M represents U, Pu or minor actinides (MA).

In the molten salt, all actinides chlorides are present in trivalent state. In view of the importance of the reductive extraction of actinides and lanthanides in the pyrochemical reprocessing, this process development is one of the crucial issues for developing the metal fuel cycle. It has to be pointed out that no experience exists in India on this metal fuel cycle and even internationally the experience is very limited and up to pilot plant scale only. The present work focuses on extraction of actinides (in the inactive form, using natural uranium as solute) from eutectic salt using cadmium alloy at high temperatures, on characterizing of the hydrodynamics of two-phase dispersion under simulated cold flow condition and on scaling up studies, with the goal of eventually utilizing the results for scaling up in pyrochemical reprocessing.

One of the challenges in the extraction is determining the agitation requirement for achieving good mixing of molten salt and cadmium alloy phases having large density

difference and interfacial tension. Good mixing is essential to increase the interfacial area and hence the mass transfer. The high temperatures of the molten metal extraction pose additional challenges by making it not possible to visually observe the dispersion. Therefore, initial hydrodynamic studies were performed at room temperature, using light solid – heavy liquid as surrogates for light molten salt and heavy molten metal in actinide drawdown process. The initial studies were done in glass contactors which are geometrically identical to the actual high temperature pyro contactors to be used for molten salt extraction.

1.7 Solvent Extraction

Solvent extraction is one of the mass transfer operations, and is widely used in nuclear industry. As mentioned earlier, it is used in aqueous reprocessing, in the purification of uranium from its ore and thorium from the rare earths in the front end of the fuel cycle as well as in the back end of fuel cycle (e.g. reprocessing) [23]. It is also used in the separation of zirconium from hafnium, separating rare earth from one another, cobalt from nickel and tantalum from niobium. It is widely employed in process industries [38-40] such as pharmaceutical, petroleum, hydrometallurgy, effluent treatment, and analytical applications besides nuclear industry.

In any mass transfer operation, the rate of transfer is controlled by the driving force for the transport, and the resistance and the relationship is given by [41]

$$\text{Rate of transfer} = \frac{\text{driving force}}{\text{resistance}} \tag{1.2}$$

Based on the phases involved, solvent extraction can be classified into solid-liquid or liquid-liquid extraction. In liquid –liquid extraction, the feed solution containing the solute and the solvent is contacted with another solvent which is immiscible with the original solvent. Here the mass transfer is based on the distribution of solute between the two phases. The driving force for the mass transfer is difference between the chemical potentials (activity) of the solute in the two phases [42]**.** At equilibrium, the chemical potential of the solutes are same

in both the phases and there is no net transfer. The extent of departure from the equilibrium determines the rate of transfer.

In mass transfer involving two phases, the transfer takes place across the interface between the phases. In the solvent extraction operation, the driving force can be optimized by controlling the solvent/feed ratio, the operating temperature and the two phase flow configuration such as co-current, counter current or cross flow. Once the process media are fixed, limited control is available to change the driving force.

Resistance to the mass transfer is governed by the interfacial area, diffusion coefficient of the solute in the medium, and the film thickness. The solute should reach the interface from the bulk of the original phase and cross the interface, and then transfer to the bulk of the other phase. Due to the convective flow, the resistances in the bulk phases are negligible compared to that in the film on both the sides of the interface. The major resistance to the transfer is in the thin film on both the sides of the interface. In the laminar film, transfer takes place mainly due to molecular diffusion, which is less than the convective diffusion by several orders [43]. The resistances in the mass transfer involving two phases are illustrated in Fig.1.5.

This laminar film thickness is in the range of tens of microns (10^{-6} to 10^{-4} m) depending upon the turbulence/stirring prevailing in the bulk phases. Diffusivities of solutes in the liquid are in the range of 10^{-9} to 10^{-10} m^2/s [44]. Once the process and solvents are fixed, the control on the solute molecular diffusivity is limited. Hence the resistance to the transfer can be reduced by increasing the interfacial area and by reducing the laminar film thickness. Dispersion of one phase into another phase in the form of droplets increases the mass transfer area by many folds. This is achieved by the selection of suitable contactors (extractors) for the two phases.

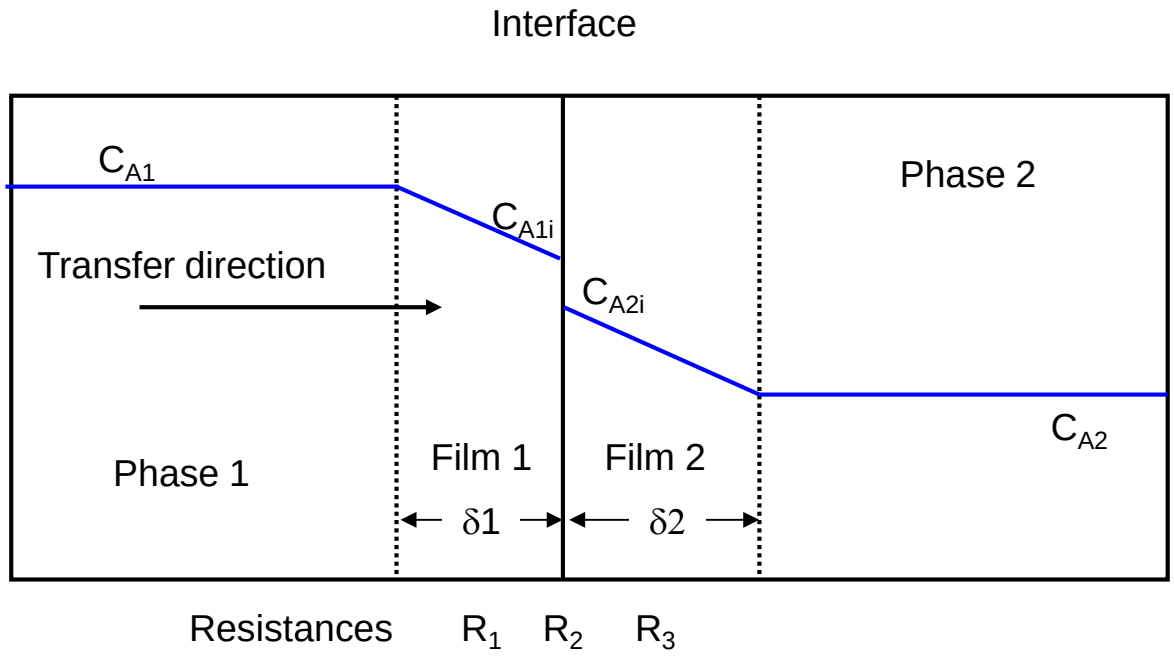

Fig. 1.5 Resistances in the two-phase mass transfer [45]

In the contactors, one phase is dispersed into the other phase in the form of droplets. These droplets increase the interfacial mass transfer area to a large extent and reduce the film thickness, which in turn reduces the resistance to mass transfer [46]. Creation of new droplets and sustaining them in the continuous phase is greatly influenced by the design and operation of the contactors. In liquid –liquid dispersion, the driving force for the creation of droplets are the turbulent energy dissipation and external velocity gradients. The resistances are density difference, interfacial tension between the two phases and internal viscous stresses which control the coalescence and the rate of settling [47].

For the dispersion of liquid-liquid mixture, various types of contactors viz. flow contactors such as jet mixers, packed tower, sieve tray tower, static mixers, etc., and mechanically agitated contactors such as mixer-settlers, rotary disc column type contactor and centrifugal contactors, are used in the industry [48]**.** Selection of suitable contactor should be based on the fluid properties such as density difference, interfacial tension, viscosity and chemical stability of the phases, mass transfer rate and specific application related parameters.

Among these, mechanically agitated type contactors are energy intensive, compact and offer high throughput per unit volume (i.e. low residence time), less volume hold up and maximum recovery. These are advantageous in the nuclear industries, in terms of fewer inventories, which in turn reduce the criticality hazard, shielding requirement and material accounting procedures for the nuclear materials.

1.8 Organization of the Thesis

This chapter provides the introduction to solvent extraction, the nuclear fuel cycle, various reprocessing options and in particular pyrochemical reprocessing. The electrorefining step used in pyrochemical reprocessing is described. The rationale for initially conducting mixing studies using light solid/ heavy liquid at room temperature is also explained.

The second chapter summarizes the relevant literature available in this field. Specifically, the experimental results published in the solvent extraction for pyrochemical reprocessing are reviewed. The experimental and simulation results for dispersion of lighter particles in heavier liquids are also reviewed. Based on the available information, the gaps in literature are identified and the objective and the scope of the work are defined.

The third chapter describes the experimental setup, results and analysis of mixing studies. The experiments were conducted using a wide variety of fluids and particles of different sizes. Three types of impellers were employed and the location of the impellers within the vessel was also varied. The results are analyzed using dimensionless numbers. A correlation is proposed to estimate the critical impeller speed at which complete dispersion is achieved.

The fourth chapter describes the experimental setup used for molten salt extraction of actinide at high temperature. The experimental setup, including the inert atmosphere used, is described in detail. Continuous extraction is employed in these studies and the results are analyzed and presented.

The fifth chapter describes the scale up studies using large glass vessel (1:10 volume). The results are analyzed using generally used scale up criteria. A correlation is proposed to estimate critical impeller speed for estimating the critical impeller speed.

The sixth chapter is conclusion chapter. This chapter summarizes the findings in the hydrodynamic studies using drawdown of floating particles in continuous liquid medium and high temperature molten salt extraction results. The scope for future work in this field is also discussed.

CHAPTER 2
LITERATURE REVIEW AND OBJECTIVE OF THE WORK

2.1 Introduction

As has been discussed in the earlier chapter, treatment of electrolyte salt from the electrorefiner containing major amounts of fission product chlorides and significant amounts of actinide chlorides to remove the actinides forms the core area of this research work. Further among the different methods that can be used for the partitioning of actinides from the electrolyte salt, extraction using molten alloys is the specific area of interest. In this chapter, a review of the literature on the studies pertaining to salt- molten alloy equilibrations for the separation of actinides and the objectives of the present study are discussed.

2.2 Literature Review

The studies reported in the literature are of two types: some investigators carried out batch equilibration experiments on salt –alloy equilibrations, while another set of investigators have carried out continuous extraction experiments. Koyama et al. [49] reported the separation factors of TRransUranium (TRU) elements and lanthanides with respect to U calculated from the activity coefficients of the elements in the eutectic salt and the Li-Cd alloy phase. The values are shown in Table 2.1. The values of actinides are almost close to each other and that of rare earth fission products forms another group. It shows that it is possible to separate the actinide elements together from the fission products. Kurata et al. [50] reported the distribution coefficients and separation factors with respect to U of some rare earth elements (Y, La, Ce, Pr, Nd, Sm, Eu and Gd) and actinides (U, Np) between LiCl-KCl eutectic /Li- Bi alloy as well as LiCl-KCl eutectic /Li-Cd alloy at 773 K.

The author has shown that the separation factors of trivalent elements are higher when Li-Bi alloy is used compared to Li-Cd alloy whereas, in case of the separation of divalent elements, they are higher with Li-Cd alloy. The reported separation factor values of actinides

Table 2.1 Separation factor for actinides and rare earths in LiCl-KCl/Cd systems at 773±5K [50]

Actinide	Separation factor	Rare earth	Separation factor
U	1.00 (basis)	Ce	45 ± 6
Np	2.12 ± 0.42	Nd	39 ± 6
Pu	1.88 ± 0.09		
Am	3.08 ± 0.78		
Cm	3.52 ± 0.59		

$$\log D_M = a + b \log D_{Li} \quad (2.1)$$

are comparable to those of Koyama et al. [49] The distribution coefficient of the elements were related as a function of lithium concentration in the form as a , b are the coefficient values estimated for U, Np, Y, La, Ce, Pr, Nd, Gd, Eu, Sm and Ba in cadmium and bismuth as the solvent.

$D_M = \frac{X_{MCl3}}{X_M}$, distribution coefficient of element (M) and

$D_{Li} = \frac{X_{LiCl}}{X_{Li}}$ distribution coefficient of lithium.

Where X_{MCl_3} and X_M are mole fraction of the element M in salt phase and metal phase respectively, X_{LiCl} and X_{Li} are mole fraction of Lithium in salt phase and metal phase respectively.

Moriyama et al. [51]reported that group partitioning of actinides is possible in LiCl-KCl/ Cd system. The elements present in the spent fuel will get reduced in the order: Pt group, actinides, lanthanides and alkaline elements Sr and Cs. Intermetallic compound formation of elements with Cd results in the distribution of compound at the interface, in the salt phase and the metal phase. These solid inter-metallics affected the recovery yield as well as the separation factor. They proposed group partitioning process by combining reductive extraction along with

filtration for the removal of solid intermetallic compounds. Sakata et al. [52] reported the distribution coefficient values of rare earth elements (La, Ce, Pr, Nd, Y) between LiCl-KCl eutectic salt and liquid Cd. The distribution coefficients of the elements were related to the lithium concentration. Intermetallic compound formation of rare earth elements was observed even at lower concentrations than their solubility limit. This leads to an uncertainty in material balance of the elements between salt and metal phase. The distribution coefficients were also estimated using the activity coefficients and the Gibbs energy of formation of the chlorides and the calculated values were comparable with the experimental values.

Moriyama et al. [53] reported the kinetics of extraction of the elements Zr, La, Ce and Th from LiCl-KCl eutectic salt by Cd phase using two film theory. The mass transfer area of the two phases in the experiments was fixed as 10 cm^2. Stirring of the phases was done by argon bubbling at a rate of few cm^3/s (3 cm^3/s). Experimental data were fitted to the equation:

$$K \propto D^n \propto \left(\frac{T}{\mu}\right)^n \qquad (2.2)$$

where D is the diffusion coefficient(m^2/s), T, temperature(K), μ is the solvent viscosity(Pa.s) and n the exponent value. The exponent values are in the range of 0.5 to 1.0. The estimated mass transfer coefficient value was in the order of 10^{-2} cm/s. Temperature dependence of mass transfer coefficient (Arrhenius plot) was found to be similar to the temperature dependence of solubility of the solutes.

Ackerman and Settle [54] reported the distribution coefficients of Pu, Am and rare earth elements (Y, Ce, La, Nd, Gd and Dy) between LiCl-KCl eutectic salt and liquid cadmium phase. They also observed that the separation of factors of TRansUranium elements (TRU such as Np,Pu, Am, Cm, Bk, Cf and other minor actinides) are in the same range whereas those of rare earth elements are different but in the same range. This enables the group partitioning of

actinides together from the fission products. The values of the separation factors are in agreement with that of those of other authors reported earlier.

Kinoshita et al. [55] carried out single stage continuous extraction studies using molten salt/ Li-Cd alloy. Ce, Gd and Y were used as the substitutes for U, other actinides and rare-earth elements, respectively. Separation efficiency was found to be better at low flow rates (10 to 25 ml/min) with sufficient agitation (300 rpm). However, the recovery was found to be lower. The concentration of the sample from extractor reached steady state in 5 to 10 min. The recovery was controlled by the amount of lithium added to the solvent (Cd) phase. With minimum lithium addition, separation efficiency equivalent to equilibrium separation factor values were attained. Separation efficiency of Gd and Y with respect to Ce was 0.27 and 0.0091 respectively. The mass transfer coefficient based on salt side was based on the agitation level, the presence of baffles and flow rate of the feed. The values are estimated to be 0.14 cm/s at an agitation speed of 300 rpm with the baffle plate in the contactor and 0.08 cm/s at 600 rpm without baffle plate. Kinoshita et al. [56] reported the results of continuous countercurrent extraction experiments using a three stage experimental set up. The rare earth elements Ce and Gd were used as the substitutes for actinides and Y for the fission products. The percentage recovery, the separation efficiency and the mass transfer coefficient were determined. It was reported that mutual mixing (axial mixing) of cadmium phases between the neighboring stages caused the experimental values for the separation factors to be less than the calculated values.

Ackerman et al. [36] described the details of a test system for molten salt extraction studies. The system was based on the centrifugal pyro-contactor having a rotor of 4 cm diameter. The throughput of the contactor was 600 ml/min of each for the salt and the cadmium alloy phases. The system included a feed preparation tank, a feed tank and a collection tank each for salt and the Cd phases. They demonstrated the contactor performance at rotor speed above 2000 rpm with a range of flow rates, 80 to 670 ml/min for the salt and 250 to 1000

ml/min for the cadmium alloy phase. They reported reductive extraction experiments using $CeCl_3$ in the salt phase and lithium as reducing agent in the cadmium phase. Stage efficiencies increase with rotor speed and exceeded 80 %.They used surrogates for trans-uranium elements and fission products (Ce for U, Ln for TRU and Y for rare earth fission products). They used the centrifugal contactor for testing with wide range of flow rates and rotor speed. Kinoshita et al. [57] reported the experimental results of pyro-partitioning for the recovery of TRU from high level liquid waste using Bi-Li alloy as the solvent. The experiments were carried out in multiple batch extraction mode in five steps. The elements taken for the reductive extraction were U, Pu, Am (actinides) and Y, La, Ce, Pr, Nd, Gd, Eu (lanthanides).They reported the recovery yield, separation factors for U and TRU with respect to Nd. More than 99 % of TRU elements were recovered from the salt phase. They compared the separation factor using Bi-Li alloy as the solvent with the Cd-Li alloy. The separation of U and TRU are better with Bi-Li alloy as the solvent.

You et al. [58] reported the conceptual design on the integrated pyroprocess plant named as PyRoprocess Integrated inactive Demonstration facility (PRIDE). This includes steps such as decladding, powder mixing device, electro-reduction equipment, electro-refining, electro-winning and waste salt regeneration and solidification. They reported the safety study results of the argon containment box for the facility using COMSOL- Multiphysics model. The PRIDE facility has been commissioned and operating in Republic of Korea.

2.3 Need for Hydrodynamic Studies

In molten salt extraction, the density difference between the two phases is very high (6400 kg/m^3) and the interfacial tension between the salt and cadmium alloy phase is 0.45 N/m (450 dyne/cm). Hence dispersion of these phases is challenging and hydrodynamics studies were undertaken in this work. The operating temperature of the facility is high which requires heaters with necessary insulation also the cadmium alloy phase is opaque. Visual observation

of dispersion in high temperature is not possible (we need to use non-intrusive techniques such as gamma tomography or resistance tomography). Hence it was decided to conduct cold flow hydrodynamic studies with a low density solid and liquid with different density to obtain the understanding of the fluid dispersion in actual pyro system. The existing literature on solid – liquid dispersion, especially the drawdown of floating particles is summarized.

2.4 Literature on Solid–liquid Dispersion

Solid-liquid suspension is applied in various industrial applications such as heterogeneous catalytic reaction, mineral processing, polymerization, fermentation, crystallization, dissolution process etc. Several works were carried out on suspension of heavy particles in liquid medium.

2.4.1 Dense solid particle suspension studies

Zwitering [59] studied the effect of agitation on complete suspension on solid particles in fully baffled vessels. Experiments were carried out in fully turbulent condition (Re > 3000). Minimum impeller speed required for the complete dispersion of particles at which no particle remained in the tank bottom for more than few seconds.

Major variables in his studies were

- Vessel diameter (0.154, 0.192, 0.24, 0.29, 0.45 and 0.60 m)
- Type of impeller viz. paddle, six blade turbine, vaned disks and propeller impeller
- Solid particle sand (2600 kg/m^3) and sodium chloride (2160 kg/m^3)
- Particle size (125 to 850 micron)
- Solid loading (0.5 to 20 wt %)
- Continuous medium viz. water, acetone, CCl_4, potassium carbonate solution, oil with different kinematic viscosity (0.39 to 11.1 cS).
- Impeller bottom clearance

Critical impeller speed (n, r/s) for complete suspension of solid particles were related with the experimental parameters vessel diameter (T, m), impeller bottom clearance (C, m), stirrer diameter (D, m), particle size (x, m), density of the solid ($\rho_s, kg/m^3$), density of the liquid ($\rho_l, kg/m^3$), solid loading (B, percent), kinematic viscosity (ν , m^2s^{-1}) and acceleration due to gravity (g, m s^{-2}). Correlation was proposed for predicting minimum impeller speed required for the complete dispersion in the form

$$nD^{0.85} = K\left(\frac{T}{D}\right)^{a} x^{0.2} B^{0.13} \vartheta^{0.13} \left(g\frac{\Delta\rho}{\rho_l}\right)^{0.45} \quad (2.3)$$

The value of the constant (K) and the exponent (a) depend on the type of impeller and impeller position (T/D). The Correlation was arranged in the form conventional dimensional form Reynolds number and modified Froude number for two phase flow.

Baldi et al. [60] reported work on the solid suspension in baffled vessels using disc turbines with 8 flat blades. Major variables were tank diameter (12.2, 19 and 22.9 cm), impeller diameter and impeller bottom clearance. Liquids used in the experiments were shown in the Table-2.1

Table 2.2 The properties of the liquids used for suspension studies in literature [12]

Medium	ρ_l (kg/m^3)	μ_l (kg/m-s)
Water (41ºC)	992	0.645 x 10^{-3}
Water (18ºC)	998	1.05 x 10^{-3}
1 mol $MgSO_4$ in water solution	1141	1.80 x 10^{-3}
2 mol $MgSO_4$ in water solution	1236	3.17 x 10^{-3}

Sand particles with density 2650 kg/m^3 and particle size were 50, 130, 370 and 545 micron was used as the solid particle. They proposed correlation to predict the minimum impeller speed for suspension in the form

$$N_m \propto \frac{\mu_l^{0.17}(\Delta\rho g)^{0.42} D_p^{0.14} B^{0.125}}{\rho_l^{0.58} D^{0.89}} \quad (2.4)$$

They have also tried mono modal and bi-modal particle and they showed that the behavior of suspension of bi-modal size distribution was similar to that of suspension of mono modal.

Nienow [61] studied solid/liquid dispersion in baffled vessels using turbine impeller. Water was used as the medium. Solid particles were soda glass Ballotini (density 1480 kg/m^3, size range: 153 to 600 micron) and other particles for dissolution studies. Here we summarize only the results of insoluble particles dispersion. The effect of impeller clearance on dispersion, suspension speed and fluid flow pattern were studied. Particle dispersion in the vessel was shown to be dependent on the impeller clearance. This work extended the Zwitering's work in terms of wider range of density difference, particle size and concentration. Minimum impeller speed required for solid suspension was related to the system parameters as

$$N_s \propto \Delta\rho^{0.43} L^{-2.21} X^{0.12} d^{0.21} \quad (2.5)$$

where N_s – impeller rotation speed (r s^{-1}), $\Delta\rho$-density difference between solid and liquid (g cm^{-3}), L-impeller diameter (cm), X-solid concentration (wt %), d-nominal particle size (cm). They concluded that efficient suspension can be achieved using small impeller bottom clearance and large impeller diameter.

Geisler et al. [62] reported scale up studies in suspension they employed physical modeling of complex fluid dynamics. The goal of their study was to determine the relationship between power input and other relevant properties such as tank size, geometrical condition and suspension properties. The model assumes that the power input needed can be divided into two parts 1) power needed for the fluid circulation and 2) sinking power of particle swam. They have considered various cases such as large particles in small vessels and medium size particles in large vessels. The large particles in small vessel usually results in heterogeneous distribution, whereas in medium (ratio of tank diameter to particle diameter, $T/d_p > 500$) and large size vessel homogeneous distribution is possible. Some of the conclusions are i) high solid hold up and large particles needed higher specific power. ii) For very large diameter ratio, the average

specific power input is constant. Major conclusion of the study is, it is not possible to obtain simple and constant rule in terms of a wider range of suspension particle properties and other parameters such as tank diameter and geometrical condition.

Raghava Rao [63] studied the solid-liquid dispersion in mechanically agitated large vessels using disc turbine and pitched downward impellers. Solid-liquid system used for the experiments was quartz particle (2520 kg/m^3) in tap water. Variables used in the studies were particle size (100 to 2000 micron), solid loading (0 to 50 wt%), type of impeller namely disc turbine, pitched downward and pitched upward impeller, impeller diameter to tank diameter (D/T) 0.175 to 0.58, ratio of impeller width to impeller diameter (W/D) and impeller blade thickness (k). He discussed the energy transfer mechanism in different type of impeller based on the flow direction and circulation loop. In case of radial impeller two circulation loops one above and one below the impeller are created. The energy associated with the bottom loop is used for the suspension of the particles. Turbulence is generated in the impeller tip region and it decays along the fluid flow path. Energy is lost during the change in flow direction at the wall and at the corner of the vessel bottom. The Pitched Turbine Downward (PTD) flow impeller generate turbulence just below the impeller and change in flow direction and flow path are minimum which results in efficient energy transfer for solid suspension than PU and disc turbine. As the particle diameter increases correspondingly settling velocity increases and requires high impeller speed for solid suspension. Solid loading is related to the impeller speed as $N_{cs} \propto X^{0.1}$. Impeller bottom clearance decreases results in low impeller speed for suspension. Fluid flow path decreases this result in (i) decay of turbulent along the flow path decreases, (ii) liquid velocity decreases. Effect of impeller diameter is related as $N_{cs} \propto D^{-1.16}$. The authors proposed the correlation for predicting the impeller speed in the form

$$N_{cs} = \frac{f\gamma^{0.1}(g\Delta\rho/\rho_l)^{0.45}X^{0.1}d_p^{0.11}T^{0.31}}{D^{1.16}} \qquad (2.6)$$

where f is the constant, γ-kinematic viscosity (m^2s^{-1}), X- solid loading (wt %), d_p- particle size (μm), T-tank diameter (m), D- impeller diameter (m).

Jirout and Riejer [64] investigated suspension of heavy solid particles in agitated vessel with dished bottom. Water was used as the continuous medium and H/T ratio was maintained at 1. Glass beads of size 0.1 to 3.79 mm were employed as the solid particles. The major variables were impeller type, 11 different impellers were used in the study namely, pitched 3 blade turbine with pitch angle of 24°, 35° or 45°, pitched six blade turbines with pitch angle of 45°, pitched 3 blade or 4 blade or 6 blade turbine with diagonally folded blades, pitched cylindrical 3 blade turbine, hydrofoil impellers, marine propellers and custom impeller were used. All the impellers were used in the pump down mode. Critical impeller speed was measured at various volume concentrations of the solid particles. The dimensionless power consumption was also calculated. They concluded that hydrofoil impellers were better compared to the standard impellers in terms of suspension efficiency. Propellers are found to be more sensitive to impeller bottom clearance, the suspension efficiency is similar for all hydrofoil impellers. The dimensionless power consumption does not depend on the number of blades (for pitched blade turbine with diagonally folded blades) and the blade angle has minimum effect on the suspension efficiency. They also showed that pitched 3 blade turbines with 45° angle needed maximum energy for suspension.

Ayranci and Kresta [65] analyzed the effect of off- bottom clearance and solid loading on suspension. They studied the limitation of Zwitering correlation at higher solid loading. Tap water was used as the medium. Five different particles were used for the studies details are shown in Table2.3. Fully baffled flat bottomed cylindrical vessel with T = 0.24 m with two impellers lightning A310 and 45º pitched blade turbine impellers was used for the studies. The authors proposed a new correlation in combination of Zwitering [59] and Baldi [60] with three exponent values for solid loadings based on the particle type 0.17, 0.23, 0.32. With modified

Table 2.3 Details of the particles used for suspension studies in literature [17]

Particle type	Size(micron)	Density(kg/m^3)
Small glass beads	74-125	2500
Urea formaldehyde	150-250	1323
Bronze	150-297	8855
Sand	350-500	2656
Large glass beads	595-841	2500
Ion exchange resin	677	1370

exponent value 0.23, just suspended speed (N_{js}) for particle suspension can be predicted up to solid loading up to 35 wt %.

2.4.2 Floating particle drawdown studies

Wojtowicz [66] studied the effect of agitator type and its position on the tank and solid properties for the drawdown of floating particles in continuous liquid medium. The minimum agitator speed necessary for the compete suspension and corresponding power required were experimentally measured. The type of impeller investigated are single impeller, dual impeller, vibromixer, Rushton turbine, pitched downward, pitched upward and reciprocating disc. Water was used as the working medium and three different types of solid particles were used for the experiments. The mass fraction of the particles was also varied. The details of the particles were given in Table-2.4 [66].

Table 2.4 The details of the floating particles used in literature [66]

Solids	Equivalent dia, d_p (mm)	Density, (kg/m^3)
MALEN	4.11	916.7
PLAST 1	3.46	883.3
PLAST 2	4.67	906.4

The results were analyzed in various dimensionless numbers, such as Froude number and modified Reynolds number (containing mixing power per unit volume, P_{min}/V). Following relationship were proposed to estimate minimum impeller speed and impeller power

$$\sqrt{Fr_{min}} = \sqrt{\frac{n_{min}^2 D}{g}} = C_1 \left(\frac{h}{D}\right)^{a1} \left(\frac{d_p}{D}\right)^{b1} \left(\frac{\Delta\rho}{\rho_l}\right)^{c1} c_m^{d1} \quad (2.7)$$

$$Re_{\frac{P_{min}}{V}} = \left[\left(\frac{P_{min}}{V}\right)\frac{d_p^4 \rho_l^2}{\mu_l^3}\right]^{1/3} = C_2 \left(\frac{h}{D}\right)^{a2} \left(\frac{d_p}{D}\right)^{b2} \left(\frac{\Delta\rho}{\rho_l}\right)^{c2} c_m^{d2} \quad (2.8)$$

The coefficients were given in the reference [66]. Based on the study the author concluded that in case of single impeller pitched upward had the lowest power requirement, where pitched downward had the highest power requirement. The impeller type and bottom clearance are the major variables which affect the N_{min} and P_{min}.

While the solid particle properties play minor role. The addition of another impeller increases the power requirement. The vibromixer was able to suspend the particles due to the axial circulation and the power requirement was half that of the classical stirred tank. The disc diameter plays a major role in determining the mean agitator velocity.

Karz and Mackiwicz [67] studied the effect of baffling on the suspension of floating particles. Four type of impellers and twelve configurations of baffles were investigated. Impeller types were pitched six bladed with UP and DOWN flow, Rushton turbine impeller and propeller impeller. Baffle arrangement were varied by changing the length of the baffles, its location and the numbers. Agitator speed was measured using photo electric method. Polyethylene particles of size 3.82 mm and density 950 kg/m^3 were used in concentration range of 1 to 4 wt% while tap water was used as the dispersion medium. They concluded that UP pumping is more energy efficient in drawdown of floating particles. They also found that when the impeller location was kept near the vessel bottom $\left(C/_H = \frac{1}{3}\right)$ baffle effect was significant, if the impeller was near the top $\left(C/_H = \frac{2}{3}\right)$ the effect of baffling was relatively less. Here, C refers to the impeller off bottom clearance and H refers to the liquid depth in the vessel.

Khazam and Kresta [68] reported experimental studies on drawdown of floating particles using expanded polyethylene beads and polyethylene grids, the specific gravity of the

particles varied from 0.3 to 1.0. The particle details are shown in Table 2.5. Tap water and another fluid Bayol (density 794 kg/m^3) were used as the dispersion medium. Tanks were either un-baffled or containing single or four baffles. Three types of stirrer were used, namely pitched blade turbine UP and DOWN and another model A340 in the UP pumping mode.

Table 2.5 The details of the floating particle used in literature [68]

Particle	Specific gravity	Particle size, d_p(mm)
EPS 1	0.9	1.0
EPS 2	0.4	1.5
EPS 3	0.3	2.0
PE grids	1	8 × 8 × 1

The effect of varying the distance from the liquid surface to the impeller location was also studied. In addition to the experimental studies computational fluid dynamics (CFD) studies were also performed to understand the flow pattern and the mechanism drawdown in this condition. Based on these results authors the authors concluded that the drawdown occurs by the combination of three different mechanisms

(i) Single vortex formation (predominant in un-baffled or single baffled cases)

(ii) Turbulent fluctuation (especially under small clearance)

(iii) Mean drag

Fully baffled vessels are better suited for drawdown of than the single baffled or unbaffled systems. The minimum impeller speed for complete drawdown increases with impeller submergence. At small submergence turbulence is the main mechanism and at large submergence mean drag is the main mechanism for drawdown. In the fully baffled system UP pumping is recommended and for small submergence and DOWN pumping is recommended for large submergence. In the experimental range studied n_{min} increases linearly with solid concentration.

Kuzmanic and Ljubicic [69] reported the experimental results of floating particles suspension in water as the dispersion medium. Polyethylene particles (840 kg/m^3) of size 205 to 600 micron were used. They employed UP pumping pitched blade turbine with four blades, different angles and different impeller diameter (D/T ratio). A cylindrical flat bottom tank with four baffles was used. The power requirement and mixing time were measured. The mixing time was measured using conductivity measurement with NaCl as the tracer. Critical impeller speed for suspension was determined by visual observation. The power consumption was measured using torque sensor. They found that the mixing time increases with the addition of floating particles and it can be as high as five times the mixing time of liquids. The mixing time depends on the particle size and concentration. On the other hand N_{min} does not vary significantly with particle size or concentration. An increase in blade angle and impeller diameter causes decrease in dimensionless mixing time ($n\ t$), but the power consumption was also found to be higher. The power consumption can be reduced by increasing the impeller off bottom clearance.

Jaworski et al. [70] measured the flow pattern of liquid in agitated vessels with pitched blade turbine impeller. The impeller was used in UP and DOWN pumping mode and two impeller diameter (D) was employed (T/2 and T/3). The off bottom clearance (C/H) varied from ¼, ½ and ¾. Laser Doppler anemometry (LDA) was used to monitor the flow pattern and CFD studies were performed and compared with the experimental results. The results show that simulations predict the mean flow variations but the turbulent parameters did not match between experiments and simulations.

Taskin and McGrath [71] investigated the effect of impeller type, submergence and number of baffles on the drawdown of floating particles. Tap water was used as the dispersion medium. Polyethylene particle (905 kg/m^3) with size 5 x 3 x 2 mm and solid loading of 1 wt% was used in the experiments. Tank diameter (D_T) was 0.31 m and standard baffles 4, 2 and 1

were used. Three impellers namely disc turbine, Pitched blade turbine and LE 20 were employed. Impeller off-bottom clearance (C/D_T) varied from 1/3 to 7/8 . The authors found two modes of mechanisms for solid suspension (i) recirculation loop, (ii) Vortices. In case of vortices, flow instabilities are more and bulk flow was predominantly in tangential direction and top to bottom mixing was significantly reduced. Instabilities lead to fluctuation in power, flow and mechanical vibrations. Radial impeller consumes high power and low N_{min}. Major findings were axial and mixed flow impellers mounted close to the base ($C/D_T \leq ¾$) in fully baffled vessel give low power demand, stable operation and the air entrainment are avoided.

Kresta [72] evaluated the effect of baffle arrangements on drawdown of floating particles. In this study 4-full baffles, 4- half baffles and surface baffles (baffle height=5/24 D_T) were employed , expandable polystyrene particles of specific gravity 0.3 and 0.9 with size of 2 and 1mm respectively were used as the solid particles and tap water was used as the fluid medium. Solid concentration and impeller submergence were varied. Pitched blade turbine impeller (PBT) of diameter T/2 and T/3 were used in UP and DOWN pumping mode and another impeller called A340 was used in UP pumping mode .The just drawdown speed (N_{JD}) ,cloud depth and the power required were monitored. Here cloud depth gives an indication of the extent of distribution of the particles in the tank. It does not directly relate to the residence time below the surface. CFD simulation was also performed to obtain better insight into the drawdown process. It was found that PBT impeller with downward flow and upward flow for D_a/D_T =½, the N_{JD} was less for surface baffles, also especially at large submergence the air entrainment is low or nil and cloud depth is larger. In case of A340 impeller all the three baffle configuration gave more or less similar results in terms of N_{JD}. For small impeller PBT secondary circulation loop is formed in the fully baffled and ½ baffled configuration, this increases the N_{JD}. At larger impeller submergence in the down pumping mode it was impossible to drawdown the particle in the fully baffled configuration.

The authors concluded that the larger impeller diameter perform better for drawdown of floating particles. In terms of cloud depth for the PBT, larger submergence results in better cloud depth. Surface baffle configuration also give better cloud comparing to the other two configurations. Relatively A340 impeller resulted in poor cloud depth, this because there is a large suction zone below this impeller which prevents the particle from going to the bottom, this actually pushes the particle towards the surface. A comparison of the power number showed that submergence has no significant effect on N_P, however if there is significant air entrainment power drawn reduces. In terms of actual power, for the impeller diameter D_a/D_T =½, surface baffle configuration resulted in substantial reduction in power consumption. The authors also reported that the effect of changes in solid concentration, density and fluid properties were similar to that of earlier results.

2.5 Objectives and Scope of the Present Work

The above literature review reveals that there are many studies on high temperature molten salt extraction using the batch experiments and a few investigators have used multistage extraction based continuous systems in their studies. Further, the extraction efficiencies and the separation factors are dependent on the design of the contactors, the rotor speed, the flow rates and the temperature of operation. As has already been pointed out in the earlier chapter, the metallic fuels will be introduced in Indian Fast Breeder Reactors in the coming decade and hence the metal fuel cycle has to be developed in our country [73]. Hence, engineering scale studies are being taken upon the various unit operations including the Actinide drawdown process step. For designing a continuous extraction facility, which is essential for engineering scale studies, it is necessary to generate our own data on the optimum design and operating parameters of the extractors for the recovery of actinides from the salt containing actinides and fission products using cadmium alloys. Between the alloys of cadmium and bismuth, cadmium

alloys were chosen for our systems, because of the fact that cadmium will be used at the bottom of the electro refiner to collect the loose deposits from the cathode.

2.5.1 Objectives

1. To setup an experimental facility with inert atmosphere to conduct the continuous molten salt extraction experiment for the extraction of U from LiCl-KCl salt using Cd-Li alloy as the solvent at 723 K.
2. To conduct batch and continuous studies to optimize the parameters for the Liquid - Liquid Extraction (LLE) of actinide using the above setup
3. To conduct hydrodynamic studies on room temperature solid- liquid dispersion, using light particles and liquids so as to have a high density difference to simulate Cd-Li/Eutectic salt system
4. To develop correlations to estimate minimum impeller speed for complete dispersion in draw-down of floating solids

2.5.2 Scope of the work

As mentioned earlier, there exists a large difference in the densities and the interfacial tension between the two phases in the high temperature molten salt extraction. In order to ensure maximum mass transfer, a thorough mixing of the two phases is essential. A study on the dispersion in the actual high temperature molten salt extraction system would be helpful. However, high temperature pyro contactors are made of stainless steel and are fitted with electrical heaters and insulation and the cadmium alloy phase is opaque. It is not possible to observe the level of dispersion within the pyro contactor without special NDT technique such as gamma tomography or electrical resistance tomography [74]. For the design and development of suitable stirred vessel contactor for application at high temperatures, experiments with room temperature two phase systems having a high density ratio were

performed. In this work, to study the dispersion phenomena, room temperature solid–liquid phases with high density difference were investigated. Solid particles used for this studies were low density cenosphere (680 kg/m^3), a kind of inert fly ash generated as waste in coal fired thermal power plant. The solid particles were sieved and segregated into 100, 230 and 325 µm particle size. Various liquids (such as acetone, kerosene, water, glycerol-water solution and aqueous $ZnCl_2$ solution) with a density range of 780 to 1830 kg/m^3 were used as the continuous medium.

In the high temperature molten salt extraction studies, natural U in the chloride form was employed as the solute. The reduction reaction involved in the molten extraction is nearly instantaneous and hence mass transfer, which depends on the hydrodynamics of the liquid-liquid contactor, controls the overall reaction rate. A facility to conduct batch and continuous studies of high temperature molten salt extraction was created and experimental runs were performed to characterize the extraction.

CHAPTER 3
EXPERIMENTAL INVESTIGATION OF STRATIFICATION USING FLOATING SOLIDS

This chapter contains the details of experimental studies on drawdown of floating solids into continuous liquid medium and the relevance of solid-liquid dispersion with liquid-liquid dispersion with high density difference. Following details are discussed in this chapter, the basis for the selection of solid /liquid materials for the experiment, description of the experimental setup, experimental procedure and results and discussion.

3.1 Introduction

Liquid extraction efficiency depends on the three important factors viz. departure from equilibrium, interfacial area and film resistance [75]. Once the process and process media are fixed, the mass transfer between the two phases is mainly dependent on the interfacial area across which transfer takes place. The interfacial area depends on the hydrodynamics of the process medium in the reaction vessels. Energy transferred to the fluids generates a flow field in the medium. Turbulence eddy and velocity fluctuation in the interface result in the breakage of droplets and creation of new droplets. On the other hand, fluid surface energy in the form of interfacial tension tends to cause coalescence of the droplets [76, 77]. In the stirred vessels with mechanical agitators, the impeller region is energy intensive and it acts as the source of droplet generation. The flow field prevailing in the stirred vessel imparts drag force to the droplets, resulting in the distribution of droplets throughout the continuous medium.

Dispersion of the two phases is governed by the applied forces, i.e. inertial force by the impeller and the resistance forces, viz. buoyancy force, viscous force, interfacial tension and gravity force. These are dependent on the fluid properties and the vessel geometry. In case of immiscible liquids with high density difference, buoyancy force dominates and this results in the stratification of phases. In this study, agitation level needed for the dispersion of such

phases and the effect of fluid parameters and geometry and the type of impellers was carried out. In ideal case, the mixing studies should be done with eutectic salt and cadmium alloy phase, but the high temperature involved and the lack of transparency in the medium as well as the setup precludes such studies. Hence a setup containing floating particles in continuous medium (with transparency of the medium and the vessel) with wide range of density ratio ($\frac{\Delta\rho}{\rho}$) 0.13 to 0.63 is employed. This study is taken as a surrogate for the dispersion of immiscible liquids with high density ratio (i.e. eutectic salt and cadmium alloy phase).

3.2 Experimental

3.2.1 Materials

Clear liquids with different densities in the range of 778 – 1830 kg/m^3 and dynamic viscosities in the range of 0.3 to 19 cP were employed as continuous media. The liquids chosen were water, kerosene, acetone, glycerol-water solution in 1:1 and 2:1 ratios by volume and aqueous $ZnCl_2$ solution (65 wt % of $ZnCl_2$). The inorganic salt $ZnCl_2$ having high solubility (>4000 kg/m^3) [78] in water is considered to prepare the solution with high density.

In each case, the liquid density was measured using a standard volume flask and the viscosity was measured using Brookfield viscometer. Cenospheres, a kind of fly ash particles sintered inside coal-fired furnaces generated in thermal power plants, were used as the solid particles. The liquid and solid properties are shown in Table 3.1. The cenosphere was sieved and segregated and particles with the average size of 100, 230 and 325 micron were used for the experiments. The reason for choosing these size ranges is explained below. In the dispersion of two immiscible liquids, the mean droplet size of the dispersed phase is measured in the form of Sauter mean diameter, d_{32}, which indicates the average surface area of dispersed phase per unit volume [79]. The droplet size varies depending upon the external forces breaking the droplets such as turbulent kinetic energy, viscous stresses due to velocity gradient and internal

resisting forces such as interfacial tension and internal viscous stress. For liquid-liquid extraction, the size of the dispersed phase is primarily determined by the turbulence level at the impeller. Zhou and Kresta [47] proposed a correlation for the droplet diameter as $d_{32}(\mu m) = 118.6\left(\varepsilon_{\max} N D_a^2\right)^{-0.270}$ where D_a is the impeller diameter. CFD studies [68, 72, 80-82]show that this varies rather widely in an impeller, with it being the highest in the region of the impeller. The measurements of Dong et al. [83] and the CFD simulations show that for radial impellers, k/U_{tip}^2, where k is the turbulent kinetic energy and U_{tip} is the blade tip velocity, is of the order of 0.05. For an impeller diameter of 0.04 m rotating at 600 rpm, the turbulent kinetic energy near the tip would be 8×10^{-3} m^2 s^{-2} and the turbulent energy dissipation rate $\approx k/(0.4 * \frac{D}{4})$ =2 m^2 s^{-3} Taking the diameter to be 0.04 m, one may get an estimated drop size of ~ 300 micron as a typical drop size in the liquid-liquid system under turbulent conditions. To verify this, the correlations of O'Connell and Mack [84] and Nagata [85] for power number in stirred tanks have been used to obtain the power, from which an average value of the dissipation rate could be obtained as $\varepsilon_{avg} = P/(\rho_l V)$. Assuming that the dissipation rate near the impeller would be about 10 times the average value gives an estimated drop size from the above equation in the range of 180 to 300 micron. One can see that these estimates of drop size are much lower (by about an order of magnitude) than the ones used in liquid-solid dispersion studies quoted above.

The particle density was measured by liquid volume displacement method and the values are in the range of 630 -730 kg/m^3. The average density of 680 kg/m^3 was used in the analysis. Using the cenospheres in acetone would give a density difference of 98 kg/m^3 while using the salt solution would give a density difference of 1150 kg/m^3. The ratio of $\Delta\rho/\rho$ could thus be changed over a wide range compared to what has been reported in the literature for drawdown experiments. The viscosity of liquids varies over a wide range. However, it is

possible to change the density difference significantly while keeping the viscosity nearly the same. For example, the use of water and kerosene allow a change in difference from 178 kg/m^3 to 320 kg/m^3 while maintaining the viscosity almost identical. Similarly, the use of $ZnCl_2$ solution and glycerol-water solution in the volumetric ratio of 2:1 allows a change in density difference from 496 to 1150 kg/m^3 while making only a small change in dynamic viscosity.

Table 3.1 Properties of solids and fluids employed in this study

No.	**Medium**	**Density, kg/m^3**	**Viscosity at 25°C , cP**	$\frac{\Delta\rho}{\rho}$
1	Acetone	778	0.30	0.13
2	Kerosene	858	0.96	0.21
3	Water	1000	1.00	0.32
4	Glycerol: water$(1:1)_{vol}$	1109	7.86	0.39
5	Glycerol: water$(2:1)_{vol}$	1174	18.8	0.42
6	$ZnCl_2$-salt solution	1830	16.5	0.63
	Solid particles	**Density, kg/m^3**	**Size, μm**	
1	Cenosphere	680	100, 230 and 325	

3.2.2 Experimental setup

The stirred vessel used for the dispersion study is geometrically identical to the metal contactor used for the molten salt extraction in pyrochemical reprocessing [86]. It was made of borosilicate glass vessel of 83 mm ID (D_T) having four vertical baffles and is shown schematically in Figure 3.1. The baffles had a width, J, of 8 mm and extended well above the liquid height in the vessel. The operating volume for the trials was 460 ml and the depth of the liquid was equal to the vessel diameter, i.e., $H = D_T$. A wide variety of stirrers [41, 80, 81, 87] such as radial, axial, mixed, anchor type helical ribbon and helical screw are used for mixing operation in industrial application. Among these, the stirrers used for the experiments were paddle type with radial and axial blades (blade angle= 45°) with upward flow and downward

flow directions which are normally used for less viscous media. The four-bladed impellers had a diameter, D_a, of 40 mm and a blade height, W, and length, L, of 8 and 12 mm each. The ratio of impeller diameter to vessel diameter, D_a/D_T, was close to 0.5. A straight bladed radial impeller and twisted blades with 45^o angle as axially up or axially down impellers were used in the study. The drive used for the stirrer is a permanent magnet direct current motor made by M/s. Remi Laboratory Instruments. It has a speed control of ±5 rpm and is capable of clockwise and anticlockwise rotations. A high speed camera was used to capture the images of dispersion in all experiments.

In the experiments, the height of the liquid in the stirred vessel was maintained as 83 mm (D_T/H =1) and the corresponding liquid volume was 460 ml. 5 wt % of cenospheres were added to the liquid in all the cases except in the $ZnCl_2$ salt solution where 2 wt % was maintained. In the $ZnCl_2$ solution, the density of the fluid was very high and correspondingly 5 wt% of solid particles would occupy a large portion of the liquid volume. In order to maintain the height of the floating solids roughly the same in all experiments, 2 wt% of solids particles were used in this case. The impeller submergence from the top free surface, S, was one of the variables investigated by conducting experiments with the impeller located at depths of 20, 40 and 60 mm, which are equivalent to s/D_a = 0.5, 1.0 and 1.5, respectively. The temperature of the liquid was maintained at 300 ±1 K during the experiment.

A number of experiments were conducted with the liquid, the impeller height, the type of impeller and the particle diameters as the main variables. The distinguishing feature of the present experiments is the wide range of the density difference between the continuous phase and the dispersed phase. With a proper choice of the continuous medium, the parameter $\Delta\rho/\rho$ could be varied between 0.13 and 0.63; in the literature, experimental data have been reported

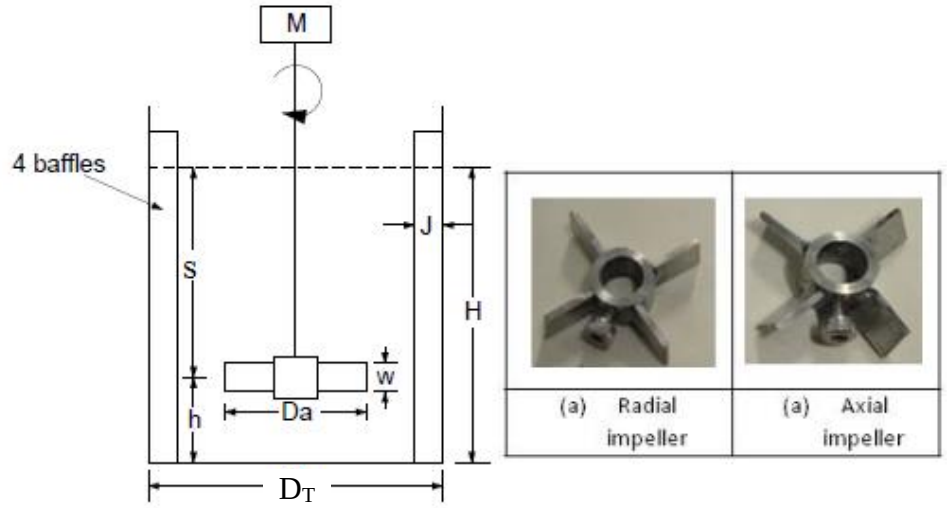

Fig. 3.1 Schematic of the stirred vessel, a) radial impeller, b) axial impeller

Table 3.2 Experimental setup dimensions

Parameter	Shape ratio
Vessel diameter, D_T	83 mm
Impeller diameter, D_a	$D_a/D_T=1/2$
Liquid depth, H	$H/D_T=1$
Impeller submergence, s	$s/D_T=0.25,0.5,0.75$
Blade height, W	$W/D_a=1/5$
Baffle width , J	$J/D_T=1/10$

for $\Delta\rho/\rho$ of only up to 0.2 and is thus far from the value of 0.80 in molten salt extraction application. High $\Delta\rho/\rho$ results in high buoyancy force which leads to stratification of the phases, hence higher impeller speeds and more turbulence are required to overcome the terminal settling velocity of the dispersed phase. The consolidated set of fluid/ solid data used to generate the present experimental data is summarized in Table 3.1. It can be seen that apart from density difference, difference in viscosity, particle size, height of the impeller from the surface and particle size could be changed significantly and independently. For each

experimental condition, experiments were conducted thrice, and the average value is taken as the critical impeller speed for that set of conditions. Results from these experiments are discussed below.

3.2.3 Drawdown criteria

In literature, different criteria have been used to mark the dispersion of solid liquid systems. (1) In one criterion, no solid particles should stay on the free surface for more than a specified time (e.g. few seconds). (2) In another criterion, there should not be any large volume of liquid (especially at the bottom) without solid particles, i.e. homogenous distribution of solid particles throughout the continuous medium. In our case, the goal is to mix the two phases to a sufficiently large extent so that the reductive extraction can occur efficiently. Therefore, it was deemed that homogenous distribution was suitable criterion to mark complete dispersion. In all the experimental results reported here, the minimum impeller speed for the complete dispersion was recorded when the entire liquid zone exhibited nearly uniform distribution of the microspheres which was clearly marked by uniform obscuration of the liquid.

3.3 Results and Discussion

The experimental results on drawdown experiments were analyzed for the minimum agitator speed required for the uniform distribution of solid particles throughout the continuous medium. The various stages of dispersion of microspheres in two different liquid media are shown in Fig 3.2. Fig 3.2a shows the photograph of the setup, with water as the medium, at three stages of dispersion. The figure on the left shows that at low impeller speeds, the lighter-than-liquid particles stayed at the top. A discernible boundary separating the particles and the fluid is seen near the top surface, and the impeller is clearly visible. As the impeller speed was increased in small steps, the stratified layer as a whole oscillated but still stayed stratified. At even higher speeds, some particle entrainment was observed from the stratified layer,

especially near the baffles. At even higher speeds, there was higher entrainment of particles but these stayed mostly in the region above the impeller. In the region below the impeller, the liquid medium remained transparent (or translucent as the case may be) and was mostly free of particles. This is shown in the middle photograph of fig. 3.2a. Here also, it is seen that a moderate level of transparency is present in the continuous medium, indicating that the particles are not fully dispersed. At the critical impeller speed, particles were spread throughout the liquid volume, both above and below the impeller, and the fluid medium turned opaque, as shown in the right side picture in fig. 3.2a. At this point, there was a significant loss of transparency in the liquid all over the vessel and only a few particles remained on the top near the baffles. Fig.3.2b shows the corresponding results in aqueous $ZnCl_2$ medium. Due to the color of the solution, the agitator blades are not visible even under unstirred conditions (left most image in fig. 3.2b). However, upon increasing the agitator speed, drawdown begins, and the color changes due to the presence of particles, as shown in the middle image of fig.3.2.b. A comparison of these images shows that the dispersion is not homogenous at this level. At the critical speed, (shown in the right most image of fig. 3.2b), the dispersion is more or less homogeneous and the speed is recorded. The measured critical speeds under various conditions are presented in Table 3.3. The effect of this critical impeller speed on the parameters investigated is summarized below.

3.3.1 Effect of parameters

3.3.1.1 Effect of liquid medium: The properties of the liquid that are of interest in particle suspension are the density and the viscosity. Of the two, the effect of density is found to be much stronger. At high liquid densities, the buoyancy force on the particle increases significantly leading to stratification. The impeller speed had to be increased to a high value to create a sufficiently high inertial force to counter this. This is reflected in the data shown in Fig 3.3

Fig. 3.2 Stages of solid-liquid dispersion, 230 micron cenosphere in liquid medium of (a)water and (b) $ZnCl_2$ solution; radial impeller, impeller submergence S/D_a =1.0, images (from left to right) nil dispersion, just drawdown and uniform dispersion.

where the critical impeller speed is plotted against $\Delta\rho/\rho$ for 230 μm particles for a dimensionless depth of immersion, s/D_a, of 1.0. The relationship between N_{crit} on $\Delta\rho/\rho$ is not linear and further analysis (section 3.4.1) shows that a power law is better suited to describe the relationship. The effect of viscosity is not clear from these data. Examining the data given in Table 3.3, one can see that effect is not monotonic. For lightly viscous fluids such as acetone and water, circulation induced by the impeller spreads all over the vessel without significant damping [82] In such cases, the effect of viscosity on N_{crit} is rather small. For highly viscous fluids, the action of the impeller is confined to the near-impeller region [88] and significant damping of the flow occurs away from the impeller. In such a case, increase in viscosity can be expected to increase N_{crit}. This can be seen in the case of data from glycerol/water solutions of 1:1 and 2:1 volume ratios. The effect of viscosity may also be seen in the case of submergence. For low submergence, i.e., when the impeller is close to the top surface where

the particles collect in a stratified layer, the effect of viscosity is not significant; for higher submergence ratios and for axially upward flow (where the flow pattern is different, as shown in Fig 3.3), increasing viscosity leads to increased N_{crit}.

Comparing the data from $ZnCl_2$ solution and glycerol/water (2:1) solution, one can see that while both liquids have nearly the same viscosity, the higher density difference in the former leads to high N_{crit} in all cases. The relatively small influence of viscosity is also evident in the Zwietering correlation[59] where it implies a weak dependence of the form $N_{crit} \sim \mu^{0.1}$.

3.3.1.2 Effect of impeller type: The effect of impeller type is somewhat contrary to expectation in that one might have expected a lower N_{crit} for axial upward impeller. The data show that of the three types investigated, the radial impeller has the lowest N_{crit} for the same conditions while the axial upward and axial downward have similar values of N_{crit} and they do not exhibit a consistent trend. The first result is understandable as a radial impeller is known to dissipate higher turbulent kinetic energy than either the upward or downward impellers [89]. This is consistent with the higher power requirement for a radial impeller for the same rotational speed. One may expect that upward pitched blade will have lower N_{crit} compared to downward pitched blade due to the flow patterns, especially when impeller submergence is high. CFD simulations of these impellers [88] show that in the case of axially downward flow, a large and strong wall-jet type of flow is created in the vessel (Fig 3.4) which extends all the way into the bottom half. In the case of axial up flow impeller, two circulation loops are created; these are in opposite direction and the wall-jet flow from the top is arrested at mid-height and is reversed. In addition, the fluid velocity in the upper loop is less than in the case of the axial down flow impeller. However, the results do not show any clear and consistent difference between upward and downward flow impellers.

Table 3.3: Measured Critical impeller speed, N_{crit} (rpm) at which solid particles dispersed uniformly throughout the medium for radial and axial impellers at impeller location s/D_a =0.5, 1.0, 1.5.

Continuous medium	Radial			Axial downward			Axial upward		
	s/D_a			s/D_a			s/D_a		
	0.5	1	1.5	0.5	1	1.5	0.5	1	1.5
	N_{crit}, rpm (avg, max,min)			N_{crit}, rpm(avg, max,min)			N_{crit}, rpm(avg, max,min)		
100 micron particles									
Acetone	133 +9/-5	149 +8/-6	203 +7/-5	173 +8/-6	189 +7/-5	220 +7/-5	151 +6/-5	189 +7/-4	220 + 7/-4
Water	240 +7/-6	253 +5/-4	300 +9/-6	230 +7/-3	300 + 8/-6	364 +8/-6	204 +7/-5	270 +8/-5	343 +6/-6
Gly: Water (1:1)	211 +8/-6	270 +7/-5	344 +9/-7	268 + 7/-5	365 +9/-5	495 +8/-6	255 +6/-4	367 +8/-6	414 + 9/-7
$ZnCl_2$ soln. (65wt %)	267 +9/-5	297 +10/-7	384 +11/-8	304 + 9/-7	439 +10/-7	557 +11/-7	335 +9/-7	458 +9/-5	521 +8/-5
230 micron particles									
Acetone	120 +8/-6	122 +4/-7	165 +6/-4	146 +7/-6	161 +12/-9	195 +13/-12	149 +8/-7	162 +6/-7	194 +9/-7
Kerosene	156 +5/-4	163 +6/-5	193 + 6/-7	173 +4/-6	200 +8/-6	253 + 7/-4	200 + 7/-6	216 + 8/-4	256 + 9/-6
Water	186 +4/-6	215 +6/-7	270 + 6/-8	223 + 7/-9	245 +13/-10	325 + 9/-8	218 +5/-6	272 +14/-11	320 + 8/-6
Gly: Water (1:1)	231 + 12/-8	282 +14/-8	330 +10/-7	252 +7/-6	352 +6/-4	477 +5/-5	249 +4/-3	342 +7/-5	429 +8/-5
Gly: Water (2:1)	256 +7/-4	316 +6/-4	382 +4/-3	310 +12/-7	400 +5/-2	610 +12/-7	327 +6/-4	420 +7/-3	572 +8/-4
$ZnCl_2$ soln. (65wt %)	272 +9/-5	343 +12/-8	425 +7/-4	293 +9/-6	423 +7/-5	631 +11/-7	362 +9/-5	457 +7/-4	600 +14/-9
325 micron particles									
Acetone	107 +6/-4	113 +5/-4	160 +6/-4	133 +5/-4	146 +6/-4	158 +5/-4	149 +6/-4	153 +7/-5	173 +6/-4
Water	172 +6/-5	250 +7/-5	320 +9/-7	261 +7/-5	300 +7/-4	377 + 8/-6	191 +5/-6	310 +6/-7	380 +9/-6
Gly: Water (1:1)	224 +7/-4	293 +9/-6	426 +11/-7	327 +8/-5	399 +8/-5	540 +11/-7	323 +7/-5	396 +8/-5	457 +8/-5
$ZnCl_2$ soln. (65wt %)	312 +6/-4	392 +8/-5	521 +9/-6	342 +7/-6	479 +7/-6	723 +13/-10	369 +8/-6	506 +9/-7	700 +11/-8

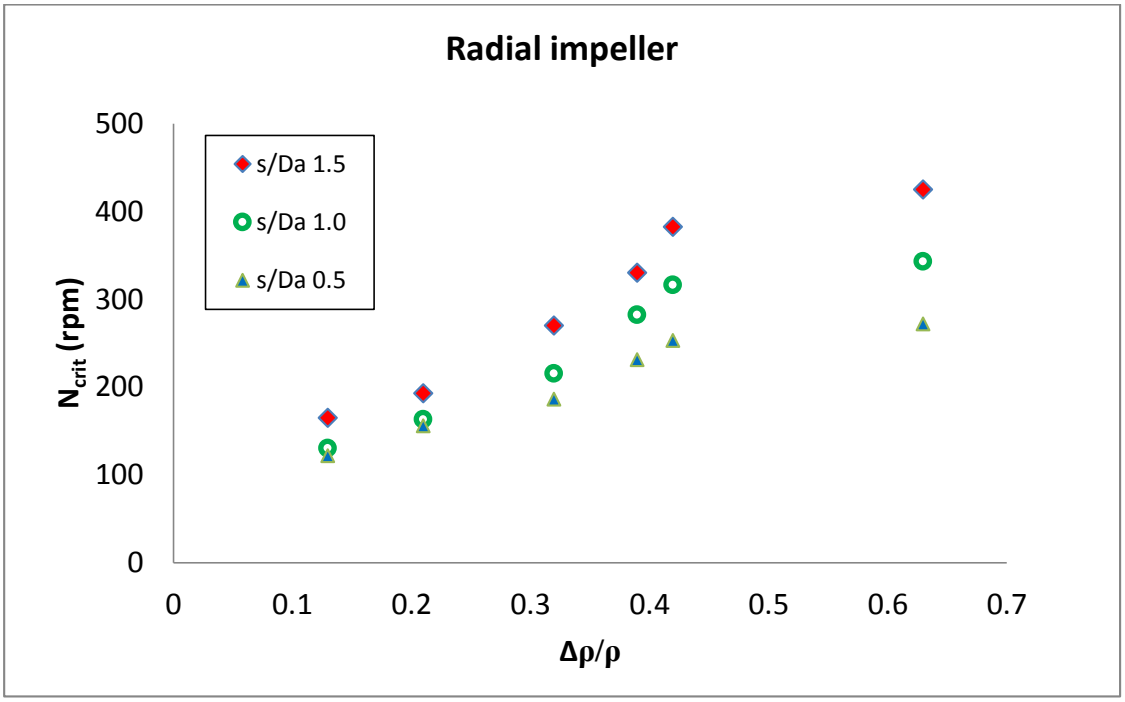

a)

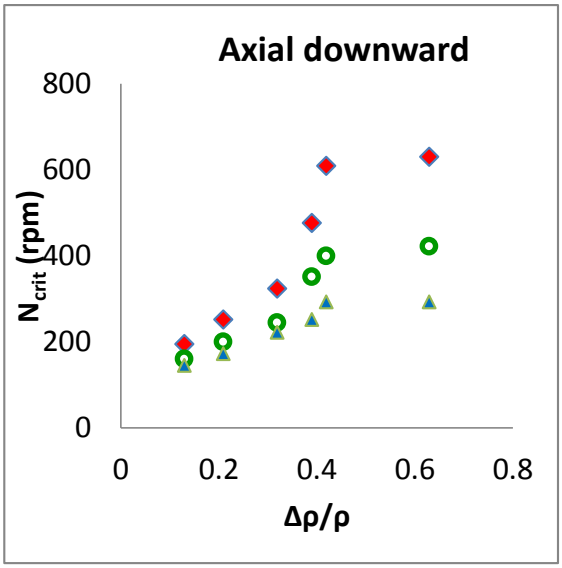

b)

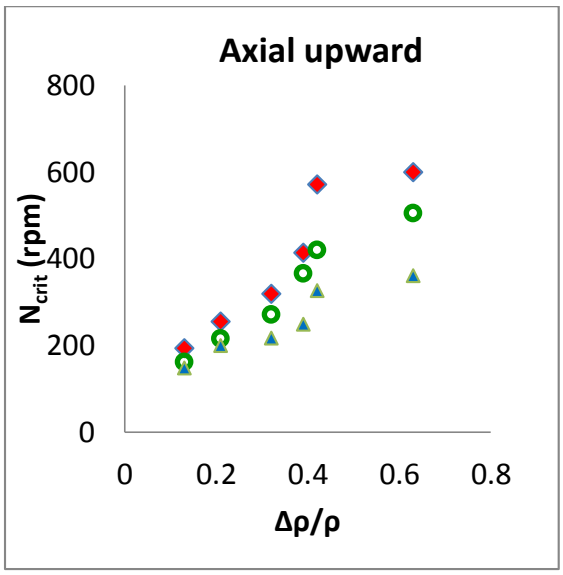

c)

Fig. 3.3 N_{crit} *vs.* $\Delta\rho/\rho$ for (a) radial (b) axial downward and (c) axial upward impeller at impeller submergence, S/D_a =0.5, 1.0 and 1.5

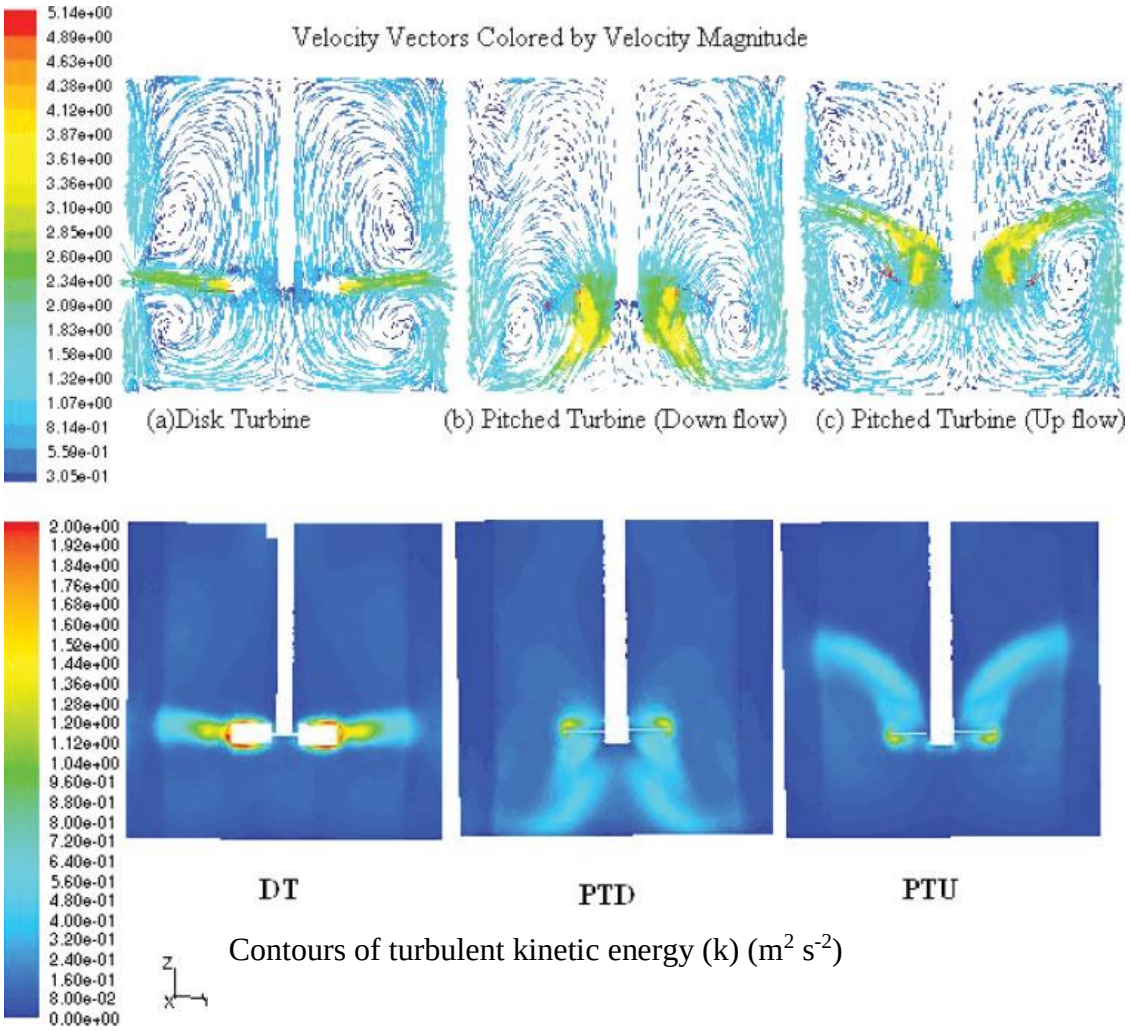

Contours of turbulent kinetic energy (k) ($m^2\ s^{-2}$)

Fig. 3.4 Fluid flow pattern in radial and axial type impellers [88]

3.3.1.3. *Effect of particle size:* The effect of particle size on the critical impeller speed is significantly different for low buoyancy and high buoyancy liquids. The principal forces acting on the particle are the buoyancy force and drag force. For a given impeller speed and liquid, the buoyancy force scales as $g\Delta\rho D_p^3$ while the drag force on the particle scales as $\rho C_d U^2 D_p^2$. Thus, for the same liquid-solid combination, increasing size leads to a higher rate of increase of buoyancy force than drag force. In low buoyancy conditions such water (or acetone)-cenosphere conditions, N_{crit} is determined primarily by drag force and N_{crit} therefore decreases as D increases. For high buoyancy force flow such as with glycerol/cenosphere or $ZnCl_2$ solution/cenosphere combinations, increasing D increases N_{crit} as this leads to relatively higher buoyancy force.

3.3.1.4 *Effect of submergence (s/D_a):* For the dispersion of particles, the fluid velocity must be higher than the terminal settling velocity of the particles. CFD predictions of [81, 82] fluid velocities in radial, axial and circumferential directions are related to impeller tip velocity (u/u_{tip}) at different planes show that the fluid velocity is reduced with distance from impeller. Thus, for solid suspension, the fluid velocity near the upper surface is important. Since this decreases with increasing submergence, one finds that the critical impeller speed increases monotonically with submergence as shown in Fig 3.5 for different fluid combinations. When the impeller position was nearer to the top interface, dispersion was observed at lower stirrer speeds. A similar effect of impeller submergence was reported in earlier studies of [65, 68, 71].

3.4 Correlation of Data and Prediction of N_{crit}

3.4.1 Correlations from cold flow dispersion studies

Since the data are showing a consistent trend, a correlation is sought for determining the critical impeller speed as a function of the relevant parameters. Several non-dimensional groupings relevant to the flow situation can be readily identified; these are summarized in Table 3.4. The fluid Reynolds number (Re) is a parameter which would characterize the fluid velocity field for a given impeller speed in a geometrically similar stirrer set-up. Archimedes number (Ar) based on the particle size, particle density and the fluid properties, is often used in particle dispersion correlations. Three additional parameters, namely, two phase Froude number (ratio of inertial force to gravity force), the density difference relative to the fluid density ($\frac{\Delta\rho}{\rho}$), and the submergence depth relative to the diameter of the impeller(s/D_a), are found to be relevant as per the discussion given in Section 3.1. Since particle dispersion is a sub-surface phenomenon, the surface tension of the liquid is assumed to be of negligible importance and is not included in the correlation. Since the critical impeller speed is of interest, a correlation of the data in the following form is sought:

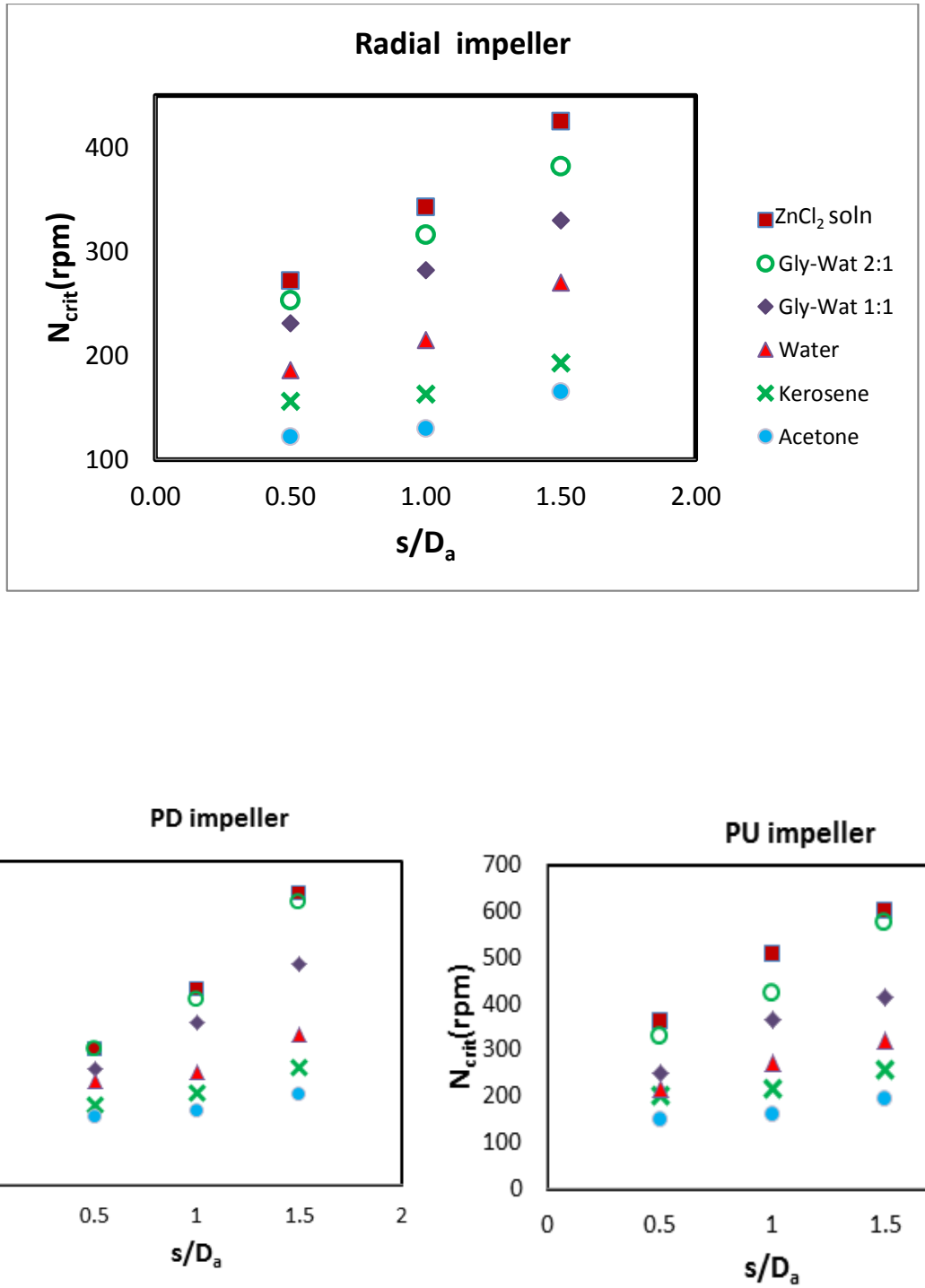

Fig. 3.5 Effect of impeller submergence on N_{crit} for water, $ZnCl_2$ soln., Glycerol-water 1:1 and 2:1 solution, Acetone and Kerosene, with 230 micro particles for Radial impeller, Axial downward impeller and Axial upward impeller.

$$Fr = C' \, Ar^{\alpha} \left(\frac{\Delta\rho}{\rho}\right)^{\beta} \left(\frac{d_p}{D_a}\right)^{\gamma} \left(\frac{s}{D_a}\right)^{\delta} \quad (3.1)$$

Since the nature of the impeller (radial or pitched blade) has an important effect on the induced flow field, the data for each of the impellers is correlated separately. The constants and the exponents of the dimensionless group are derived by data analysis of the experimental results and the values were given in the Table-3.5.

Table 3.4 Non-dimensional group used for correlation

Dimensionless group	Min value	Max value
Reynolds number ,Re= $\frac{D_a{}^2 N\rho}{\mu}$	420	15200
Archimedes number, Ar = $\frac{g\, D_p{}^3 \rho\, \Delta\rho}{\mu^2}$	0.11	285
Froude number, Fr=$\frac{\rho N^2 D_a^2}{g\Delta\rho D_p}$	12.67	250
Density difference,$\frac{\Delta\rho}{\rho}$	0.13	0.63
Impeller immersion depth, s/D_a	0.5	1.5

The values of exponents are in the range of α = - 0.04 to - 0.10, β - 0.056 to 0.068, γ = - 0.62 to - 0.92 and δ = 0.72 to 0.85. The values of C´,α, β, γ and δ obtained for each case are listed in Table 3.5. A nearly equally good correlation was obtained for the data from all impellers in the form:

$$Fr = C_i' \, Ar^{-0.11} \left(\frac{\Delta\rho}{\rho}\right)^{-0.08} \left(\frac{d_p}{D_a}\right)^{-0.65} \left(\frac{s}{D_a}\right)^{0.72} \quad (3.2)$$

The constant C_i' is impeller dependent and has the values of 1.50, 2.45 and 2.30 for radial, pitched down and pitched up impellers respectively. This indicates that the critical impeller speed, which is proportional to $\sqrt{Fr}$, is 28 and 24 % higher for pitched down and pitched up impellers compared to a radial impeller.

Table 3.5 Exponents' values in correlation given in equation (3.1)

Type of impeller	C'	α	β	γ	δ	R^2 value
Radial	0.39	-0.04	0.0679	-0.92	0.72	0.9693
Axial downward	1.36	-0.09	0.0032	-0.77	0.85	0.9528
Axial upward	2.83	-0.10	-0.0561	-0.62	0.81	0.9599

The performance of the above correlation is summarized in figure 3.6 which shows a parity plot between the predicted and the measured critical impeller. The prediction is good with most of the points lying within ± 20% deviation, the overall standard deviation being 11.6%. The comparison of predicted N_{crit} with that of experimental values unified correlation (3.2) for all impellers was shown in the Fig 3.6. The influence of major variables on N_{crit} can be obtained by rewriting equation (3.2) in the following form

$$N_{crit} = C' D_a^{a1} (\Delta\rho)^{a2} \rho^{a3} s^{a4} D_p^{a5} \mu^{a6} \quad (3.3)$$

Substituting the values of the exponents from equation (3.2),

$$N_{crit} \sim D_a^{-1.04} (\Delta\rho)^{0.41} \rho^{-0.51} s^{0.36} D_p^{0.01} \mu^{0.11} \quad (3.4)$$

The above relation (for radial impeller) indicates that impeller diameter is playing important role in N_{crit} for the drawdown of floating solids [90]. Density difference between the two phases and impeller submergence [69, 70, 91] are showing significant effect whereas particle diameter and liquid viscosity [59] having week effect on dispersion. The impeller tip speed is $U_{tip} = N \times D$ and the impeller speed is related to impeller diameter as $N \sim D^{-1}$. The equation (3.4) can be interpreted as

$$U_{tip,\ crit} \sim (\Delta\rho)^{0.41} \rho^{-0.51} s^{0.36} D_p^{0.01} \mu^{0.11} \quad (3.5)$$

The above relation showing strong influence of density difference and submergence on the impeller tip speed for drawdown of floating particles.

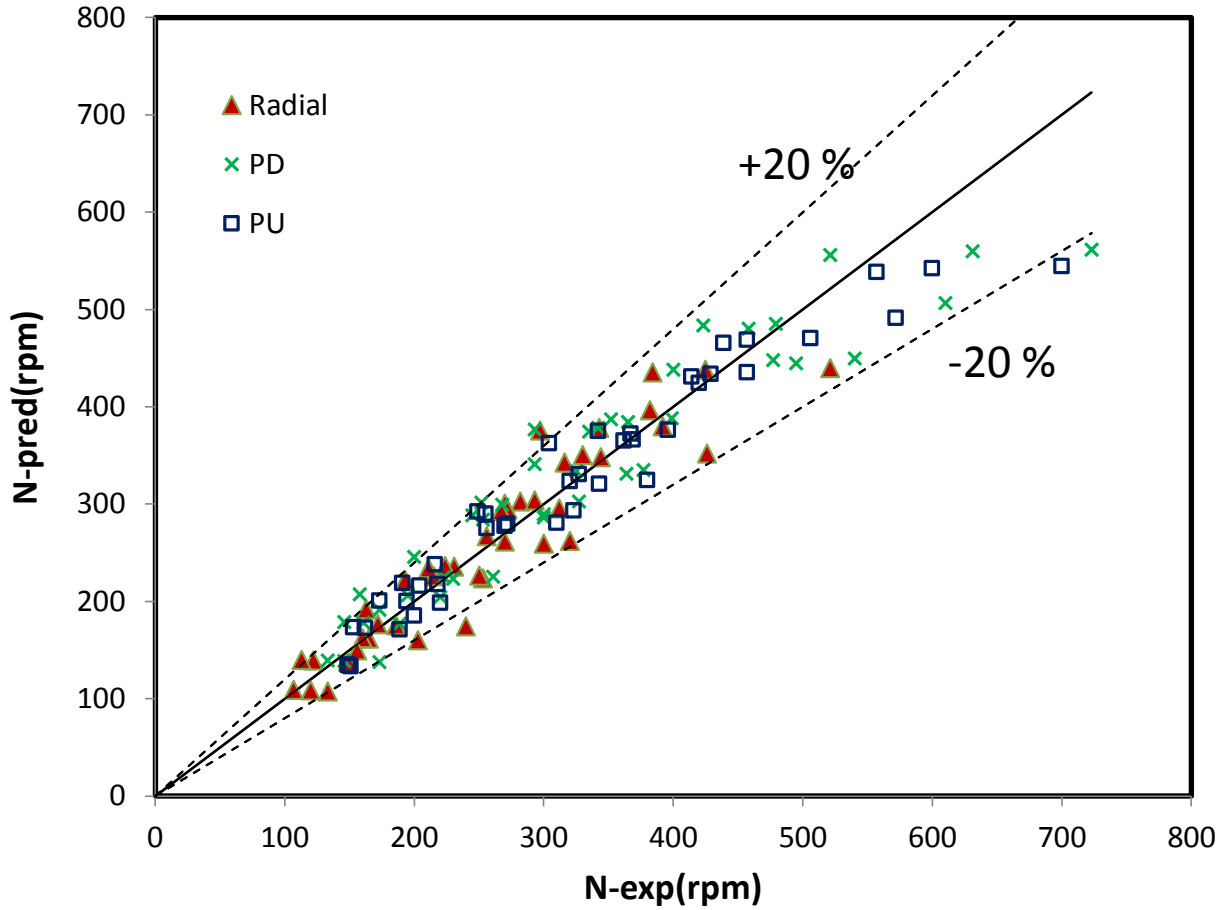

Fig. 3.6 Parity chart N_{crit} vs. actual impeller speed using correlation 3.2 for radial, PD and PU impellers with ±20 % deviation lines.

3.4.2 Prediction of N_{crit} for eutectic salt/cadmium alloy dispersion

The correlation was used to predict the N_{crit} required for the dispersion of molten salt-cadmium alloy system. The predicted N_{crit} using correlation (3.2), (radial impeller, D_a=40 mm, ρ_s = 1600 kg/m^3, ρ_l = 8000 kg/m^3, μ_l =0.0018 kg /m-s for droplet size 100, 230 and 325 μm) for molten salt dispersion in cadmium alloy was shown in Table 3.6.

In case of molten salt extraction with radial impeller and position near interface N_{crit} required for the dispersion of droplets are in the range of 214 to 412 rpm depending upon the droplet size. The above prediction indicates that with 40 mm diameter radial impeller and impeller position near the interface around 300 rpm stirrer speed is sufficient for the dispersion of molten salt phase in to cadmium alloy phase. This study is useful for the

Table 3.6 N_{min} predicted for molten salt system

s/D_a	D_p(micron)	Radial impeller	PD impeller	PU impeller
0.5	100	214	274	266
	230	216	276	268
	325	217	277	269
1	100	275	352	341
	230	278	355	344
	325	279	356	345
1.5	100	319	408	395
	230	322	411	398
	325	323	412	400

selection of suitable stirred vessel for liquid- liquid extraction in pyrochemical reprocessing application.

3.5 Effect of Multiple Impellers on N_{crit}

When the liquid level is high (H/T > 1.25), multiple impellers are preferred. High liquid levels may be seen in solvent extraction, fermentation and gas-liquid operations. The recommended number of impellers for a turbine agitator is given by the relationship [92]

$$\text{Number of turbines} = \frac{\text{WELH}}{\text{T}} \tag{3.6}$$

where WELH is the water equivalent liquid height and T is the tank diameter. WELH is the product of the liquid height and the average specific gravity of the contents of the vessel. In our case (molten salt extraction), the molten salt (ρ=1600 kg/m^3) and cadmium alloy phase (ρ = 8000 kg/m^3) in 1:1 volume ratio were dispersed. The liquid height in the contactor was 100 mm, of which 50 mm was for cadmium alloy phase and 50 mm was for eutectic salt. The tank diameter was 83 mm, the average specific gravity of the liquid contents is 4.8 and the recommended number of impellers is calculated as

$$= \frac{100 \times 4.8}{83} = 5.8 \approx 6$$

However, if 6 impellers were used, the distance between two adjacent impellers would be too small. Generally, the distance between adjacent impellers must be at least equal to the impeller diameter. Using that criterion, in our case, only two impellers can be used at the most. Considering the stratification tendency of our system, due to the large density difference between the phases and the large interfacial tension, we have used three impellers with a distance of 20 mm (= half the impeller diameter) between the impellers.

Drawdown of floating particles was tried with three impellers in the agitator shaft. The top and bottom impellers were of axial type, while the middle impeller was of radial type. Two combinations (PD-radial-PD, and PU-radial-PU) were studied. The position of the top, middle and bottom impellers were maintained at s/D_a =0.5, 1.0 and 1.5 respectively. The submergence was kept invariant. The critical impeller speed (N_{crit}) values were measured and are presented in the Table 3.7.

Table 3.7 Effect of multiple impellers on N_{crit}
(Average, maximum and minimum values for solid- 5 wt %, 230 micron particles)

Liquid medium	Single-stage, radial at s/D_a=1.0	3-stage (PU-radial-PU)	3-stage (PD-radial-PD)
Water	215 +6/-7	158 +8/-4	156 +7/-4
Glycerol-water(1:1)	282 +14/-8	180 +9/-6	190 +6/-4
Glycerol-water(2:1)	316 +6/-4	187 +7/-4	206 +13/-7
$ZnCl_2$ soln.	343 +12/-8	211 +8/-6	226 +11/-8

The results show that complete dispersion can be achieved at a lower speed in a three stage impeller compared to the speed needed in a single stage impeller. A comparison of PD-radial-PD and PU-radial-PU results show that there is no significant difference in the performance of the two types of three stage impellers for the case of water. For the more difficult to disperse cases N_{crit} for the PD-radial-PD is about 10% higher than the PD-radial-

PD impellers. The results can be explained as follows. In case of a three stage impeller, the flow pattern created by the top impeller facilitates drawdown of the particles, while the middle and bottom impellers help with dispersion of the particles throughout the continuous medium. In case of single stage impeller, a higher speed is needed to generate the flow pattern needed to drawdown and simultaneously maintain the dispersion uniformly throughout the continuous medium.

3.5 Summary

Solid –liquid dispersion studies were carried out with low density cenosphere of size few hundred microns in different liquid medium. Density difference between the solid and liquid was in the range of 100 to 1150 kg/m^3. Minimum impeller speed required for the uniform dispersion of particle throughout the liquid phase was estimated. Results indicated that stirrer speed is minimum for radial impeller followed by axial downward flow and axial upward flow impeller. Stirrer speed N_{crit} is lowest when impeller position was near to the interface. Correlation was proposed in the form of dimensionless number for predicting minimum stirrer speed required for dispersion. The effect of viscous force is not significant in all type of impellers and impeller position. Impeller diameter is playing significant role in all cases. Effect of multiple impellers was studied using 3-stage impeller and significant reduction in impeller speed for dispersion was observed.

CHAPTER 4
EXPERIMENTAL STUDY OF DRAWDOWN PROCESS FOR RECOVERY OF ACTINIDE FROM MOLTEN SALT

4.1 Introduction

The actinide drawdown process, as pointed out earlier in Chapter 1, is aimed at the recovery of valuable actinides from the spent electrolyte LiCl-KCl salt which is obtained from the electro refining process. This mixture contains alkali, alkaline earth and rare earth fission products in the form of chlorides. The challenge here is to achieve >99% recovery of the actinides, and at the same time, to minimize the co-extraction of the rare earth fission products. One way of achieving this is by using reductive extraction using molten cadmium– lithium alloy at 773 K. In this work, an experimental facility was installed inside an argon atmosphere glove box, for carrying out studies on the actinide drawdown process. The experimental facility and the results of the extraction studies are presented and discussed in this chapter.

4.2 Experimental

4.2.1 Facility

A schematic diagram of the experimental set up used in this study is shown in Fig. 4.1. A photograph of the setup without heaters is shown in Fig. 4.2. This set up comprises of four tanks, viz. a salt feed tank, a salt collection tank, a cadmium feed tank and a cadmium collection tank, each of 10 L capacity. The salt tanks are made of AISI 304L, while the cadmium tanks are made of AISI 430. Austenitic stainless steels (such as AISI 304L) usually contain significant fraction of nickel (8 to 10 wt %) and cadmium, if stored in these tanks, will form an alloy [93]. On the other hand, ferritic stainless steels type AISI 430 does not contain nickel (< 0.75 %) and is suitable for storing Cd alloy phase.

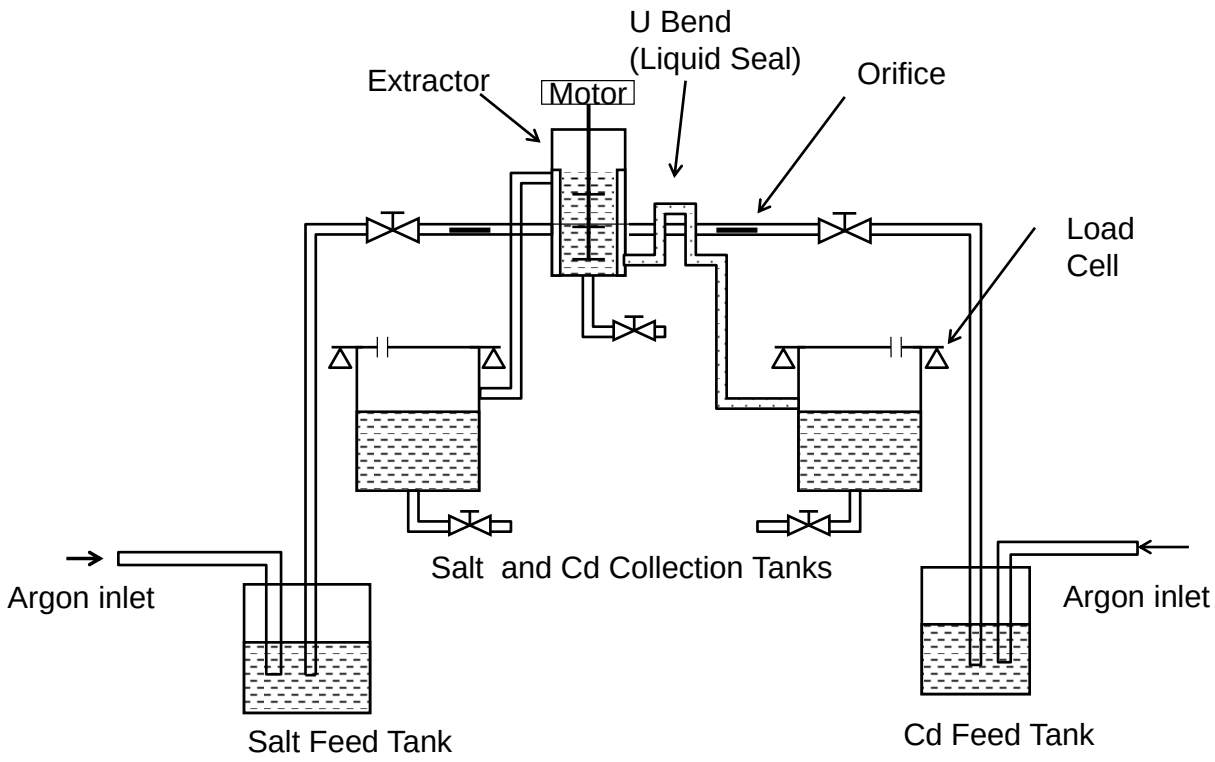

Fig. 4.1 Process flow diagram of actinide drawdown Process

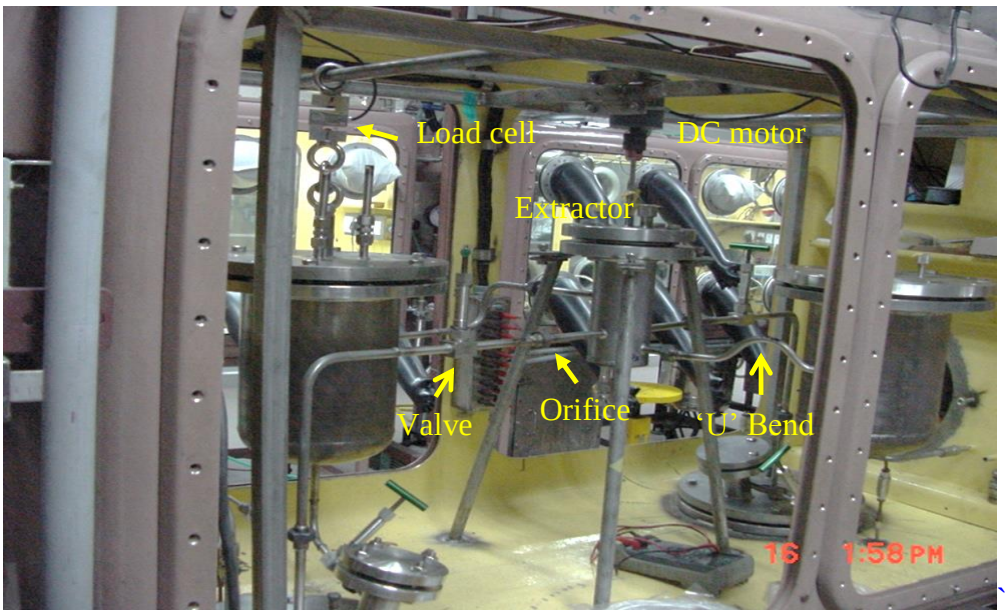

Fig. 4.2 Photograph of the extraction system, without heaters

A 1 L capacity single stage extractor, also made of AISI 430, is provided in the set up where 250 mL each of molten salt and alloy is brought into contact with each other. The design basis for the extractor volume is to maintain the residence time (5- 10 min) of salt and cadmium phases required for the reductive extraction. The design flow rate of the feed and solvent phases is 25 ml/min each. This is equivalent to treating the eutectic spent electrolyte salt at the rate of 2.4 kg/hr. This throughput is sufficient to handle and recycle the spent electrolyte salt from the batch electrorefiner in pyroreprocessing. Since pressure transfer is adopted for the transfer of molten salt and cadmium alloy from their respective feed tanks, these tanks are designed to operate at a pressure of 2 bar and at a temperature up to 773 K. The salt tanks with AISI 304L were made with standard 8" schedule 10 pipe with wall thickness 3.76 mm whereas the cadmium tanks were fabricated using AISI 430 sheet with thickness 3 mm. The pressure vessel design calculation was done using the ASTM codes and the details are given below.

Circumferential Stress$= \frac{S \times E \times t}{(R+0.6t)}$

Longitudinal stress$= \frac{2S \times E \times t}{(R-0.4t)}$

Stress at the tori-spherical dished end $= \frac{2S \times E \times t}{(R_C\, M+0.1)}$

where S is the maximum allowable stress, E is the welding efficiency, t is the wall thickness, R is the inner radius, R_c is the radius of dished end curvature and M is the stress intensification factor given by

$M= \frac{1}{4}\left(3+\sqrt{R_C/R_k}\right)$ Here R_k is the knuckle radius of the dished end.

Hydrostatic test pressure $= 1.3\, P_{design}\, \frac{S_{test}}{S_{design}}$

The results are shown in Table 4.1. The tanks were subjected to dye penetration test and hydrostatic pressure test at 5 bar (gauge). The tanks were connected through a ½" AISI 316L tubing and the lines were fitted with high temperature bellow seal valves and

dismountable fittings. The salt and cadmium collection tanks were attached with load cells in order to monitor the rate at which molten salt and cadmium fill up in the respective tanks.

Table 4.1 Pressure vessel design calculation for salt and cadmium feed tank.

(Calculated as per the code ASME-SEC-8, Div-1 and ASME –SEC-2, Part-D [94, 95])

Design Pressure = 2 Bar		
Design temperature = 500^0C		
	Salt tank	Cd tank
Material of construction	SS 304L	SS 430
Max. Allowable stress @ 38ºC,S , N/m^2	9.8×10^7	12.8×10^7
Max. Allowable stress @ 510ºC,S , N/m^2	5.8×10^7	6.3×10^7
Weld efficiency, E	0.75	0.75
Radius- inner, R, mm	105.5	105.5
Thickness, t, mm	3.76	3.00
Circumferential Stress, N/m^2	1.5×10^6	1.33×10^6
Longitudinal stress, N/m^2	3.13×10^6	2.73×10^6
Dished end, N/m^2	7.6×10^5	6.7×10^5
Hydrostatic test pressure, N/m^2	4.4×10^5	5.2×10^5

Four vertical baffles were fitted to the extractor. High energy is required to disperse one phase into another because of the large interfacial tension (450 dyne/cm). To meet this requirement, a stirrer with a 3-stage turbine impeller [96] in which the top and bottom impellers pitched downward and upward respectively at an angle of 45° is provided. The middle impeller is a straight one and is positioned at the interface between the two phases. The stirrer is driven by a DC motor with variable speed control. The level of the interface between the two phases is maintained by hydrostatic balance using a 'U' loop, provided in the outlet line of the dense cadmium phase. The physical properties of the eutectic salt and cadmium are given in Table 4.2 and these were used to design the setup. A schematic of the extractor is shown in Fig. 4.3. The setup was incorporated inside an argon atmosphere glove box. The glove box was maintained at a positive pressure of 20-40 mm WG with respect to the ambient.

Table 4.2 Physical properties of the reagents [97, 98]

Properties of the reagent	Eutectic salt	Cadmium
Density (kg/m^3)	1620	7820
Melting point (°C)	352	321
Viscosity (cP)	1.6	1.8
Heat capacity (J/kg-K)	1160	268
Heat of fusion (kJ/kg)	340	55
Thermal conductivity (W/m-K)	0.42	96
Surface tension (mN/m)	129	620

All the tanks and transfer lines were provided with resistance heaters with ceramic beads and quartz fiber insulation. The heating elements in the heaters were made of thin-wire of Nichrome (80% Ni, 20% Cr alloy). The insulation resistance of the heaters was tested at 5000 V. The earthing for the vessels and transfer lines and Earth Leakage Circuit Breaker (30 mA current operated ELCB) are provided to trip the power supply system in case of any failure in the insulation of the heaters. Thermocouples (K-type) were provided at various locations of the set up the details of which are shown in Fig. 4.4. The tag number of the control and monitoring thermocouples are given in the Table 4.3. Photograph of the line heaters (Fig. 4.5a) and vessel heater (Fig. 4.5b) are also shown. The experimental setup (whose photograph without heaters is shown in Fig. 4.2) including the heaters, is shown in Fig. 4.6. The instrument signals from thermocouples, pressure transmitter and load cell were received through the feed through provided in the glove box and also by using wireless signal transmission as shown in Fig. 4.7.

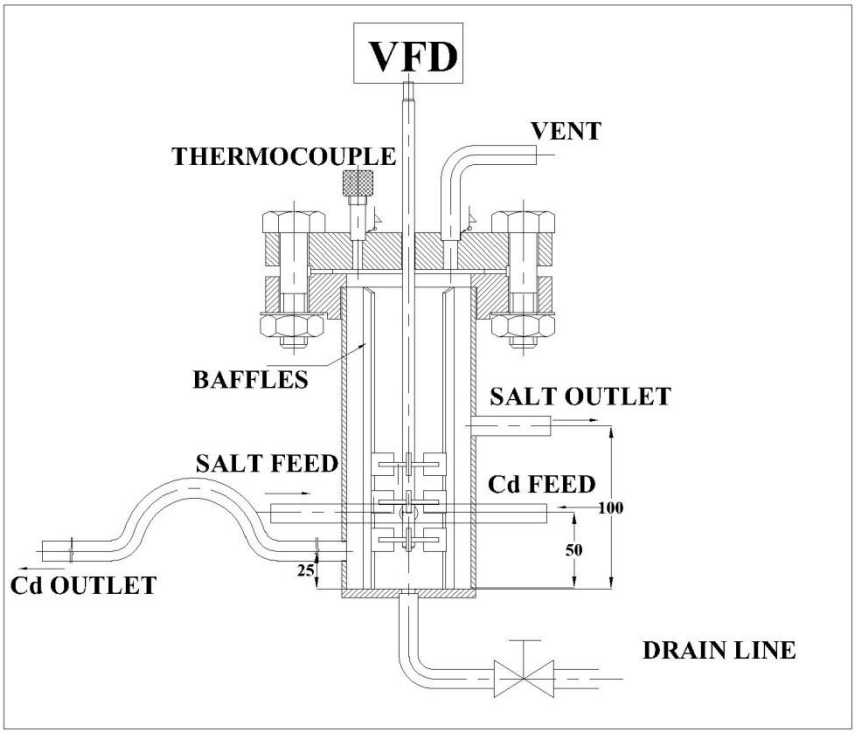

Fig. 4.3 Schematic of the continuous extractor

The temperature of the entire actinide drawdown set up was controlled using PID controller. The power being fed to these heaters was controlled by a multi-channel (8 channel) thyristor based control system. Thyristor units control the voltage feed to the individual heater by controlling the phase angle of the power supply. The tanks and the extractor were controlled by individual controllers whereas the transfer liners were grouped and controlled by three controllers. The temperature of the glove box is monitored by thermistors provided in the bottom of the glove box near the salt and cadmium feed tank. The feed tank top flange was provided with ½" copper coil with cooling water circulation. This prevents the heat transfer from the feed tanks to the glove box. The pressure switch is provided in the cooling water return line to ensure the flow.

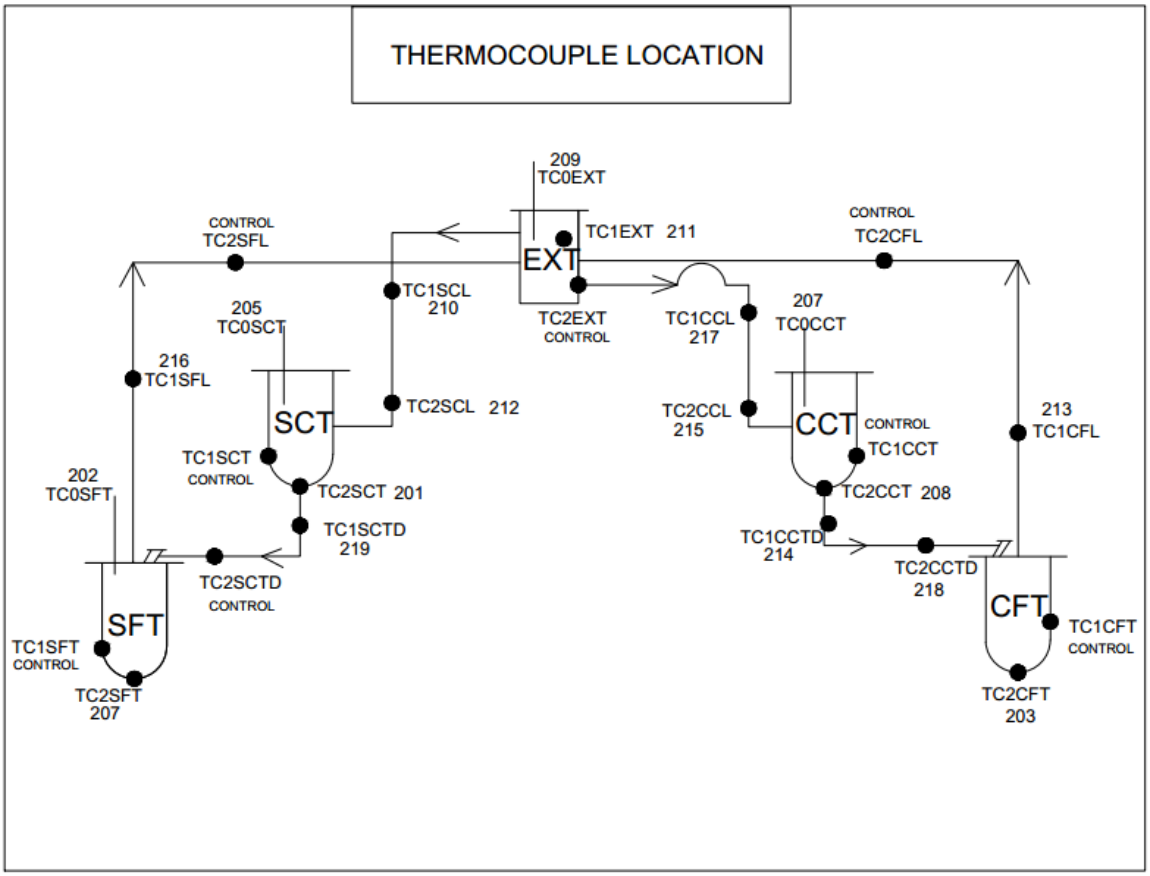

Fig. 4.4 Process flow diagram with thermocouple locations. The locations of thermocouples are marked by large black dots.

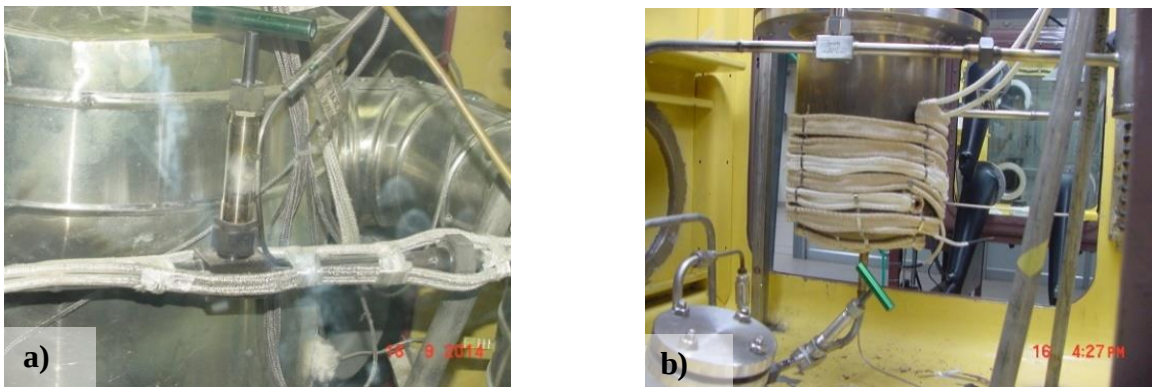

Fig. 4.5 Photograph of (a) Line heater and (b) Vessel (tank) heaters used in the setup.

Table 4.3 Thermocouple tag number and location corresponding to the tags in fig.4.4

Tag no.		location
201	TC2SCT	Bottom of salt collection tank
202	TC0SFT	Inside molten salt in Salt Feed Tank
203	TC2CFT	Bottom of Cadmium feed tank
204	TC1EXTD	Drain line of extractor
205	TC0SCT	Inside molten salt in Salt collection Tank
206	TC0CCT	Inside molten Cadmium in Cd Collection tank
207	TC2SFT	Bottom of salt feed tank
208	TC2CCT	Bottom of Cadmium collection tank
209	TC0EXT	Inside molten salt in extractor
210	TC1SCL	Salt collection line near extractor
211	TC1EXT	Lighter phase in Extractor(top)
212	TC2SCL	Salt collection line near collection tank
213	TC1CFL	Cadmium feed line in vertical transfer line
214	TC1CCTD	Drain line near Cd collection tank
215	TC2CCL	Cd collection line near collection tank
216	TC1SFL	Salt feed line in vertical transfer line
217	TC1CCL	Cd collection line bottom of the inverted U tube
218	TC2CCTD	Drain line near Cadmium feed tank
219	TC1SCTD	Drain line near Salt Collection tank
CH - 1	TC1SFT	Salt feed tank , Outside, On the curved surface of the tank
CH - 2	TC1CFT	Cadmium feed tank , Outside, On the curved surface of the tank
CH - 3	TC1SCT	Salt collection tank , Outside, On the curved surface of the tank
CH - 4	TC1CCT	Cd collection tank , Outside, On the curved surface of the tank
CH - 5	TC2EXT	Extractor, Dense phase in extractor(bottom)
CH - 6	TC2SFL	Salt feed line, In horizontal transfer line, b/n orifice and valve
CH - 7	TC2CFL	Cd feed line, In horizontal transfer line, b/n orifice and valve
CH - 8	TC2SCTD	Salt collection tank drain line, Near salt feed tank

4.2.2 Heater power calculation

Heater power rating of the electrical resistance heaters used in the set up was arrived from the process heat load and the heating period to reach the operating temperature [99]. Process load included the sensible heat of the process materials (eutectic salt/alloy) and stainless steel container, latent heat of fusion of the process materials and heat losses through the insulation. Heating period was conservatively fixed as 1 hour, in actual heating, temperature was raised gradually from ambient to operating temperature over a period of 6 to 8 hr. Tape heaters were used in the vessels whereas cord heaters were used in the transfer lines. The power ratings of the heaters were selected based on the following calculation.

Sensible heat = m. C_p.ΔT (for process materials and container materials)

Latent heat = m. ΔH_f (for process materials only)

The specific heat capacity (C_p) of the materials is given in the Table 4.2. Heat loss per unit area from the insulation surface is calculated from the relation

$$\frac{Q}{A} = h(\Delta T) \tag{4.1}$$

where h is the heat transfer coefficient. For our case, the heat transfer coefficient for heat loss from aluminum surface to ambient is 9.7128 W/m^2/K [100]. Insulation outer surface temperature, T_s was taken as 60 ºC (333 K) and ambient temperature, T_a as 30 ºC (303 K). Using the above relation, insulation surface heat loss was arrived as 300 W/m^2

Heater power rating = heat load / heating period

Heater power was calculated for the process vessels and transfer lines. Heaters resistance value was arrived from the relation, $P = \frac{V^2}{R}$, where V is the applied voltage and R, is the heating element resistance. R value for the resistance heaters were calculated by keeping the applied

voltage as 230V for the required heater power. The heater resistance, R is related to the heating element specific resistance by $R = \rho \frac{l}{A}$, where ρ is the specific resistance of the heating element (~ 1.0×10^{-6} ohm-m), l- length and A – cross sectional area of the heating element[101]. To minimize stocking many different heaters in the inventory, it was decided to use identical heaters for all the storage vessels and a conservative estimate was used for the heat loads. Thus, all storage vessels were provided with 3200 W heaters. The details of the heaters are listed in Table 4.4

Table 4.4 Details of various heaters used in the setup

Location	Type of heater	Heater power (W)	Length (m)	Resistance (Ω)
Salt feed tank (SFT) Salt collection tank (SCT) Cd alloy feed tank (CFT) Cd alloy collection tank (CCT)	Tape heater	3200 (each)	4	16
Extractor (EXT)	Tape heater	1000	1	58
Feed lines (SFL, CFL)	Cord heater	450(each)	2	116
Collection lines (SCL, CCL) Drain lines (SDL, CDL, EDL)	Cord heater	300(each)	1	177

All the heaters were provided with 4 inch thick ceramic wool hot insulation with aluminium cladding. Insulation thickness was calculated using the relation (Equation 4.2), where Q is the heat loss per unit area (W/m^2), T_h and T_s are hot and insulation outer side surface temperature (K) respectively, r_1 and r_2 are respectively the inner and outer radius of the insulation (m) and k is the thermal conductivity of the insulation (W/m-K). The thermal conductivity of the ceramic wool insulation was taken as 0.07 W/m-K.

$$Q=\frac{(T_h-T_s)}{\left(r_2 \ln\left(\frac{r_2}{r_1}\right)\Big/_k\right)} \quad (4.2)$$

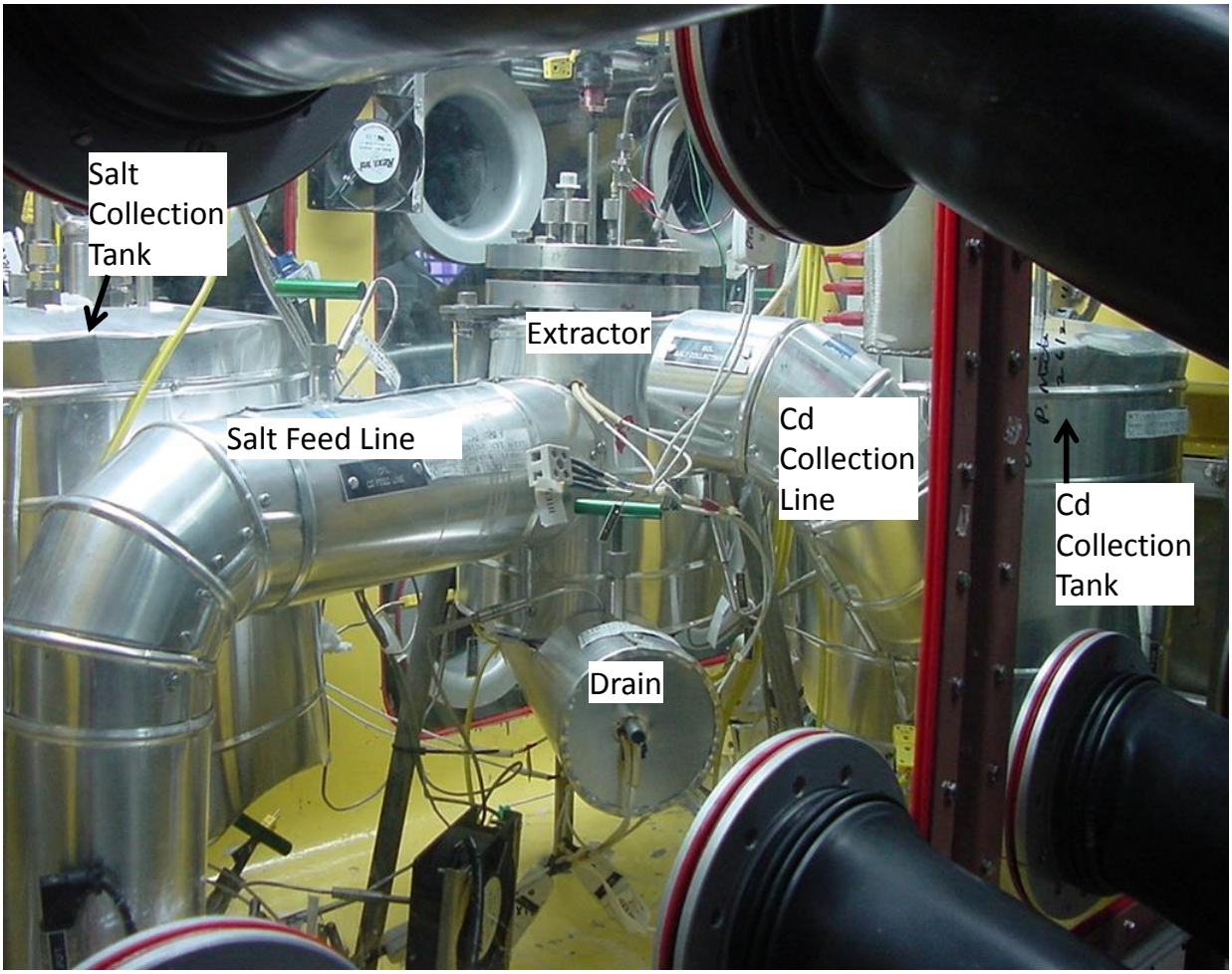

Fig. 4.6 Photograph of the high temperature molten salt extraction setup with heaters

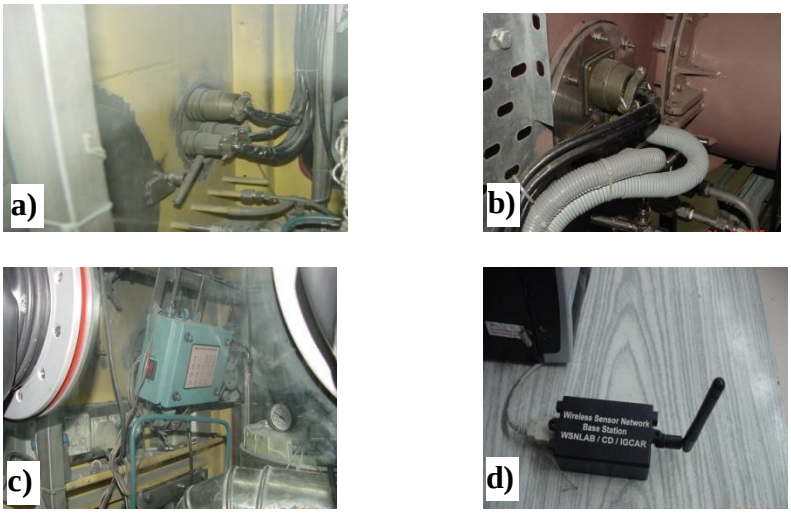

Fig. 4.7 Photographs of glove box signal transmission devices. a) Signal feed through-inside, b) feed through-outside c) wireless signal transmitter, d) signal receiver

4.2.3 Flow control system

Molten salt and cadmium were fed from the feed tanks to the extractor by pressure transfer using Ultra High Purity (UHP) argon gas (O_2 and moisture < 2 ppm). Capillaries of 1.0 mm diameter are provided in the molten salt and molten cadmium transfer lines to achieve the required flow rate of 25 mL min^{-1}. The orifice was actually a capillary with 10 mm length and 1.0 mm diameter, with converging and diverging sections in the up and down stream. The schematic of the capillary is shown in the Fig. 4.8. The transfer lines were provided with strainers with holes of about 1 mm diameter, to prevent the entry of any solid particles into the transfer line.

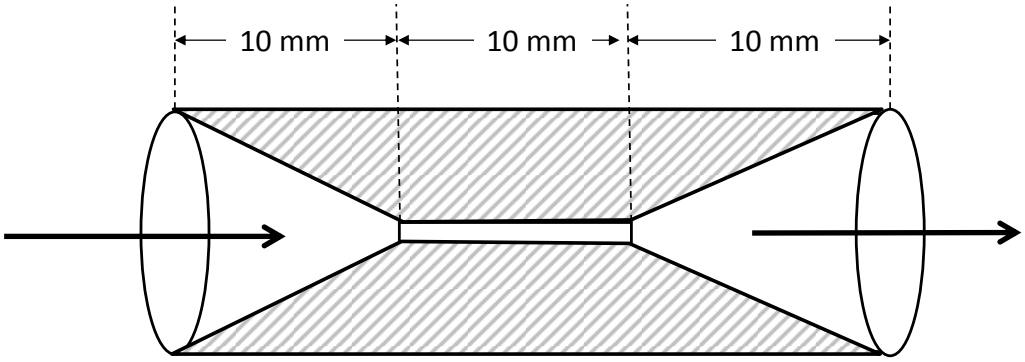

Fig. 4.8 Schematic of the 1 mm dia. capillary in the salt and cadmium phase feed line.

The argon gas line that is used to pressurize the tank for feeding the salt/cadmium was extended up to the bottom of the tank so as to maintain a constant the flow rate. The pressures used to maintain a flow rate of 25 mL min^{-1} of molten salt and cadmium were 125 mbar and 625 mbar, respectively. These values were arrived at using Bernoulli's energy balance equations [87, 102]. A simplified schematic of the setup, with the relevant variables marked, is shown in Fig. 4.9. Head required for the transfer of feed from the feed tank to extractor arrived by using Bernoulli's energy balance equation between point 1 and 2.

$$\frac{P_1}{\rho g} + Z_1 + \frac{V_1^2}{2g} = \frac{P_2}{\rho g} + Z_2 + \frac{V_2^2}{2g} + h_L \qquad (4.3)$$

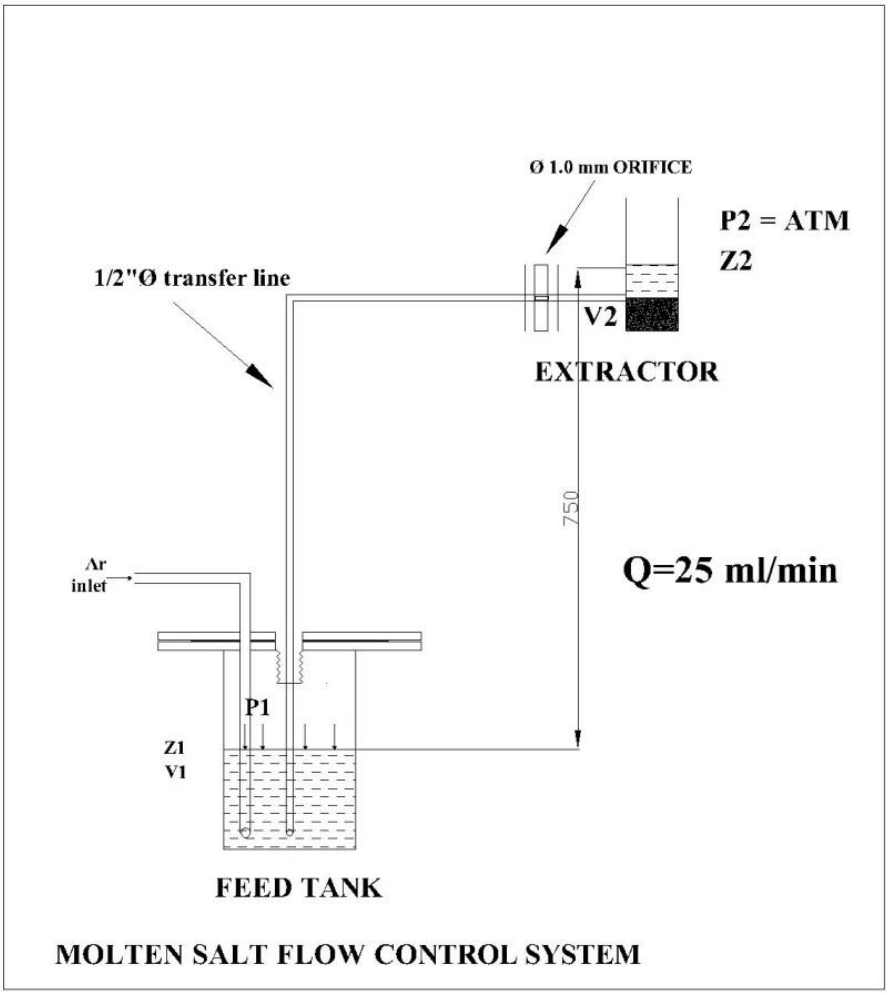

Fig. 4.9 Simplified schematic of molten salt flow control system. (The pressure, velocity and elevation variables are marked.)

The terms involved in this equation are pressure head, potential head, velocity head and frictional head losses. In this, the receiver (extractor) was maintained at glove box pressure (20 mm WC) which was fixed and almost negligible. Potential head is based on the elevation between the feed and delivery locations, and this was also fixed (750 mm). The velocity of the liquids in the transfer line, V_2 (½" SS tube with tube id =10 mm) corresponding to a flow rate of 25 ml/min, is nearly 5 mm/sec. Hence the velocity head in the pipe is negligible.

The frictional head loss in the transfer liner is calculated using Darcy's equation $h_L = \frac{fL}{D}\frac{V_2^2}{2g}$, where f is the Darcy's friction factor. For laminar flow, $f = 64/N_{Re}$. The Reynolds number,

$N_{Re} = \frac{DV\rho}{\mu}$ = 50 (i.e. laminar flow condition). Hence, the corresponding frictional head loss, h_L = 0.5 mm (the length of the transfer line, L is 3 meter including the equivalent length of the beds and valves). Total head required for the transfer is sum of the potential head and frictional head loss (750 + 0.5 = 750.5 mm). In this, potential head is fixed irrespective of the flow rate.

If the applied pressure is below the potential head, then flow does not occur (i.e. no flow condition). If the applied pressure exceeds the potential head by at least 0.5 mm, then flow will be high, which is practically difficult to control. Hence, to control the flow rate, an orifice was provided in the transfer line. The pressure drop across the orifice is calculated using the following relation[87]

$$Q = C_O A_o \sqrt{\frac{\Delta P}{\rho\left(1-\left(\frac{A_o}{A}\right)^2\right)}} \quad (4.4)$$

Using this relation, the frictional head loss across the orifice for 25 ml/min is calculated to be 40 mm of liquid column. It may be noted that the orifice discharge coefficient (C_o) is taken as 0.61. The total head required for the obtaining a flow of 25 ml/min, is 790 mm of liquid column. In terms of pressure, this is equivalent of 125 mbar for salt (density 1600 kg/m^3), 625 mbar for cadmium alloy (8000 kg/m^3) and 75 mbar in case of water. Before commissioning the facility, the flow through the orifice was calibrated with water. The measured flow rates were within ± 5 % of the calculated values.

4.2.4 Safety measures - high level detector in extractor

If the outlet of the extracted material were to be blocked due to any reason and the inlet continues to be open, then the liquid level in the extractor will continue to increase and then overflow. The overflow would cause damage to the glove box components, and has to be avoided at all costs. Therefore, a high-level detector probe is used in this set up. If the liquid level reaches a set value, then the pressure in the feed tanks will be released and the inflow will

be automatically stopped. The details of the high level detector probe are described below. The extractor top flange is fitted with a level probe to detect the buildup of level in the extractor during operation. This is spark plug type (NO/NC) discrete level detector fitted at 75 % of the total volume of the extractor (i.e. 50 mm from the top flange, total height of the extractor being 200 mm normal operating level is 100 mm). In case of level build up in the extractor, the probe gives a signal which is interlocked with the solenoid valves in the argon gas vent lines in the salt and cadmium feed tanks. These solenoid valves would be actuated and release the argon pressure in the feed tank and hence further transfer would stop.

4.3 Argon Atmosphere Glove Box System

The extraction set up containing all the tanks with transfer lines are installed inside the glove box system under argon gas atmosphere [103]. The glove box is double modular type, made of stainless steel and fitted with glass panels on the two sides and the top. Side glass panels are fitted with aluminum glove ports with silicone rubber 'O' rings and butyl rubber gloves. The volume of the glove box is ~ 1.4 m^3 (dimension:1.7 × 1.0 × 0.8 m).The box contains a transfer port on one side and a bag-out facility at the other side to facilitate the transfer of materials from/to the box under argon atmosphere. The box was leak tested with pressure hold test and helium leak detection (HLD) test. The leak rate is within 0.05 % of box volume at 100 mm water column box pressure. The schematic of the glove box system is shown in Fig. 4.10.

The box was maintained at a positive argon pressure in the range of 20-60 mm WG. The pressure was maintained in this range by the use of a pressure monitoring and controlling system consisting of a photohelic gauge in conjunction with two solenoid valves (normally closed), one connected at the argon gas inlet and the other connected to the exhaust system. The photohelic gauge (Dwyer Instruments Inc., USA) displays and controls the pressure of the box within the pre-set range by giving appropriate signals to the corresponding solenoid valves.

The oxygen and moisture contents of argon inside the boxes were maintained at less than 20 ppm (by volume) by continuous circulation of the gas through an argon gas purification system. It is a closed loop and consists of an adsorption tower, a gas recirculation blower (capacity: 89 m^3/hr, Gardner Denver Inc., Germany) and necessary piping connections to the boxes, all connected in series. The gas maintenance system, piping and the gas recirculation system are shown in Fig. 4.10. In the gas purification system, each adsorption tower was filled with a mixture of copper de-oxo catalyst (Sud-Chemie India pvt. ltd.) and molecular sieves (Sorbead, India). The regenerated copper catalyst in the towers serves as oxygen absorber whereas the molecular sieves absorbs moisture from the gas stream. The purification towers were provided with heaters with control system, argon- hydrogen mixture gas line and purge lines for regenerating the adsorbents.

4.3.1 Argon gas analyzer

Monitoring the oxygen and moisture concentrations in the argon gas inside the argon atmosphere glove box was done by on-line analysis of the gas sample using calibrated oxygen and moisture sensors. For this purpose, the gas inside the box was sampled out by a suitable blower kept inside the glove box and the oxygen content was analyzed using a trace oxygen analyzer (NUCON, Delhi, India). The moisture content was analyzed with a moisture meter (SYSTECH, UK). The oxygen analyzer measures the oxygen content based on the reduction – oxidation reaction taking place in a Pb/PbO electrolytic cell. The *emf* generated was calibrated with respect to the oxygen concentration. The moisture analyzer works on the principle of change in conductivity of a pair of P_2O_5 coated thin parallel metal wires. The moisture present in the sample would be absorbed by P_2O_5 which changes the conductivity of the wires, and this was also calibrated.

4.3.2 Regeneration of argon gas purification tower

Continuous use of the tower for a long time would lead to the purification agent becoming fully utilized. The regeneration of these catalysts was carried out by a two-step operation. In the first step, all the absorbed moisture was removed from the molecular sieves by heating the tower to 423 K – 473 K under argon purge, till all the water comes out as steam.

In the second step, the tower was purged with Ar-4% H_2 mixture to regenerate the oxidized copper catalyst back to metallic copper. Hydrogen reduces copper oxide back to elemental copper, with water as the by-product. When there was no water released through the outlet tube, the completion of regeneration was ensured. The tower was then finally dried by application of vacuum to remove traces of moisture, if present, in any inaccessible parts of the tower. The tower was finally allowed to cool under argon flow and closed tight and was ready for use in the gas purification system.

4.4 Chemicals

Laboratory grade LiCl (99.5 %, Leonid Chemicals Pvt. Ltd., India), KCl (99.5 %, Sisco Research Lab. Pvt. Ltd., India), cadmium metal (99.9%, SARU Smelting Pvt Ltd., India), cadmium chloride and lithium metal (99.9 %, Sigma-Aldrich Co., India) were obtained from indigenous suppliers. Natural uranium metal required for the preparation of LiCl-KCl containing UCl_3 was received from Bhabha Atomic Research Centre, Mumbai, India.

4.4.1 Drying of eutectic salt

The eutectic salt of LiCl-KCl with a composition of 59 and 41 mole %, respectively (44.48 wt % LiCl- 55.52 wt% KCl), was prepared and dried by vacuum drying, followed by chlorination at 773 K [9]. The eutectic salt was prepared in a 5 kg batch, eutectic composition

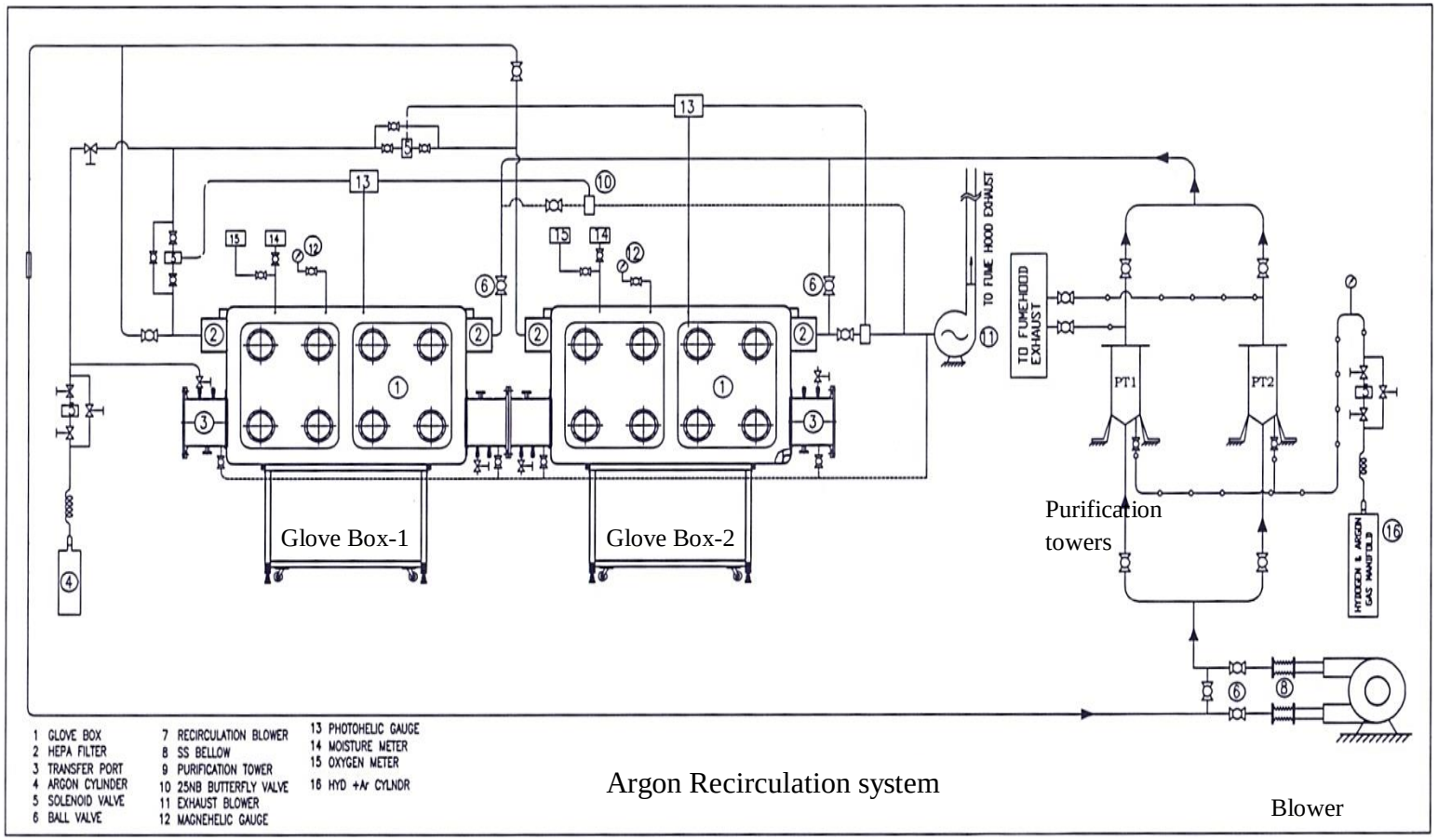

Fig. 4.10 Inert atmosphere glove box with argon purification system

of LiCl and KCl fine crystals (1-2 mm size) were mixed and dried in oven (Digiqual Systems, India) for nearly 48 hour. The oven temperature is maintained at 423 K and vacuum less than 5 torr. The trace level of moisture was removed by chlorination, chlorine gas has high affinity to moisture [104] and reacts as per the following reaction

$$H_2O + Cl_2 \leftrightarrow HOCl + HCl \quad (4.5)$$

Vacuum dried salt mixture was loaded in to the graphite crucible, heated to 773 K gradually under vacuum (< 5 torr). At molten condition, argon gas was passed through the melt followed by bubbling of chlorine at 100 to 150 ml/min for 2 h. This would ensure the complete removal of moisture from the eutectic salt. The free chlorine coming out of the setup was treated in caustic scrubber system. After the completion of chlorine addition, argon gas was purged through the eutectic salt melt to remove the free chlorine from the melt. The salt was transferred to the receiver tank cooled and transferred to the glove box for extraction studies.

4.4.2 Cleaning of cadmium balls

Cadmium received as balls (90 – 100 g each ball with 25 mm diameter) were cleaned with distilled water. They were then cleaned with 0.1M HNO_3 for the removal of oxide layer in the outer surface, again rinsed with distilled water and acetone.

4.4.3 Preparation of UCl_3 loaded LiCl-KCl salt mixture

UCl_3 was loaded in the salt by equilibrating U metal chips with eutectic salt containing $CdCl_2$ in a separate set up. U metal reacted with $CdCl_2$ to form UCl_3, which is soluble in the molten salt. Eutectic salt containing up to 5-8 wt. % UCl_3 was obtained by this process. A Li-Cd master alloy having 15 -18 wt. % lithium was prepared separately and cast into 25 to 50 g pieces and this master alloy was used for adjusting lithium concentration in cadmium phase that was used for extraction. A photograph of the eutectic salt piece, cadmium metal and UCl_3 loaded LiCl-KCl salt mixture is shown in Fig 4.11.

a)  b) 

Fig. 4. 11 Photograph showing a) feed eutectic salt (whitish cylindrical material) and cadmium balls (metallic spherical material), b) UCl_3 loaded eutectic salt

4.4.4 Analytical methods

4.4.4.1 Inductively Coupled Plasma – Optical Emission Spectroscopy (ICP-OES) This technique is used to measure the U concentration in the salt and cadmium samples. A known quantity of the sample was initially dissolved in 1:1 HNO_3 and made up to 1 mg/ml using 0.1 M HNO_3. The solution was analyzed for solute (U) concentration by ICP-OES (Model Ultima-C, Horiba Jobin Yvon, France***).*** In ICP-OES high energy plasma is used for the decomposition of the samples. A peristaltic pump delivers the sample into a nebulizer where it is nebulized and the generated aerosols passes through the spray chamber where the bigger droplets are filtered and only small droplets reach the plasma. At plasma temperature (8000 to 10000 K) the sample undergoes decomposition ,atomization, excitation and ionization *[105, 106]*. Light emitted from these excited state atoms and ions are then dispersed by the monochromoter, which consists of lenses and grating. The intensity of the dispersed light is measured by the photomultiplier. The intensity of the light is calibrated against concentration with standard solutions.

4.4.4.2 Inductively Coupled Plasma – Mass Spectroscopy (ICP-MS): An ICP-MS (PQ Excel model, Thermo Fischer Scientific Inc.) was used to measure very low concentration (ppb level) of U. This is a multi-elemental technique, where the detection is based on the difference in

charge to mass ratio (e/m ratio) for different elements. The sample is placed in a plasma and the constituents are dissociated into the respective ions. The elements in ionic state are separated based on their mass and the detector receives the signal intensity, which is proportional to the concentration.

4.4.4.3 Atomic Absorption Spectroscopy (AAS): AAS was used to measure the lithium and cadmium concentration in the solution (GBC Avantha, Australia). AAS technique is based on the principle of Beer – Lamberts law, which relates the absorption of light to other variables by the following equation $A = \varepsilon l c$. Here, A = Absorption, ε – molar absorptivity, l – length of the sample and c =molar concentration. The absorption of light through the sample solution is compared with that of the blank solution.

4.4.4.4 High Performance Liquid Chromatography (HPLC): Here, the detection is based on the difference in interaction of elements with the adsorbents in the chromatographic column. Chromatography adsorption column is packed with micro size adsorbents which gives high theoretical plates (50,000 to 100,000 per meter).The sample solution with carrier is eluted through the column at high pressure (70 to 400 bar) and the components retention time varies in the column based on their interaction with the adsorbents. The eluted phase is analyzed by UV-visible spectrometer for their concentration.

4.4.4.5 Davies –Gray Potentiometric method: This is a potentiometric method [107] for the determination of U in high concentration (% level). In this technique U in the sample solution is reduced from U^{6+} state to U^{4+} state in a phosphoric acid medium by excess of Fe(II) in sulphamic acid. The excess of ferrous ion is oxidized with nitric acid in the presence of Mo (VI) and sulphamic acid. Then U (IV) is titrated with a standard solution of $K_2Cr_2O_7$.To obtain precise potentiometric endpoint, vanadyl sulphate solution in sulphuric acid solution was added to the solution.

4.5 Experimental Procedure

Experiments were carried out at 723K instead of 773K to minimize the cadmium vapor loss to the argon atmosphere. LiCl-KCl eutectic salt containing 0.5 wt. % of UCl_3 was used as the feed in these experiments. It was prepared by adding required amount of LiCl-KCl salt containing 5-8 wt. % UCl_3 into the salt feed tank, in which LiCl-KCl eutectic salt was maintained at 723 K. The mixture was agitated by bubbling UHP argon gas through the molten salt in the feed tank. Salt samples were taken and analyzed by ICP-OES as well as HPLC techniques to measure the U concentration. Cadmium-lithium alloy used in the experiments was prepared by adding required amount of Li-Cd master alloy (15-18 wt. % Li) into the molten cadmium at 723 K in the feed tank. The alloy was agitated by argon bubbling and samples were analyzed for lithium concentration by AAS. Lithium concentration was maintained in the range of 200 - 300 ppm (by wt.) in cadmium which was nearly twice the stoichiometric amount of lithium needed for the reduction of UCl_3.

$$UCl_{3\,(\text{salt phase})} + 3Li_{\,(\text{Cd phase})} \leftrightarrow U_{\,(\text{Cd phase})} + 3LiCl_{\,(\text{salt phase})} \qquad (4.6)$$

The uranium in the salt exists in trivalent state, hence as per the stoichiometric, one mole of U in salt phase reacts with 3 mole of reducing agent lithium present in the alloy phase. At dilute concentration (0.5 wt % of U in feed salt, equivalent to 0.1 mole % of U) in single stage continuous extractor exact stoichiometric composition of reducing agent (Li) may not results in complete recovery of U, hence excess Li (200 to 300 ppm, equivalent to 0.56 mole of Li) was taken in the alloy phase. In an experiment, initially, feeding the cadmium alloy to the extractor was started until it filled up to the liquid seal in the cadmium outlet line of the extractor. Then feeding the molten salt containing UCl_3 was started by pressurizing the salt feed tank using UHP argon. The salt and cadmium alloy phase were fed to the extractor continuously at a flow rate of ~25 ml/min. The three stage stirrer in the extractor was then

started. The salt and alloy streams, after contacting each other in the extractor, were collected in to the respective collection tanks.

During the extraction, samples of salt and cadmium were taken from the extractor periodically, using syringes and 2 mm diameter quartz tubes. The stirrer speed was maintained at 300 rpm. Once the feed tanks of the salt and cadmium feed were empty, samples were taken from the collection tank and analyzed to determine the overall extraction efficiency. After the completion of experiments, both the salt and cadmium phases were drained by gravity from the collection tanks into the respective feed tanks and feed concentrations were adjusted for the next runs by adding fresh UCl_3 loaded salt into the salt tank and Li-Cd alloy to the cadmium tank. Since the uranium concentration in the cadmium is well below the solubility limit (0.77 atom% or 1.6 wt% at 723 K) [50, 108], back extraction was carried out after few runs of reductive extraction.

4.6 Results and Discussion

4.6.1 Continuous runs

Six runs of molten salt continuous extraction experiments were carried out at 723 K. The details of the experiments are given in Table 4.5. The U concentration in the feed salt was maintained around 0.5 wt. % and that of lithium (reducing agent) in the cadmium phase was maintained in the range of 200 to 300 ppm. The flow rates of the salt and cadmium alloy streams were maintained in the range of 25 -50 ml/min. The residence time of both the phases in the extractor was in the range of 5 – 10 min. Photograph of the salt before extraction and after extraction from the salt feed tank, salt collection tank and extractor are shown in Fig. 4.12. Presence of U in the salt solution gives it a grayish appearance.

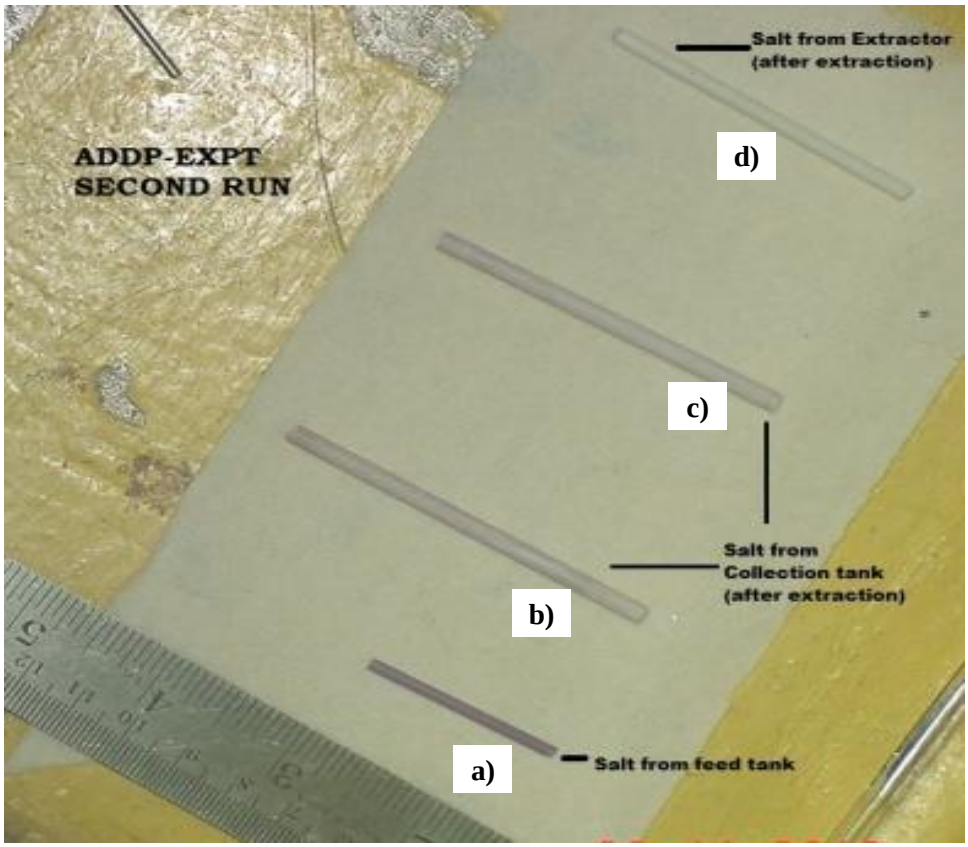

Fig. 4.12 Photograph of salt samples at various stages (a) grayish material from the initial feed salt containing U, (b) and (c) whitish material from the collection tank after extraction (d) white sample from the extractor after extraction. The grey complexion in the (a) indicates the presence of U while the nearly white sample in (d) indicates the complete absence of U.

Table 4.5 Percentage recovery of U in different experimental runs. (All the runs are carried out at 723 K and stirrer speed at 300 rpm)

	Run 1	Run 2	Run 3	Run 4	Run 5	Run 6
Salt flow rate, (ml/min)	17	50	51	31	25	30
Cadmium flow rate, (ml/min)	6	32	30	28	16	24
Salt feed U conc. (wt. %)	0.36	0.20	0.50	0.33	0.40	0.35
Lithium conc., ppm (Cd phase feed)	300	170	270	220	320	196
Salt outlet U conc. (wt.%)	0.1	0.08	0.10	0.007	0.002	<0.0007
Extractor salt conc. (wt %)	0.07	0.06	0.07	0.007	<0.001	<0.0007
% Recovery of U	72	60	80	97	99	99

One can see that before extraction (Fig.4.12 a), the sample is grey and after extraction from the extractor as shown in (Fig. 4.12 d), it is nearly white indicating the absence of U, The samples from the collection tank at different time (Fig. 4.12 b and c) are nearly white indicate slight contamination of U presumably due to the fluctuations in the flow rates. These results show that uranium recovery from the salt solution is nearly complete. In uranium analysis, possible sources of errors are sample weight measurement (<1 %), solution preparation (<1%) and error in analysis (<5%). These are uncorrelated, and the overall error is estimated to be $\sqrt{0.01^2 + 0.01^2 + 0.05^2} \approx 0.052$ or about 5 %

Sampling error and repeatability analysis is given below.

Six runs were carried out with U concentration in the feed salt 0.20 to 0.50 wt %. Overall sampling error – It is the cumulative error of sampling, sample weight measurement, solution preparation and analytical error in emission spectroscopy.

- Extractor sampling error – negligible (the solution is homogeneous in the extractor, and all samples can be considered as representative of the bulk)
- Error in weight measurement: 1 % (sample weight 100 – 200 mg, weighing balance accuracy is +/- 1 mg)
- Error in solution preparation: < 1 % (sample is dissolved in 0.1 N HNO_3 and made up to 100 ml)
- Analytical error (Optical Emission Spectroscopy): +/- 5%
- Overall error: approximately 5 %

The results from the Table 4.5 confirm the recovery of U. The final concentration of U in the salt outlet from the extractor went down to less than 0.1 wt% in some cases up to less than 10 ppm in Run 6 which is the detection limit of U by HPLC technique. The percentage recovery of uranium was calculated from the U concentrations in the inlet and outlet of the salt, as shown below:

$$\% \text{ recovery of U} = \frac{\text{Feed salt U conc} - \text{outlet salt U conc}}{\text{Feed salt U conc}} \times 100\ \% \qquad (4.7)$$

The percentage recovery of U from the last three runs range from 97-99%. This is in line with the results of Kinoshita et al [55]. Equilibration studies reported by Kurata et al. [50] revealed that the distribution coefficient of actinides between the salt and the cadmium alloy is dependent on the lithium concentration in the cadmium phase. For 10 % excess of lithium above the required stoichiometric concentration in cadmium phase, the equilibrium distribution coefficient is higher by two orders of magnitude or more. With such a high distribution coefficient value, a recovery of greater than 99 % of actinides is possible in single stage and the results are thus in the expected range. The percentage recovery of first three runs is less than the latter runs. In these initial runs, some problems were encountered in maintaining the flow rates of the salt and cadmium alloy. That could have led to lower recovery. The consistently high recovery obtained in the last three runs confirms the possibility of ~ 98% recovery with a single stage of a well stirred continuous extractor.

4.6.2 Material balance of U in salt and alloy phases

Apart from visual observation (Fig. 4.12) and concentration measurements (Table 4.5), the evidence of recovery can also be adduced from material balance of U. This was done in three ways. Firstly, the uranium extracted from the salt phase by reductive extraction was calculated from the amount of feed during the run and the difference between feed and outlet U concentration. Secondly, the amount of U transferred to the Cd phase was calculated from the increase in U concentration in the Cd phase. Thirdly, material balance of U was also possible from the topping up of the U in the salt before each run. This was done in the feed preparation stage by adding UCl_3 in the required quantity pertaining to reach the target feed salt concentration. The data of these three methods are summarized in Table 4.6.

Table 4.6 Uranium material balance (based on salt and cadmium phase concentration and U loading in the feed preparation)

	Run1	Run 2	Run 3	Run 4	Run 5	Run 6	Total
Salt phase							
Feed quantity (g)	4504	4504	5061	4890	5057	5279	
Feed U conc. (wt%)	0.355	0.20	0.50	0.345	0.40	0.345	
U in the feed (A) (g)	16.00	9.00	25.30	16.90	20.23	18.20	
Outlet U conc. (wt %)	0.14	0.12	0.09	0.10	0.03	0.0007	
U in the collection tank (B) (g)	6.31	5.41	4.55	4.89	1.52	0.04	
U removed (=A-B) (g)	9.68	3.60	20.75	11.98	18.71	18.16	82.90
Cadmium phase							
Feed quantity (g)	17910	17910	17910	19450	19450	19450	
Feed, U conc. (wt %)	0.00	0.01	0.025	0.02	0.04	0.03	
U in Cd feed (B) (g)	0	1.80	4.48	3.90	7.80	8.34	
Cd Outlet, U conc.(wt %)	0.045	0.02	0.04	0.05	BDL	0.001	
U at Cd outlet (A) (g)	8.06	3.58	7.16	9.73	-	0.20	
U transferred (=A-B) (g)	8.06	1.79	2.69	5.84	-	BDL	4.95
U accounting %	83	50	13	49	Nil	Nil	
UCl_3- LiCl-KCl salt mixture loaded in feed preparation							
Amount (g) – lot (1)	318	nil	556	230	90	182	
U, conc. (wt %)	5.20	-	4.05	8.05	8.05	5.07	
Amount (g) – lot (2)	112	nil	nil	nil	77	40	
U, conc. (wt %)	3.80	-	-	-	3.84	8.4	
Total U loaded (g)	20.81	-	22.54	18.47	10.22	12.59	84.63

One can see that the material balance on U obtained in the first method agrees well with that obtained in the third method. However, the material balance in the cadmium shows gross under-recovery of U. The reason for this may be due to the inhomogeneity in Cd phase. After every run, heaters were stopped and the phases solidified and reached the ambient temperature. For the successive runs again the feed salt and the alloy phases were melted and maintained at operating temperature 723 K (due to the high vapor pressure of cadmium (10 mm Hg at 773 K) [97, 109]). At low temperatures, there is a possibility for the formation of an intermetallic

compound (mainly UCd_{11}) which leads to the precipitation (segregation of U) of the compound. This intermetallic compound may get accumulated in the low temperature region in the storage vessels. The dissolution kinetics of the intermetallic compound depends on the prevailing temperature and diffusion rate. There is a possibility of a temperature gradient in the lines and storage vessels, such as thermo-well, argon pressurization line, feed withdrawal lines and fittings in the transfer lines.

The low temperature region in the system may act as the cold trap for the intermetallic compounds. Such inhomogeneity in cadmium phase resulted in the sampling error and difference in material balance. Similar observations have been reported earlier by Moriyama et al. [51, 53]. This may be the reason for the difference in material balance of U between salt and alloy phase.

4.6.3 Mass transfer coefficient

Mass transfer coefficient in continuous molten salt extraction is calculated based on the salt side U concentration. A simplified schematic of the two phase mass transfer is shown in Fig. 4.13. The Conservation equation for the U balance in the extractor is written in the form

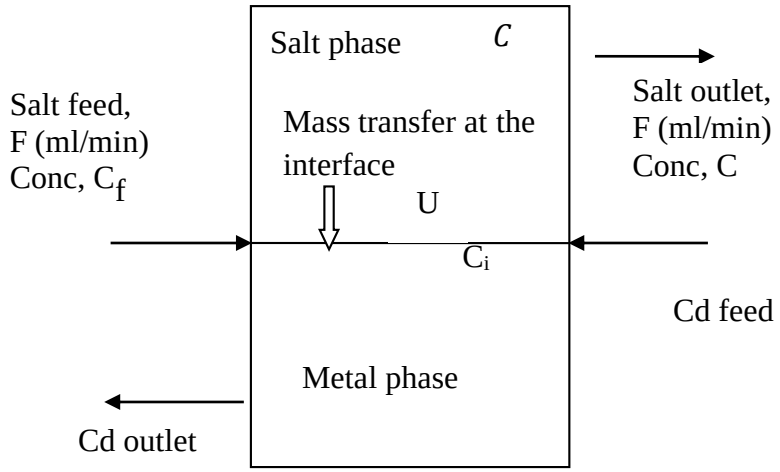

Fig. 4.13 Schematic illustrating the mass transfer across the interface in the extractor

Rate of U in	-	Rate of U out	+	Rate of U generation	=	Rate of U Accumulation	(4.8)

At steady state condition in continuous molten salt extraction, the rate of accumulation term is equal to zero. The rate of generation term is equal to the rate mass transfer across the interface. Rate of mass transfer across the interface = k.a .ΔC, where the concentration difference, ΔC= C – C_i , C - concentration in the bulk phase, C_i - concentration in interface, k = salt side mass transfer coefficient, a = interfacial area. Conservation equation (4.8) can be mathematically written in the form

$$F (C_f - C) = k.a .\Delta C \quad (4.9)$$

$$= k . a . (C - C_i)$$

However, the interfacial area cannot be easily measured during two phase mixing. In one of the earlier reports, the contactor area has been used instead of interfacial area [53] to estimate the mass transfer coefficient. Moriyama et al. [53] estimated the mass transfer coefficient for the elements Zr, La, Ce and Th using contactor area as basis, and the values were in the order of 10^{-2} cm/s. Kinoshita et al. [55] carried out continuous molten salt extraction with Ce, Gd and Y. They did not report whether actual interfacial area or contactor area was used as basis. The estimated mass transfer coefficient value was about 0.14 cm/s. Based on contactor area, the mass transfer coefficient in our system is estimated to be k = 0.31 cm/s.

During typical operation, the actual interfacial area will be lot more than the contactor area, and using the contactor area in the formula will lead to overestimation of the mass transfer coefficient. It is possible to estimate the interfacial area in some cases. For example, Zhou and Kresta [47] studied mixing of water – silicone oil system and have proposed a correlation to estimate the mean droplet size, as discussed in section 3.2.1. Since there is no literature data or correlation available to estimate the mean droplet size for systems with high interfacial tension, the one proposed by Zhou and Kresta can be used as a first order approximation, For

our system, this yields a mean droplet size of 300 μ, and corresponding interfacial area of 2.5 m^2, which yields an estimated mass transfer coefficient of k = 7 × 10^{-4} cm/s. Naturally this depends on the applicability of the correlation to our system. However, a volume based mass transfer coefficient (k·a) calculation will avoid this issue, and hence is calculated as shown below.

$$(k.a) = F\frac{(C_f - C)}{C} \quad (4.10)$$

For a fixed salt feed flow rate, mass transfer coefficient depends mainly on the outlet U concentration. In the molten salt concentration runs, the salt outlet concentration in the runs varied from 0.001 to 0.1 wt%. In a typical runs with feed flow rate 30ml/min, concentration, C_f =0.35 and outlet concentration, C = 0.01 wt %, Mass transfer coefficient calculated based on the above equation (4.10) is 16.7 cm^3/s. The uncertainty in the sampling and analysis is ± 5 %.

4.6.4 Reductive extraction at higher U concentration in batch mode

Extraction kinetics study was carried out with 3 wt % U concentration in salt phase. Due to the large requirement of U to increase the U concentration in the entire salt in feed tank, extraction was conducted in batch mode. UCl_3 loaded eutectic salt was prepared by in-situ oxidation of U metal in extractor using the oxidizing agent $CdCl_2$ as per the following reaction.

$$2U + 3CdCl_2 \leftrightarrow 2UCl_3 + 3Cd \quad (4.11)$$

Natural U in 3 mm rod form was loaded in perforated rotating basket, and was inserted into the salt phase. This basket is connected to the stirrer motor and used as the stirrer. $CdCl_2$ was added to the salt phase and stirred for 48 hour. The U metal was converted to UCl_3. The U concentration in the salt sample was analyzed (ICP-OES) and was found to be 3.10 wt %.

For the reductive extraction, 2 g of lithium in the form of Li-Cd alloy (10 wt % Li) was added to the extractor. The extractor was maintained at 723 K and the stirrer speed was maintained at 300 rpm. The salt and Cd phases were contacted for 1 h duration. The salt samples were taken at regular intervals and analyzed, and the results are shown in the Table 4.7. U concentration in cadmium sample increased from below detectable level (BDL) before extraction, to 0.32 wt % after the completion of extraction. Batch experiments (run 2) were carried out with 5.6 wt % of initial U concentration. Lithium equivalent to 4.48 g (20 % excess than stoichiometric) was added in the form of Li-Cd alloy (Li- 9 wt %). Extraction was carried out at 773 K and stirrer speed was maintained at 300 rpm, salt samples were analyzed with time for U concentration. In the batch extraction runs U concentration in salt phase reached steady state value in nearly 30 min. Though the reaction kinetics is fast, in batch mode Li-Cd alloy was added to the extractor at the beginning of the experiment, it may take some time to melt and become homogeneous solution. This may be the reason for the excess time taken to reach the equilibrium state.

Table-4.7 Uranium concentration in batch extraction experiments (in the runs amount of salt 400 g and Cd phase 2000 g, stirrer speed 300 rpm and Extractor temperature 723 K)

	Run 1		Run 2	
location	Time (min)	U conc. (Wt. %)	Time (min)	U conc. (Wt. %)
Salt phase Sample in extractor	Before extraction	2.98		5.6
	12	0.57	6	0.59
	24	0.2	17	0.20
	33	0.092	27	0.17
	67	0.093	60	0.14
U recovery (%)	-	96.8	-	98
Cd phase sample	Initial conc.	BDL	-	0.03
	Final conc.	0.32	-	0.32

The amount of U loaded for the experiments and U extracted during the extraction were shown in Table 4.8. The quantity of U removed from salt phase based on salt sample was almost equal to the U loaded in the beginning of the experiments, whereas the U loaded in the Cd phase based on Cd sample is less, it is shown in Table 4.8.

Table 4.8 Uranium material balance in batch experiments

	Run 1	Run 2
Amount of U loaded (g)	11.92	22.4
U removed base on salt sample(g)	11.54	22.02
U transferred based on Cd phase sample(g)	6.4	5.8

This difference may be due to the intermetallic compound formation of U in the alloy phase which leads to the inhomogeneity in sampling. Taken together, the results presented in Table 4.6 and 4.7 show that uranium recovery to the extent of 95 to 99% is possible through liquid-liquid extraction either in a continuous mode or in batch mode.

4.7 Challenges Encountered During the Experiments

During the experimental setup and runs, certain difficulties were encountered, and they are listed below so that future setup and runs can be made by taking these into consideration. Firstly, lithium is extremely reactive and pyrophoric. i.e. It cannot be stored in ambient, and has to be stored in an inert atmosphere, free from oxygen and moisture. The salt LiCl/KCl is hygroscopic and should also be maintained under inert atmosphere. This means, the setup must be installed in an inert atmosphere containment box, and the operations had to be carried out using glove box. This also limits the size of the experimental setup and throws challenges in sampling and maintenance.

The electrical resistance heater as well as the insulation failed frequently. This could be addressed by ensuring that all the vessels and lines were grounded (earthed) properly. In

addition, fuses and MCB (Miniature Circuit Breaker) should be included in the system design. In this study, quartz with ceramic beads insulated tape and cord heaters were employed. Instead, stainless steel sheathed mineral (magnesium oxide) insulated heaters may be used in the future, to ensure longer life for heating element and insulation.

In this study, the flow of molten materials is achieved by pressurizing the feed tank. The level of control provided by this method is not very high. Instead, especially in larger systems, pumping devices such as centrifugal pump or metering pump such as gear pump can be adopted. If pressurized tank is used, a safety relief valve is a must in the feed tank. The typical pressure in Ar cylinder is above 100 bar, whereas the pressure required (corresponding to the flow rates in our system) is less than 1 bar. To achieve a reasonable control in the flow, two stage pressure regulators are needed in the argon line. Since the system was at high temperature and was under positive pressure during the experiments, the system must be thoroughly checked using dye penetration test and hydro test at high pressure (e.g. @ 5 bar gauge pressure, as per the standards). During the actual runs, the maximum allowed pressure (set using a pressure relief valve) was 1.5 bar.

At the operating temperatures (~ 723 K), cadmium has high vapor pressure. In our setup, there was no mechanical seal between the shaft and the top flange of the extractor. A small clearance (1 mm) was provided for the free rotation of the stirrer. The cadmium vapors would escape through this clearance. At high temperatures, a significant amount of cadmium came through this clearance and deposited on the glass viewing panels, and limited the visibility. This also led to additional periodic maintenance. It should be noted that cadmium is a carcinogenic (permissible threshold limit value = 0.05 mg/m^3), and the containment box confined the cadmium vapor to the inside and prevented its outflow into the ambient. Otherwise, additional actions would be necessary to limit the cadmium concentration in the

ambient. In large feed tanks (e.g. in our case 8 inch dia) operated at high temperature, copper gaskets may not provide sufficient leak-tight operation. In these cases, spiral wound metallic gaskets are used to obtain leak-tight operation. It is worth noting that any leakage of the fluid (in this case, conducting materials), will trip the power supply, due to short circuit.

In our setup, the top flange of the salt and cadmium feed tanks were attached to the bottom of the glove box. During the operation, the tanks were heated to maintain the contents in liquid state, and the temperature of the top flange would also be high. However, the glove box frame (made of steel) should not get heated too much. Otherwise, it would lead to uneven expansion of the steel, which can cause stress at (i) the joint connecting the top-flange of the tank to the glove box leading to mechanical failure or (ii) in the glass panels, leading to cracks which would result in failure to maintain inert atmosphere. Hence, cooling water jacket was provided outside the glove box, to limit the increase in temperature of the glove box.

4.8 Summary

An experimental set up for carrying out studies on the actinide drawdown step of the pyroprocess flow sheet has been assembled inside an argon atmosphere glove box. It is a single stage continuous molten salt extraction facility. Experiments were carried out at 723 K to recover U in the molten salt into Li-Cd alloy and about 99 % could be recovered. The results match with the estimates based on the thermodynamic parameters (specifically, distribution coefficients) of the salt and the cadmium alloy. Batch experiments were carried out at higher U concentrations and the results show that about 96 % recovery is possible. The material balance based on the UCl_3 loading confirmed the % recovery of U. The material balance based on the cadmium phase grossly under predict the recovery, this may be due to the formation of intermetallic compounds. The results obtained are in agreement with the reports in the literature.

CHAPTER 5
SCALE UP STUDIES

In pyrochemical reprocessing of spent metallic nuclear fuel, for continuous molten salt extraction, a five liter size stirred vessel would be sufficient to handle the expected process load. However the process studied here, (i.e. dispersion of floating solids in continuous medium) has application in wide variety of industries, such as effluent treatment, fermentation, catalytic reactor etc. In those cases, vessels of large volume, of the order of m^3 or more would be in use. In order to calculate the power requirement and operational mode (such as vessel geometry, agitator type and stirrer speed) of the large vessels, it is likely that small and medium scale experiments using similar solid/liquid combination would be performed as a part of scale up studies. In this chapter the experimental results of the two different size vessels were described. The results are analyzed to obtain insights into how scale up can be performed.

5.1 Scale up Principles

There are different criteria that can be used to scale up, as described in the literature [92] and they are summarized below. Usually, lab scale and pilot scale studies are carried out before the design of large scale experiments. This is done in order to ensure that the operation of the large scale vessel can be predicted with a good accuracy.

5.1.1 Similarities

i. Geometric similarity – When the ratios of corresponding dimensions in one system are equal to those in the other system.
ii. Kinematic similarity – In addition to geometrical similarity, the ratios of velocities between corresponding points in each system should be equal.
iii. Dynamic similarity – in addition to geometric and kinematic similarity, the ratios of forces between corresponding points in each system should be equal

For proper scale up, the above similarities need to be maintained. In this study, the goal of the process is to ensure dispersion of particles throughout the liquid volume. In molten salt

extraction using alloy phase as the solvent, reductive extraction is the goal. Since the chemical reaction is fast, the actual mass transfer rate is controlled by the hydrodynamics in the stirred vessel. It is worth noting that in other industries, mass transfer may or may not be the limiting step. Once the agitation needed to completely disperse the particles in lab and pilot scale are studied, we need to predict the required agitation in the large scale (production unit). A list of possible scale up criteria used in stirred vessel is given in Table 5.1 [92].

Table 5.1 Scale up criteria generally used in stirred vessels

	Criteria	Formula	Proportional to
1	Reynolds number, N_{Re}	$\frac{\rho N D_a^2}{\mu}$	$\propto N D_a^2$
2	Froude number, N_{Fr}	$\frac{N^2 D_a}{g}$	$\propto N^2 D_a$
3	Weber number, N_{we}	$\frac{\rho N^2 D_a^3}{\sigma}$	$\propto N^2 D_a^3$
4	Tip speed, TS	$\pi N D_a$	$\propto N D_a$
5	Power number, N_P	$\frac{P}{\rho N^3 D_a^5}$	$\propto N^3 D_a^5$
6	Power per unit volume, P/V	$\frac{P}{D_a^3}$	$\propto N^3 D_a^2$
7	Volumetric flow per velocity head, Q_V/H	$\frac{D_a^3 N}{(v^2/2g)}$	$\propto \frac{D_a}{N}$

It is not possible to simultaneously maintain all the criteria. For example, if tip speed is constant, the case with a larger impeller diameter would correspond to a lower stirrer speed for the same process medium (in this case, solid/liquid). For fixed fluid properties, if tip speed is fixed, then N_{Re}(α N D_a^2) will be more in the larger vessel. Similarly, Froude number (α N^2 D_a) will be less in the larger vessel, as the stirrer speed will be lower there.

5.2 Experimental

Experimental details of the smaller vessel have been described in chapter 4, and a geometrically similar 1: 10 volume scale up system was used in this study. The volume of the

vessel was 5 liters. A transparent acrylic vessel with 180 mm diameter was used for the dispersion studies. The liquid level was maintained equal to the vessel diameter (H/D_T =1). The baffles were dismountable type, made of stainless steel. The impellers used in the experiments were four blade-paddle type with radial and axial flow direction. A schematic of the vessel is given in figure 5.1a and a photograph of the impellers is given in figure 5.1b. The major variables in the experiments are type of impeller, impeller submergence, impeller diameter and dispersion medium. The variables are listed in Table-5.2. Experiments were carried out with 230 micron floating particles. The liquids used for the experiments are water, glycerol-water (1:1 volume ratio) and aqueous $ZnCl_2$ (65 wt %) solution. The axial impellers were 45^o angle pitched, and by reversing the motor direction from clockwise to anticlockwise the same impeller was used in upward and downward pumping mode. The diameter of the impeller was 90 and 60 mm (D_a/D_T = 1/2 and 1/3). The dimensions of the stirred vessel are given in the Table-5.3.

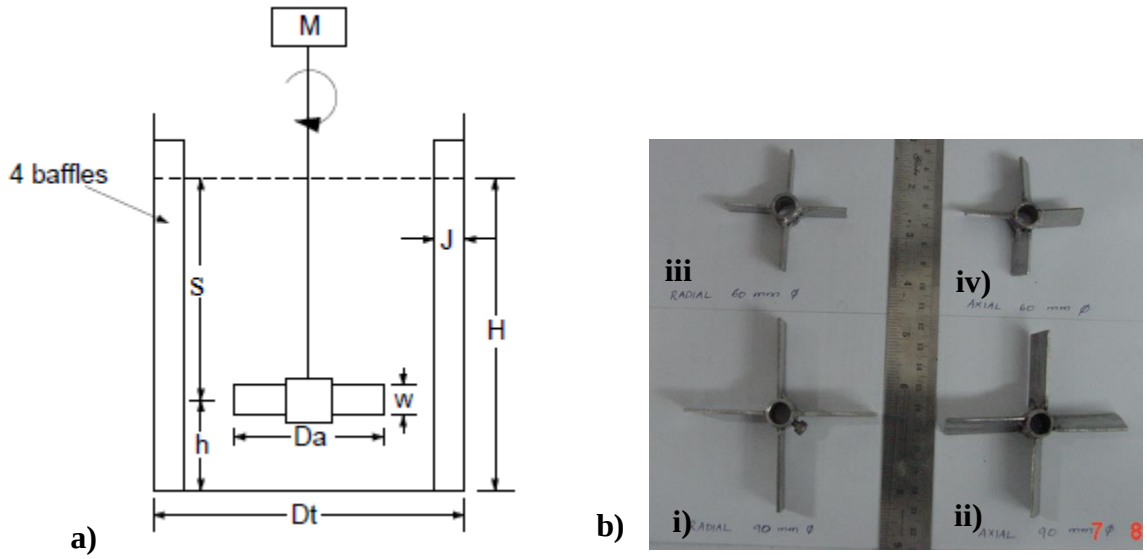

Fig. 5.1 Schematic of a) the experimental set up and b) i) radial 90 mm, ii) axial 90 mm, iii) radial 60 mm and iv) axial 60 mm impellers

Table 5.2 Variables in the scale up experiments

Impeller type	Radial, Axial upward and Axial downward
Continuous medium	Water, Glycerol-water 1:1 solution and Aqueous $ZnCl_2$ salt solution
Impeller location	s/D_a =0.5,1.0 and 1.5
Impeller diameter	D_a/D_T = 1/3 and 1/2

Table-5.3 Vessel dimensions in scale up studies

Parameter	mm	Shape ratio
Vessel dia. D_T	180	
Imp. dia. D_a	90 and 60	D_a/D_T=1/2, 1/3
Liquid depth, H	179	H/D_T=1
Impeller submergence, s	45, 90, 135	s/D_T=0.25, 0.5, 0.75
Blade height, W	18 and 12	W/D_a=1/5
Baffle width , J	18	J/D_T=1/10

5.3 Results and Discussion

The experiments on drawdown of floating solids were carried out with three different fluids, three stirrers, and three impeller locations and two vessel sizes. The relevant scale up criteria such as Reynolds number, impeller tip speed, Froude number, power per unit volume and volumetric flow rate per velocity head are evaluated.

5.3.1. Effect of vessel size

Figure-5.2a shows the effect of change in volume on tip speed for radial impeller, at various positions of impeller submergence (s/D_a ratio). The data corresponding to all the three fluid media are presented here. Except for one pair of data, all other results show that the impeller tip speed must be maintained constant (for the given solid/fluid system) to ensure complete mixing, regardless of the size of the vessel. This suggests that in large vessel, a smaller rpm is sufficient to get complete dispersion. The remaining parts of the figure also present the results from radial impeller, at different submergence values.

The value of Reynolds number *vs.* vessel size is given in figure 5.2b. It is seen that N_{Re} increases with volume. This is expected since maintaining constant impeller tip speed at larger size leads to lower rpm. Hence N_{Re} ($\propto ND_a^2$) will be higher at larger vessel. The trend of Froude number as a function of vessel volume is presented in figure 5.2c. It is seen that N_{Fr} ($\propto N^2 D_a$) decreases with vessel volume. Figure-5.2d presents the power per unit volume as the function of vessel volume. In these experiments, power was not measured and instead, the value of P/V is derived. For a given process medium, Impeller power $\propto \rho N^3 D_a^5$ and vessel volume $\propto D_a^3$. Hence, P/V $\propto N^3 D_a^2$. The values of P/V are calculated for the two vessel volumes. The results show that P/V decreases with an increase in vessel volume. The volumetric flow per velocity head as the function of vessel volume, Q_v/H is shown in figure 5.2e. Here volumetric flow rate is $\propto D_a^3 N$ and velocity head is $\frac{v^2}{2g}$ (or $\frac{D_a^2 N^2}{2g}$). Therefore, $Q_V/_H \propto \frac{D_a}{N}$. The results show that the Q_v/H increases with an increase in vessel volume. The results for axial downward and axial upward impellers (along with those of

Table 5.4 Effect of scale up (1:10) on critical impeller speed, N_{crit} (rpm) in small and large vessel with three impeller submergences

	Radial			Axial downward			Axial upward		
	s/D_a			s/D_a			s/D_a		
Continuous medium	**0.5**	**1**	**1.5**	**0.5**	**1**	**1.5**	**0.5**	**1**	**1.5**
Water-small vessel	186	215	270	223	245	325	218	272	320
Water-large vessel	56	89	113	74	89	114	56	95	118
Gly+ Wat (1:1)-small	231	282	330	252	352	477	249	342	429
Gly+ Wat (1:1)-large	104	129	139	112	127	173	95	135	168
$ZnCl_2$ soln. -small	272	343	425	293	423	631	362	457	600
$ZnCl_2$ soln. - large	123	146	167	136	148	196	127	146	177

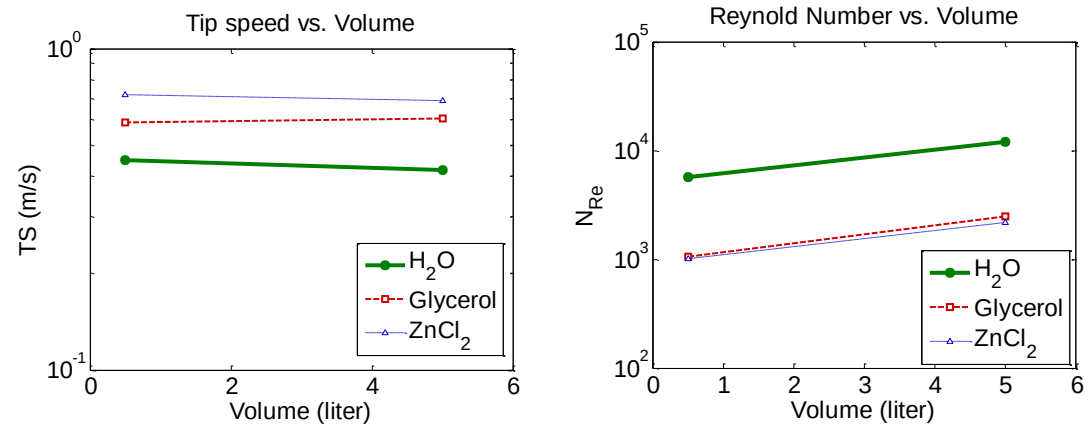

(a)

(b)

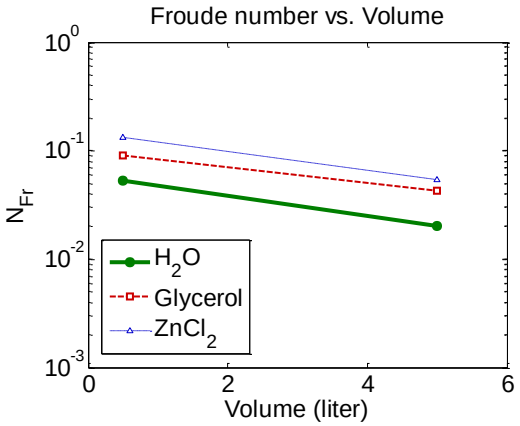

(c)

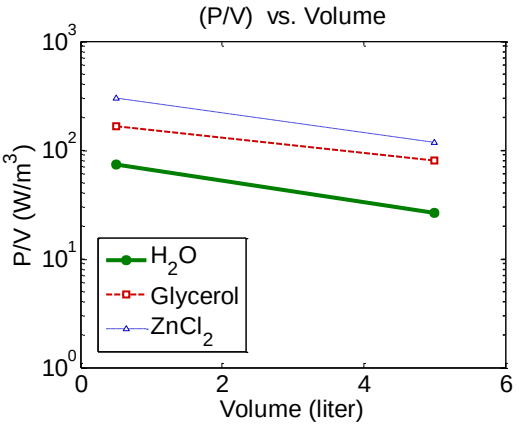

(d)

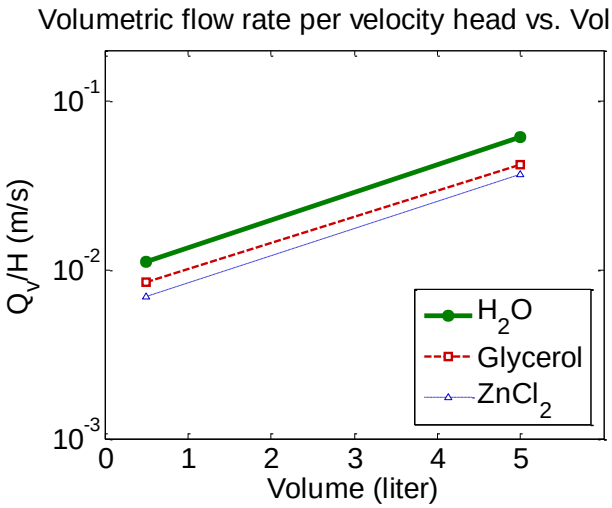

(e)

Fig. 5.2 Effect of vessel volume on (a) Tip speed (b) N_{Re}, (c) N_{Fr}, (d) P/V and (e) Q_v/H. (Radial impeller data, at impeller location of s/Da =1.0 are shown here).

radial impellers) are presented in Table 5.4, and the trends are similar to those of radial impeller results (figures not shown).

5.3.2 Effect of impeller diameter

The impeller diameter of the larger vessel was changed from 90 mm to 60 mm, and the results corresponding to radial impeller at $s/D_a = 1.0$ are presented in figure 5.3. The data for all the impellers at all the three submergence values studied are shown in table 5.5.The effect of increase in diameter on the critical impeller speed is presented as tip speed vs. impeller diameter, in figure 5.3a. The results clearly show that at larger diameter, lower tip speed (and significantly lower rpm) is sufficient to obtain complete dispersion. The reasons for this trend are not obvious. One possibility is that at the smaller diameter, the clearance between the impeller tip and the vessel wall is relatively higher, which results in the reduction in fluid velocity due to velocity decay with distance.

Table 5.5 Effect of impeller diameter on critical impeller speed in large vessel. N_{crit} (rpm) in 5 liter stirred vessel with 60 and 90 mm diameter impeller

Continuous medium	D_a (mm)	Radial			Axial downward			Axial upward		
		s/D_a			s/D_a			s/D_a		
		0.5	1	1.5	0.5	1	1.5	0.5	1	1.5
Water	90	56	89	113	74	89	114	56	95	118
Water	60	161	195	209	192	233	281	150	186	216
Gly: Water (1:1)	90	104	129	139	112	127	173	95	135	168
Gly: Water (1:1)	60	181	272	363	260	322	396	197	253	384
$ZnCl_2$ soln	90	123	146	167	136	148	196	127	146	177
$ZnCl_2$ soln.	60	205	355	464	354	406	542	212	360	476

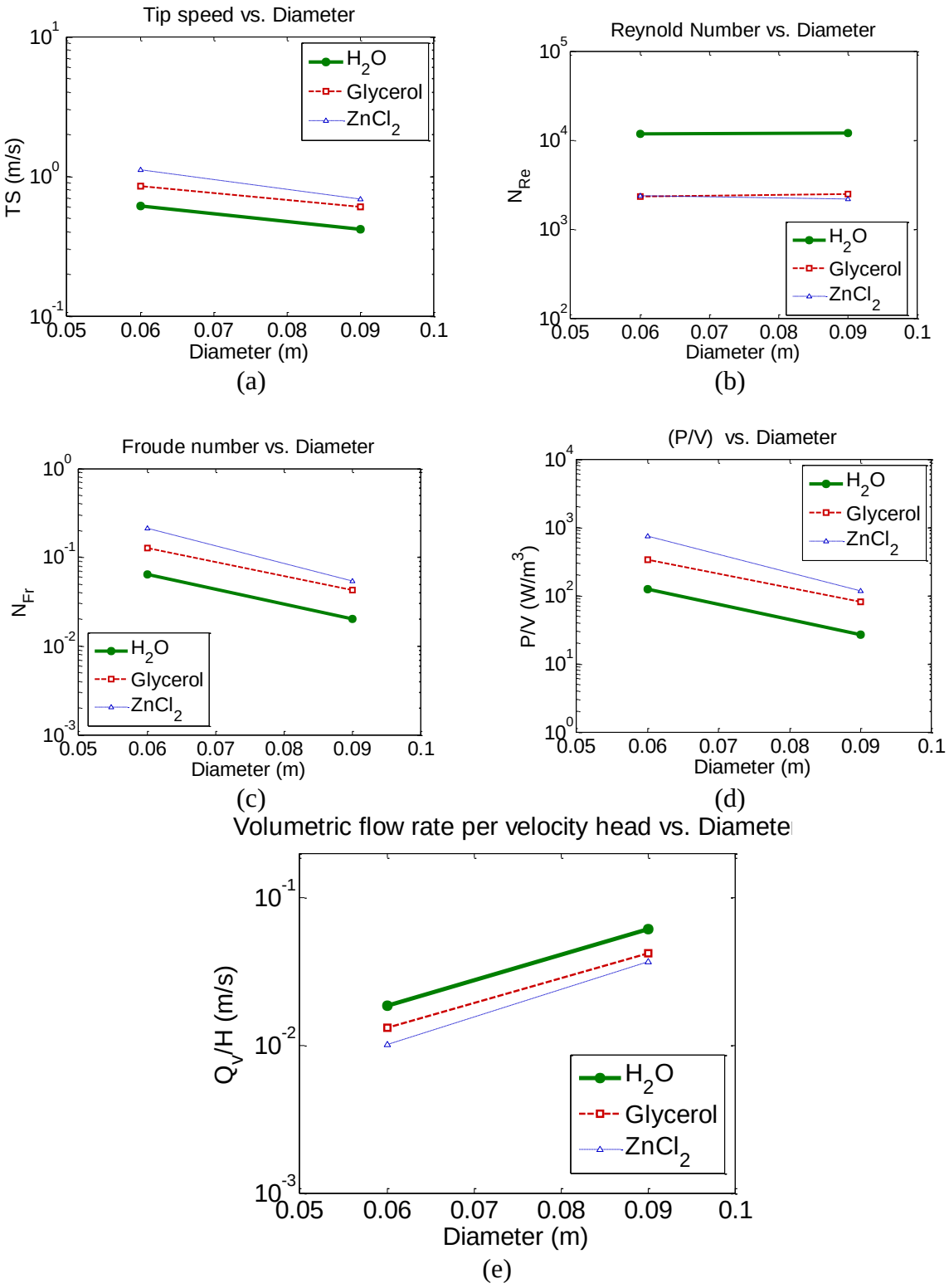

Fig. 5.3 Effect of impeller diameter on (a) Tip speed (b) N_{Re} (c) N_{Fr} (d) P/V and (e) Q_V/H. (Radial impeller data, at impeller location of s/Da = 1.0 are shown here).

Fig. 5.3b shows Reynolds number vs. impeller diameter and this is more or less constant for the two impellers. The decrease in diameter is compensated by the higher rpm required and velocity of the fluid, across the diameter would be so much, that it is not sufficient to cause good dispersionhence the Re does not change significantly. The variation of Fr with diameter is presented in Fig. 5.3 c. Since $\propto N^2 D_a$, at smaller agitator diameter (with a corresponding higher N), a larger Fr is observed. The trend of P/V vs. D_a, shown in Fig. 5.3d indicates that the power requirement will be significantly more if a smaller agitator is employed. This is related to the fact that lower tip speed is necessary to obtain sufficient mixing. The volumetric flow rate per velocity head is less for the smaller agitator, as seen in Fig. 5.3e.

5.3.3 Correlation of data

Similar to small scale vessel, a correlation in the form of $Fr = C' Ar^{\alpha} C_d^{\beta} \left(\frac{\Delta\rho}{\rho}\right)^{\gamma} \left(\frac{S}{D_a}\right)^{\delta}$ was attempted and the exponents in the relation were found by regression analysis. The results show that the exponents of drag coefficient and density ratio are negligible. Hence a simple correlation in the form of $Re = C^{"} Ar^{\alpha} \left(\frac{s}{D_a}\right)^{\delta}$ was evaluated. The values of the constants and exponents are estimated by regression analysis and are presented in Table-5.6

Table 5.6 Exponents of correlation equation, from the large scale vessel data.

Type of impeller	C″	α	δ
Radial	2234	0.43	0.36
Axial downward	2607	0.43	0.35
Axial upward	2279	0.43	0.41

By substituting the exponent's values and rearranging the above correlation, the following relationships for N_{crit} for radial, axial downward and axial upward impeller were obtained.

$$N_{crit} \propto \boldsymbol{D_a^{-2.36}}(\Delta\rho)^{0.43}\rho^{-0.57}\boldsymbol{s^{0.36}}D_p^{1.29}\mu^{0.14} \quad (5.1)$$

$$N_{crit} \propto \boldsymbol{D_a^{-2.35}}(\Delta\rho)^{0.43}\rho^{-0.57}\boldsymbol{s^{0.35}}D_p^{1.29}\mu^{0.14} \quad (5.2)$$

$$N_{crit} \propto \boldsymbol{D_a^{-2.41}}(\Delta\rho)^{0.43}\rho^{-0.57}\boldsymbol{s^{0.41}}D_p^{1.29}\mu^{0.14} \quad (5.3)$$

The values predicted by the correlations were compared with the measured values and are presented as parity chart and shown in figure 5.4. The comparison shows that the predicted values are mostly fall within the ±20% deviation lines.

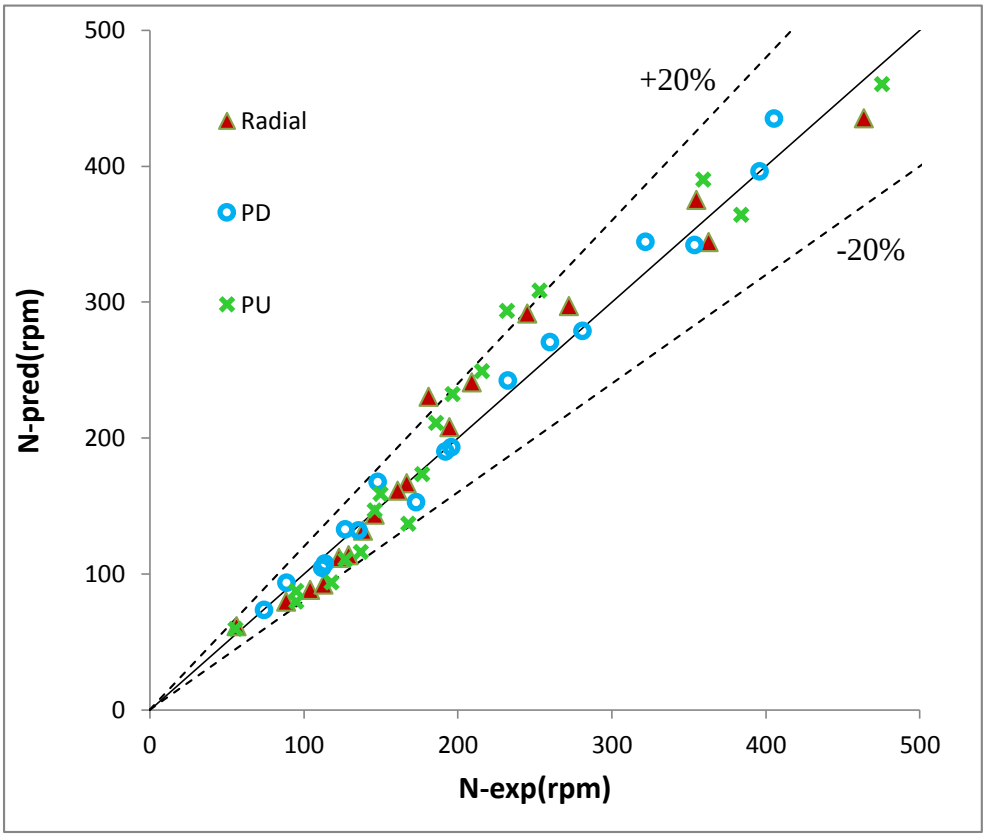

Fig. 5.4 Parity chart comparing experimental impeller speed with predicted values with +/- 20 % deviation lines for radial impeller, axial downward impeller and axial upward impeller

5.3.4 Multistage impeller results

The effect of multiple impellers on critical impeller speed for drawdown of floating particles was investigated. The setup was similar to the small scale setup described in the sec. 3.5. Three impellers in two combinations of axial-radial-axial (PU-radial-PD and PD-radial-

PU) were employed. The impellers were positioned at fixed position at the submergence of s/Da= 0.45, 1.0 and 1.5. The photograph of the setup and stirrer with multiple impellers are shown in Fig. 5.5. The dispersion experiments were carried out with 230 micron solid particles and with three fluids viz. water, glycerol-waster (1:1) solution and aqueous $ZnCl_2$ (65 wt%) solution. The critical impeller speed (N_{crit}) for the three fluids are shown in table 5.7. The results show that, with multiple impellers, dispersion taking place at lower impeller

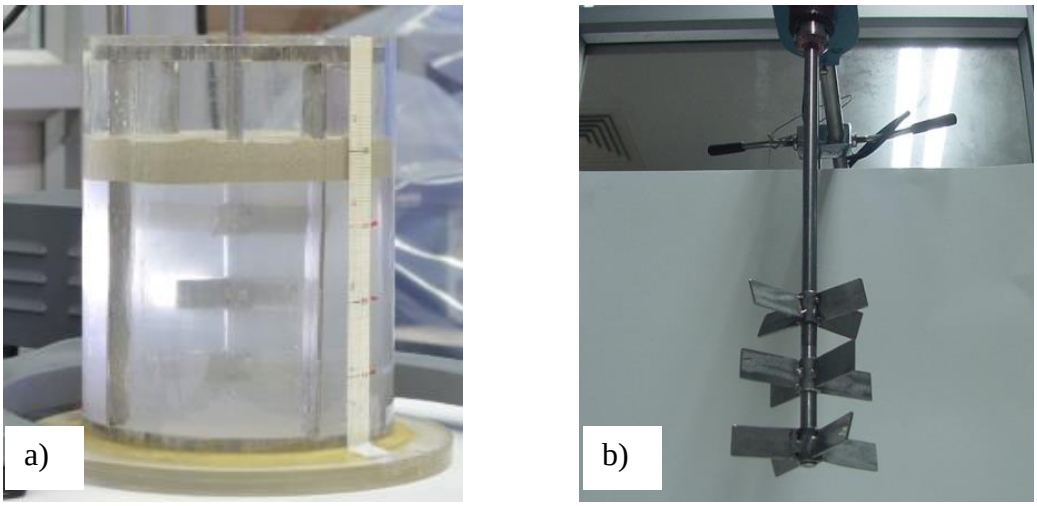

Fig. 5.5 Photograph of a) experimental set up and b) 3-stage impeller

Table 5.7 Effect of 3-stage impellers compared with single stage impeller (using 230 micron particles)

Liquid medium	N_{crit}(rpm)		
	Single- stage, radial at s/D_a=1.0	3-stage (PD-radial-PU)	3-stage (PU-radial-PD)
Water	89	45	45
Glycerol-water(1:1)	129	89	83
$ZnCl_2$ soln.	146	114	113

speed compared to the values for single impeller**.** In case of water which exhibits low buoyancy force, the dispersion was observed at a lower impeller speed of 45 rpm. There is no difference between the results corresponding to the two combinations of the impeller configuration. In other two liquids, PU-radial- PD combination was able to disperse the particles at slightly lower

impeller speed compared to PD –radial – PU combination. The reason for this is probably due to the fluid flow pattern generated by axial upward-radial-axial downward, which covers the entire volume of the fluid. In contrast, in case of PD-radial-PU impeller, visual observation indicates that the flow was mainly in the middle region.

5.4 Summary

Cold flow experiments were conducted with larger vessel to understand the effect of scaling up and the impeller type, impeller diameter, submergence and fluid medium were varied. The N_{crit} was measured and compared with the corresponding values in the smaller vessel. The results showed that in case of geometrically similar vessels, the impeller tip speed has to be maintained constant, to obtain complete dispersion. If the impeller diameter was reduced while keeping the vessel diameter the same, then a higher tip speed as well as power per unit volume is necessary to obtain complete dispersion. The data was analyzed to correlate the relevant dimensionless variables, and a relatively simple equation was sufficient to match the experimental results. A few experiments were also conducted with multi-stage impellers and, similar to the results in the smaller scale, the N_{crit} in multi-stage impeller was found to be lower than that in the corresponding single stage impeller in all the cases studied.

CHAPTER 6
CONCLUSIONS AND FUTURE STUDIES

In Indian nuclear program, sodium bonded ternary metal alloy fuel (U-Pu-19%Zr-10%) is likely to be used in the near future and pyroreprocessing can be used to close the fuel cycle. Electrorefining is an important step in pyroreprocessing of metallic fuel, and in this process, the fission products accumulate in the Li-KCl eutectic electrolyte and should be removed periodically. In the present study liquid-liquid extraction using cadmium alloy has been evaluated as a candidate process for this step and the results are summarized below.

6.1 Conclusions

In actual molten salt extraction set up, the entire process is operated at 723 K and visual inspection is not possible. To understand the hydrodynamics of dispersion in the actual process, floating particles drawdown in continuous liquid medium was carried out. The density ratio between the floating particles and liquid medium $\left(\Delta\rho/\rho\right)$ was varied from 0.13 to 0.63. The latter value is close to the value (0.8) in the actual system. The effect of impeller type, impeller submergence and particle size on drawdown floating particles was studied. Critical impeller speed (N_{crit}) required for the dispersion of floating particles in liquid medium was determined and a correlation using non-dimensionless groups, viz. Froude number, Archimedes number, density ratio, ratio of particle diameter to impeller diameter and ratio of impeller submergence to impeller diameter, to predict the critical impeller speed (N_{crit}) was developed. The experimental values were within ±20 % of the predictions. The correlation was used to predict the N_{crit} required for molten salt extraction system. The results also showed that the N_{crit} can be reduced by using multiple impellers.

An inert atmosphere experimental facility was set up to conduct the molten salt extraction experiment at 723 K. The extraction experiments were carried out using natural

uranium as the solute at 0.5 wt % concentration in the feed salt. The feed to the extractor was maintained at 25 ml/min of both salt and alloy phase. The U recovery up to 99% was observed in typical runs. Batch extraction studies were carried with 5.6 wt % U concentration and 98% recovery of U was observed. In this continuous reductive extraction process, the mass transfer coefficient based on volume was estimated to be around 16.77 cm^3/s. These results are in agreement with the values reported in the literature. This confirms that a high U recovery is possible in a single stage continuous well stirred liquid-liquid extractor.

The effect of scale up on dispersion was studied using 5 liter baffled glass vessel (1:10 volume ratio) and the type of impeller, impeller submergence, impeller diameter and the liquid medium were varied. In case of the larger vessel, the impeller tip speed needed for dispersion was less than or equal to that of smaller vessels. A correlation to predict N_{crit} from Reynolds number, Archimedes number and impeller submergence was developed. A comparison of the results in small and large scale indicates that, the dispersion hydrodynamics depends strongly on the scale of the process and independent studies need to be performed at each scale in order to characterize the system accurately.

6.2 Scope for Future Studies

Molten salt extraction, in continuous counter current multi stage setup, with multicomponent representing fission products extraction needs to be investigated for selective separation of actinides. In addition, process optimization as a function of various operating conditions and feed properties should be studied. Alternative contactors such as jet mixer, centrifugal contactors, ultrasonic mixtures etc can be evaluated for molten salt extraction.

REFERENCES

[1] G. Aydin, "The Modeling and Projection of Primary Energy Consumption by the Sources," *Energy Sources, Part B: Economics, Planning, and Policy,* vol. 10, pp. 67-74, 2015.

[2] F. Meunier, "The greenhouse effect: A new source of energy," *Applied Thermal Engineering,* vol. 27, pp. 658-664, 2007.

[3] B. Raj and M. Vijayalakshmi, "Ferritic steels for sodium-cooled fast reactors: Design principles and challenges," *Journal of Minerals Metals and Materials Society,* vol. 62, pp. 75-83, 2010.

[4] M. M. Abu-Khader, "Recent advances in nuclear power: A review," *Progress in Nuclear Energy,* vol. 51, pp. 225-235, 2009.

[5] X. Sun, H. Luo, and S. Dai, "Ionic liquids-based extraction: a promising strategy for the advanced nuclear fuel cycle," *Chemical reviews,* vol. 112, pp. 2100-2128, 2011.

[6] C. Degueldre, J. Bertsch, G. Kuri, and M. Martin, "Nuclear fuel in generation II and III reactors: research issues related to high burn-up," *Energy & Environmental Science,* vol. 4, pp. 1651-1661, 2011.

[7] A. K. Upadhyay, K. Jain, and U. Chandra, "Modularity in design and construction of nuclear power plants," in *International Congress on Advances in Nuclear Power Plants , ICAPP 2010*, pp. 2222-2238.

[8] B. Raj, M. Vijayalakshmi, P. Vasudeva Rao, and K. Rao, "Challenges in materials research for sustainable nuclear energy," *MRS bulletin,* vol. 33, pp. 327-337, 2008.

[9] Outlook, BP Energy, "2030," *London, January,* 2012.

[10] B. Raj, H. Kamath, R. Natarajan, and P. V. Rao, "A perspective on fast reactor fuel cycle in India," *Progress in Nuclear Energy,* vol. 47, pp. 369-379, 2005.

[11] S. Jain, "Inevitability of nuclear power in the Asian region," *Energy Procedia,* vol. 7, pp. 5-20, 2011.

[12] R. Chidambaram and C. Ganguly, "Plutonium and thorium in the Indian nuclear programme," *Current Science,* vol. 70, pp. 21-35, 1996.

[13] M. Lung and O. Gremm, "Perspectives of the thorium fuel cycle," *Nuclear Engineering and Design,* vol. 180, pp. 133-146, 1998.

[14] M. Menon, U. Mishra, B. Lalit, V. Shukla, and T. Ramachandran, "Uranium, thorium and potassium in Indian rocks and ores," *Proc. Indian Acad. Sci.,*, vol. 91, pp. 127-136, 1982.

[15] S. Glasstone and A. Sesonske, "Nuclear reactor engineering: Reactor Design Basics," 1994.

[16] S. Chetal, V. Balasubramaniyan, P. Chellapandi, P. Mohanakrishnan, P. Puthiyavinayagam, C. Pillai, *et al.*, "The design of the prototype fast breeder reactor," *Nuclear Engineering and Design,* vol. 236, pp. 852-860, 2006.

[17] P. Dey and N. Bansal, "Spent fuel reprocessing: a vital link in Indian nuclear power program," *Nuclear Engineering and Design,* vol. 236, pp. 723-729, 2006.

[18] B. Y. Moratilla Soria, M. Uris Mas, M. Estadieu, A. Villar Lejarreta, and D. Echevarria-López, "Recycling versus long-term storage of nuclear fuel: Economic factors," *Science and Technology of Nuclear Installations,* vol. 2013, 2013.

[19] S. Chetal and P. Chellapandi, "Indian fast reactor technology: Current status and future programme," *Sadhana,* vol. 38, pp. 795-815, 2013.

[20] A. Kakodkar, "Nuclear power in India: an inevitable option for sustainable development of a sixth of humanity," in *World Nuclear Association Annual Symposium, London*, 2002.

[21] N. Takaki, "Neutronic potential of water cooled reactor with actinide closed fuel cycle," *Progress in Nuclear Energy,* vol. 37, pp. 223-228, 2000.

[22] S. F. R. Options, "IAEA-TECDOC-1587," *IAEA, Vienna*, 2008.

[23] M. Benedict, T. Pigford, and H. Levi, "Nuclear Chemical Engineering," ed: McGraw-Hill Book Co, Inc., New York, 1981.

[24] D. D. Sood and S. K. Patil, "Chemistry of nuclear fuel reprocessing: current status," *Journal of radioanalytical and nuclear chemistry,* vol. 203, pp. 547-573, 1996.

[25] K. Venkatesan, T. Srinivasan, and P. V. Rao, "A review on the electrochemical applications of room temperature ionic liquids in nuclear fuel cycle," *Journal of Nuclear and Radiochemical Sciences,* vol. 10, pp. 1_R1-1_R6, 2009.

[26] R. Natarajan and B. Raj, "Fast reactor fuel reprocessing technology: successes and challenges," *Energy Procedia,* vol. 7, pp. 414-420, 2011.

[27] C. E. Till and Y. I. Chang, "Plentiful energy: the story of the integral fast reactor," *ISBN,* vol. 978, p. 116, 2011.

[28] J. P. Ackerman, "Chemical basis for pyrochemical reprocessing of nuclear fuel," *Industrial & Engineering Chemistry Research,* vol. 30, pp. 141-145, 1991.

[29] Y.-L. Liu, Y.-D. Yan, W. Han, M.-L. Zhang, L.-Y. Yuan, K. Liu, *et al.*, "Extraction of thorium from LiCl–KCl molten salts by forming Al–Th alloys: a new pyrochemical method for the reprocessing of thorium-based spent fuels," *RSC Adv.,* vol. 3, pp. 23539-23547, 2013.

[30] K. Kim, D. Ahn, J. Shim, S. Paek, I. Kim, and Y. Jung, "Pyrochemical extraction analysis of an immiscible molten LiCl–KCl/Cd system," *Journal of Radioanalytical and Nuclear Chemistry,* vol. 304, pp. 329-335, 2015.

[31] H. Lee, G.-I. Park, J.-W. Lee, K.-H. Kang, J.-M. Hur, J.-G. Kim, *et al.*, "Current status of pyroprocessing development at KAERI," *Science and Technology of Nuclear Installations,* 2013.

[32] K. Nagarajan, B. P. Reddy, S. Ghosh, G. Ravisankar, K. Mohandas, U. K. Mudali, *et al.*, "Development of pyrochemical reprocessing for spent metal fuels," *Energy Procedia,* vol. 7, pp. 431-436, 2011.

[33] A. E. Waltar and A. B. Reynolds, *Fast breeder reactors*: Alan E. Waltar, 1981.

[34] C. Ganguly, *Seminar on nuclear scince and technology for diplomats, IAEA, Vienna, 3 February 2009.*, 2009.

[35] K. Kim, S. Choi, S. Kim, J. Shim, S. Paek, and I. Kim, "Computational electrochemo-fluid dynamics modeling in a uranium electrowinning cell," *Journal of Radioanalytical and Nuclear Chemistry,* vol. 299, pp. 165-170, 2014.

[36] J. Ackerman, T. Johnson, L. Chow, E. Carls, W. Hannum, and J. Laidler, "Treatment of wastes in the IFR fuel cycle," *Progress in Nuclear Energy,* vol. 31, pp. 141-154, 1997.

[37] G. J. Janz, *Molten Salts Handbook*: Elsevier, 2013.

[38] G. Ladha, "Transport Phenomena in Liquid Extraction (Ladha, GS and Degaleesan, TE, eds.)," ed: McGraw-Hill, New Delhi, India, 1976.

[39] T. C. Lo, M. H. Baird, and C. Hanson, *Handbook of Solvent Extraction*: Krieger, 1991.

[40] R. E. Treybal, *Mass-Transfer Operations*: McGraw-Hill Book Company, 1981.

[41] C. Geankoplis, *Transport Processes and Separation Process Principles* Prentice Hall Press, 2003.

[42] M. Abbott, J. Smith, and H. Van Ness, *Introduction to Chemical Engineering Thermodynamics*: McGraw-Hill, 2001.

[43] P. Roberto Danesi, R. Chiarizia, and C. F. Coleman, "The kinetics of metal solvent extraction," 1980.

[44] R. E. Treybal, *Liquid Extraction*: McGraw-Hill New York, 1963.

[45] J. Davies, "Heterogeneous Reactions.: by LK Doraiswamy and MM Sharma. John Wiley and Sons, New York, 1984, 2 Vols," ed: Pergamon, 1985.

[46] L. Qi, X. Meng, R. Zhang, H. Liu, C. Xu, Z. Liu, *et al.*, "Droplet size distribution and droplet size correlation of chloroaluminate ionic liquid–heptane dispersion in a stirred vessel," *Chemical Engineering Journal,* vol. 268, pp. 116-124, 2015.

[47] G. Zhou and S. M. Kresta, "Correlation of mean drop size and minimum drop size with the turbulence energy dissipation and the flow in an agitated tank," *Chemical Engineering Science,* vol. 53, pp. 2063-2079, 1998.

[48] J. Seader and E. Henly, "Seperation Process Principles, 2nd," ed: John Wiley and Sons. Inc., New York, 2006.

[49] T. Koyama, K. Kinoshita, T. Inoue, M. Ougier, R. Malmbeck, and J.-P. Glatz, "Equilibrium distribution of actinides including Cm between molten LiCl-KCl eutectic and liquid cadmium," *Radiochimica Acta,* vol. 96, pp. 311-313, 2008.

[50] M. Kurata, Y. Sakamura, T. Hijikata, and K. Kinoshita, "Distribution behavior of uranium, neptunium, rare-earth elements (Y, La, Ce, Nd, Sm, Eu, Gd) and alkaline-earth metals (Sr, Ba) between molten LiCl・KCI eutectic salt and liquid cadmium or bismuth," *Journal of Nuclear Materials,* vol. 227, pp. 110-121, 1995.

[51] H. Moriyama, K. Kinoshita, Y. Asaoka, K. Moritani, and Y. Ito, "Equilibrium Distributions of Actinides and Fission Products in Pyrochemical Separation Systems, (II) LiCl-KCl/Cd System," *Journal of Nuclear Science and Technology,* vol. 27, pp. 937-943, 1990.

[52] M. Sakata, M. Kurata, T. Hijikata, and T. Inoue, "Equilibrium distribution of rare earth elements between molten KCl-LiCl eutectic salt and liquid cadmium," *Journal of Nuclear Materials,* vol. 185, pp. 56-65, 1991.

[53] H. Moriyama, D. Yamada, K. Moritani, T. Sasaki, I. Takagi, K. Kinoshita, *et al.*, "Reductive extraction kinetics of actinide and lanthanide elements in molten chloride and liquid cadmium system," *Journal of Alloys and Compounds,* vol. 408-412, pp. 1003-1007, 2006.

[54] J. P. Ackerman and J. L. Settle, "Distribution of plutonium, americium, and several rare earth fission product elements between liquid cadmium and LiCl・KCl eutectic," *Journal of Alloys and Compounds,* vol. 199, pp. 77-84, 1993.

[55] K. Kinoshita, T. Tsukada, and T. Ogata, "Single-stage extraction test with continuous flow of molten LiCl-KCl salt and liquid Cd for pyro-reprocessing of metal FBR fuel," *Journal of Nuclear Science and Technology,* vol. 44, pp. 1557-1564, 2007.

[56] K. Kinoshita and T. Tsukada, "Countercurrent extraction test with continuous flow of molten LiCl-KCl salt and liquid Cd for pyro-reprocessing of metal FBR fuel," *Journal of Nuclear Science and Technology,* vol. 47, pp. 211-218, 2010.

[57] K. Kinoshita, T. Inoue, S. Fusselman, D. Grimmett, J. Roy, R. Gay, *et al.*, "Separation of uranium and transuranic elements from rare earth elements by means of multistage extraction in LiCl-KCl/Bi system," *Journal of Nuclear Science and Technology,* vol. 36, pp. 189-197, 1999.

[58] G.-S. You, W.-M. Choung, E.-P. Lee, D.-H. Hong, W.-K. Lee, and J.-H. Ku, "Concept and safety studies of an integrated pyroprocess facility," *Nuclear Engineering and Design,* vol. 241, pp. 415-424, 2011.

[59] T. N. Zwietering, "Suspending of solid particles in liquid by agitators," *Chemical Engineering Science,* vol. 8, pp. 244-253, 1958.

[60] G. Baldi, R. Conti, and E. Alaria, "Complete suspension of particles in mechanically agitated vessels," *Chemical Engineering Science,* vol. 33, pp. 21-25, 1978.

[61] A. Nienow, "Suspension of solid particles in turbine agitated baffled vessels," *Chemical Engineering Science,* vol. 23, pp. 1453-1459, 1968.

[62] R. Geisler, C. Buurman, and A. Mersmann, "Scale-up of the necessary power input in stirred vessels with suspensions," *The Chemical Engineering Journal,* vol. 51, pp. 29-39, 1993.

[63] K. Raghava Rao, V. Rewatkar, and J. Joshi, "Critical impeller speed for solid suspension in mechanically agitated contactors," *AIChE Journal,* vol. 34, pp. 1332-1340, 1988.

[64] T. Jirout and F. Rieger, "Impeller design for mixing of suspensions," *Chemical Engineering Research and Design,* vol. 89, pp. 1144-1151, 2011.

[65] I. Ayranci and S. M. Kresta, "Critical analysis of Zwietering correlation for solids suspension in stirred tanks," *Chemical Engineering Research and Design,* vol. 92, pp. 413-422, 2014.

[66] R. Wójtowicz, "Choice of an optimal agitated vessel for the drawdown of floating solids," *Industrial & Engineering Chemistry Research,* vol. 53, pp. 13989-14001, 2014.

[67] J. Karcz and B. Mackiewicz, "Effects of vessel baffling on the drawdown of floating solids," *Chemical Papers,* vol. 63, 2009.

[68] O. Khazam and S. M. Kresta, "Mechanisms of solids drawdown in stirred tanks," *The Canadian Journal of Chemical Engineering,* vol. 86, pp. 622-634, 2008.

[69] N. Kuzmanić and B. Ljubičić, "Suspension of floating solids with up-pumping pitched blade impellers; mixing time and power characteristics," *Chemical Engineering Journal,* vol. 84, pp. 325-333, 2001.

[70] Z. Jaworski, K. Dyster, and A. Nienow, "The effect of size, location and pumping direction of pitched blade turbine impellers on flow patterns: LDA measurements and CFD predictions," *Chemical Engineering Research and Design,* vol. 79, pp. 887-894, 2001.

[71] G. Özcan-Taskin and G. McGrath, "Drawdown of light particles in stirred tanks," *Chemical Engineering Research and Design,* vol. 79, pp. 789-794, 2001.

[72] O. Khazam and S. M. Kresta, "A novel geometry for solids drawdown in stirred tanks," *Chemical Engineering Research and Design,* vol. 87, pp. 280-290, 2009.

[73] B. Raj, "Plutonium and the Indian atomic energy programme," *Journal of Nuclear Materials,* vol. 385, pp. 142-147, 2009.

[74] R. Gholipour-Peyvandi, S. Islami-Rad, and M. Ghannadi-Maragheh, "Influence of Gamma Energy in the Image Contrast for Material with Different Density," *International Journal of Pure and Applied Physics,* vol. 6, pp. 447-454, 2010.

[75] C. Musikas, G. R. Choppin, and J. Rydberg, *Principles and Practices of Solvent Extraction*: Dekker, 1992.

[76] Z. Chen, J. Prüss, and H.-J. Warnecke, "A population balance model for disperse systems: drop size distribution in emulsion," *Chemical Engineering Science,* vol. 53, pp. 1059-1066, 1998.

[77] C. Kotoulas and C. Kiparissides, "A generalized population balance model for the prediction of particle size distribution in suspension polymerization reactors," *Chemical Engineering Science,* vol. 61, pp. 332-346, 2006.

[78] W. M. Haynes, *CRC Handbook of Chemistry and Physics*: CRC Press, 2014.

[79] K. Singh, S. Mahajani, K. Shenoy, and S. Ghosh, "Representative drop sizes and drop size distributions in A/O dispersions in continuous flow stirred tank," *Hydrometallurgy,* vol. 90, pp. 121-136, 2008.

[80] A. Sahu, P. Kumar, and J. Joshi, "Simulation of flow in stirred vessel with axial flow impeller: zonal modeling and optimization of parameters," *Industrial & Engineering Chemistry Research,* vol. 37, pp. 2116-2130, 1998.

[81] T. Kumaresan and J. B. Joshi, "Effect of impeller design on the flow pattern and mixing in stirred tanks," *Chemical Engineering Journal,* vol. 115, pp. 173-193, 2006.

[82] S. M. Shekhar and S. Jayanti, "CFD study of power and mixing time for paddle mixing in unbaffled vessels," *Chemical Engineering Research and Design,* vol. 80, pp. 482-498, 2002.

[83] L. Dong, S. Johansen, and T. Engh, "Flow induced by an impeller in an unbaffled tank—II. Numerical modelling," *Chemical Engineering Science,* vol. 49, pp. 3511-3518, 1994.

[84] F. OCONNELL and D. Mack, "Simple turbines in fully baffled tanks-Power characteristics," *Chemical Engineering Progress,* vol. 46, pp. 358-362, 1950.

[85] S. Nagata, *Mixing: Principles and Applications*: Halsted Press, 1975.

[86] S. Vannia Perumal, B. P. Reddy, G. Ravisankar, and K. Nagarajan, "Actinides draw down process for pyrochemical reprocessing of spent metal fuel," *Radiochimica Acta,* vol. 103, pp. 287-292, 2015.

[87] D. W. Green, *Perry's Chemical Engineers' Handbook* vol. 796: McGraw-hill New York, 2008.

[88] T. Srinivasa and S. Jayanti, "An Eulerian/Lagrangian study of solid suspension in stirred tanks," *AIChE Journal,* vol. 53, pp. 2461-2469, 2007.

[89] D. Sechremeli, A. Stampouli, and M. Stamatoudis, "Comparison of mean drop sizes and drop size distributions in agitated liquid–liquid dispersions produced by disk and open type impellers," *Chemical Engineering Journal,* vol. 117, pp. 117-122, 2006.

[90] A. Tagawa, N. Dohi, and Y. Kawase, "Dispersion of floating solid particles in aerated stirred tank reactors: Minimum impeller speeds for off-surface and ultimately homogeneous solid suspension and solids concentration profiles," *Industrial & Engineering Chemistry Research*, vol. 45, pp. 818-829, 2006.

[91] P. M. Armenante and E. U. Nagamine, "Effect of low off-bottom impeller clearance on the minimum agitation speed for complete suspension of solids in stirred tanks," *Chemical Engineering Science*, vol. 53, pp. 1757-1775, 1998.

[92] F. A. Holland and F. S. Chapman, *Liquid Mixing and Processing in Stirred Tanks*: Reinhold Pub. Corp., 1966.

[93] F. Shunk and P. Nash, "The Cd− Ni (Cadmium-Nickel) system," *Journal of Phase Equilibria*, vol. 8, pp. 122-124, 1987.

[94] "Pressure Vessel Design," in *ASME Boiler and Pressure Vessel Code*, ed: ASME, USA, 2001.

[95] "Material Properties," in *ASME Boiler and Pressure Vessel Code*, ed: ASME, USA, 2001.

[96] R. R. Hemrajani and G. B. Tatterson, "Mechanically stirred vessels," *Handbook of Industrial Mixing: Science and Practice*, pp. 345-390, 2004.

[97] D. R. Lide, *CRC Handbook of Chemistry and Physics*: CRC press, 2004.

[98] K. Sridharan, S. Martin, M. Mohammadian, J. Sager, T. Allen, and M. Simpson, "Thermal properties of LiCl-KCl molten salt for nuclear waste separation," *Transactions of the American Nuclear Society*, vol. 106, pp. 1240-1241, 2012.

[99] S. Som, *Introduction to Heat Transfer*: PHI Learning Pvt. Ltd., 2008.

[100] E. A. Avallone, T. Baumeister, and A. Sadegh, *Marks' Standard Handbook For Mechanical Engineers (Standard Handbook for Mechanical Engineers)*: Mcgraw-Hill Professional, 2006.

[101] B. Theraja, A. Theraja, U. Patel, S. Uppal, J. Panchal, B. Oza, *et al.*, "A Textbook of Electrical Technology Vol II," *S. Chand publishers*, 2005.

[102] W. L. McCabe, J. C. Smith, and P. Harriott, *Unit Operations of Chemical Engineering* vol. 5: McGraw-Hill New York, 1993.

[103] W. F. Holcomb, "Experience with glovebox inert atmosphere control system," *Nuclear Engineering and Design*, vol. 6, pp. 213-216, 1967.

[104] H. Laitinen, W. Ferguson, and R. Osteryoung, "Preparation of Pure Fused Lithium Chloride-Potassium Chloride Eutectic Solvent," *Journal of the Electrochemical Society*, vol. 104, pp. 516-520, 1957.

[105] D. A. Skoog and D. M. West, *Principles of Instrumental Analysis* vol. 158: Saunders College Philadelphia, 1980.

[106] J. H. Moore, C. C. Davis, M. A. Coplan, and S. C. Greer, *Building Scientific Apparatus*: Cambridge University Press, 2009.

[107] M. Bickel, "The Davies-Gray titration for the assay of uranium in nuclear materials: a performance study," *Journal of Nuclear Materials*, vol. 246, pp. 30-36, 1997.

[108] Y. Sakamura, T. Inoue, O. Shirai, T. IWAI, Y. ARAI, and Y. SUZUKI, "Studies on pyrochemical reprocessing for metallic and nitride fuels: behaviour of transuranium elements in LiCl-KCl/liquid metal systems," in *International Conference on Future Nuclear Systems, GLOBAL'99*, 1999.

[109] R. C. Paule and J. Mandel, "Analysis of interlaboratory measurements on the vapor pressure of cadmium and silver," *Pure and Applied Chemistry*, vol. 31, pp. 395-432, 1972.